UNIVERSITY OF OKLAHOMA

GRADUATE COLLEGE

PALEOENVIRONMENTS AND SEDIMENTS AROUND THE FRASNIAN/FAMENNIAN (F/F) TRANSITION IN THE WOODFORD SHALE, SOUTH CENTRAL OKLAHOMA – A MULTIPROXY APPROACH

A DISSERTATION

SUBMITTED TO THE GRADUATE FACULTY

In partial fulfillment of the requirements for the

Degree of

DOCTOR OF PHILOSOPHY

By

CARLOS EDUARDO MOLINARES BLANCO

Norman, Oklahoma

2019

PALEOENVIRONMENTS AND SEDIMENTS AROUND THE FRASNIAN/FAMENNIAN (F/F) TRANSITION IN THE WOODFORD SHALE, SOUTH CENTRAL OKLAHOMA – A MULTIPROXY APPROACH

A DISSERTATION APPROVED FOR THE

SCHOOL OF GEOSCIENCES

BY THE COMMITTEE CONSISTING OF

Dr. Roger Slatt, Chair

Dr. Deepak Devegowda

Dr. Douglas Elmore

Dr. Kurt Marfurt

Dr. Miguel Etayo

Acknowledgements

I would like to express my sincere appreciation and deepest gratitude to Dr. Roger Slatt, my research advisor and committee chairman: Thanks for his time, guidance, mentoring, support and help throughout more than seven years, and particularly during the hardest time in my life. Thanks to his continuous support, my hope and love for geology keep it up.

I also like to thank the members of my committee, Dr. Deepak Devegowda, Dr. Douglas Elmore, Dr. Kurt Marfurt and Dr. Miguel Etayo for their support and valuable time reviewing my ideas in this dissertation and during informal discussions taking their classes and after that. Special thanks go to Miguel Etayo, who opened BP's doors and facilitated resources for part of this research.

I want to extend my gratitude also to the Institute of Reservoir Characterization (IRC) colleagues, friends and families for providing support, help, ideas, scientific discussions, field trips, cheering my days and countless laughs during my PhD life time. I also want to thank the OU Geoscience school staff and faculty members for their kind support during my research and always being friendly during my school time. I want to thank the Oklahoma Geological Survey (OGS) and OPIC facilities staff for providing kind help during hundreds of hours checking cores at the core library and specially thanks to Mr. Brian Cardott for providing valuable references and discussions about the Woodford Shale in Oklahoma.

I wish to extend my gratitude to Colfuturo, the Colombian Student Association Alumni (COUAA), the Geological Society of America (GSA), the American Association of Petroleum Geologists (AAPG), the Houston Geological Society (HGS), the Society of Independent

Professional Earth Scientists (SIPES), Oklahoma City Chapter, for their grants and monetary support. To the CPSGG for the Gen P Morell and ConocoPhillips Scholarships and all the benefactors and companies that have been part of the IRC-Shale Consortium phases. All these contributions significantly supported this research.

My sincere thanks go to Dr. Paul Philp, his students and staff at the Organic Geochemistry Laboratory, for helping me in rock preparation and letting me use lab facilities for sampling preparations. I want to thank Dr. Andy Elwood Madden and Emma Bachman for kindly explaining to me the XRD analysis routines and checking my results. Also, thanks to Dr. Douglas Elmore, Gerhard Heij and Cory Terrel for their kind assistance and support using the SEM-EDX lab.

My deepest appreciation to Dr. Seth Young and Nevin Kozik for their incredible support and help during my time in the National Magnetic Lab in Tallahassee, Florida. Their support processing and interpreting the carbon stable isotopic results let us know the Upper and Lower Kellwasser events location in the Woodford Shale.

I want to recognize and thank my parents for their love, encouragement and support. To Lindy Herrera and the NSFC family church for their incredible and continuous support and finally but no less to my daughter Maria Camila, who patiently helped me and supported me hours, and hours, and hours, during field trips, trips, classes, labs, conferences and library rooms. I really appreciate your sacrifices and support. Love you!

Thank God… to Cami with all my love!

Table of Contents

Acknowledgements……v

Table of contents ……vii

List of figures ……ix

List of tables …… xi

Abstract……x

Chapter 1: Thomas Amsden's Pre-Woodford sub-crop maps and the Late Devonian – Early Mississippian unconventional plays in the Arkoma Basin, Oklahoma …… 1

1. Introduction …… 2
2. Importance of the Thomas Amsden's Pre-Woodford sub-crop maps …… 3
3. Conclusions …… 9
4. References……10

Chapter 2: The effect of anisotropy (lamination/bedding) on shale brittleness in the Woodford Shale Unconventional deposits, Oklahoma……12

1. Introduction ……14
2. Materials and Methods……18
3. Results ……21

3.1 Effects of the anisotropy (VTI) on the rock brittleness ……25

3.2 Rock brittleness, lamination and sequence stratigraphy……27

4. Conclusions ……29
5. References …… 30

Chapter 3: The Frasnian/Famennian (F/F) Transition in the Woodford Shale, South Central Oklahoma…… 32

1. Introduction……35

2. Stratigraphic Framework……40

3. Methods ……44

4. Results ……47

4.1 Chronoestratigraphic Framework…… 47

4.2 Natural gamma-ray spectrometry analysis…… 50

4.3 Trace and Major element concentrations…… 54

4.3.1 Organic matter production…… 55

4.3.2 Oxygenation and redox proxies…… 60

4.3.3 Weathering and dilution…… 71

5. Conclusions……77

6. Ackowledgements ……79

7. References ……80

List of Figures

Figure 1.1. Location of “Stack” and “SCOOP” plays in the Oklahoma basins (After, Cardott 2012).4

Figure 1.2. Woodford shale wells with first production from 01-01-2001 to 06-01-2011 (Modified from EIA (2012)……5

Figure 1.3a) Woodford Shale sub-crop map in the Arkoma Basin from Amsden (1980) ……..6

Figure 1.3b) Flattened section B-B’ located northeast of the Arkoma Basin (see Figure 3a for cross section location). The thicknesses of the Sylvan Shale and older units are not to true vertical scale. Synclinal structures cored by the Hunton Group may have been more resistant to erosion, whereas anticlinal structures cored by the Sylvan Shale may have been less competent and easier to erode (modified from Amsden, 1980)……7

Figure 1.4. Well correlation in the Arkoma Basin. In general, the Woodford Shale is thicker to the southwest in the Arkoma Basin, but this trend is interrupted in the center of the basin where the Hunton Group is not present along some narrow corridors ……8

Figure 2.1 a) The Wyche-1 core well was a research well drilled, cored and logged near an active quarry in the Wyche shale pit, Pontotoc County, Oklahoma. b) The Wyche-1 core well Gamma Ray (GR) quartz-rich brittle intervals (yellow areas) and organic-rich ductile intervals (purple areas) compared with the Acoustic (A) Impedance, Young's modulus (E3) and the Poisson's ratio (v3) calculated from sonic and density well logs……..15

Figure 2.2. The Vertical Transverse Isotropy can be generated from nanno- to meso- scales in organic-rich, self-storage unconventional deposits……..17

Figure 2.3. The elastic compliance matrix for the Vertical Transverse Isotropy (VTI) cases expressed in terms of the Young’s modulus (E), Poisson’s ratio (ν) and the Shear modulus (μ), along the symmetry axis (E, ν and μ) and perpendicular (E’, ν’ and μ’)……..21

Figure 2.4. Cross plot between the Tensile Strength (*T*) and Fracture Toughness (K*ic*) versus compositional brittle index (Bi), Epsilon (ε) and Gamma (γ) anisotropy coefficients calculated from UPV analysis for the upper and middle Woodford samples……..22

Figure 2.5. VTI differences between the Upper Woodford (HST - right) and middle Woodford (TST - left) shale deposits. The sample with less laminae corresponds with HST upper Woodford interval (111 ft) and the more laminae with the TST middle Woodford (136 ft)……..23

Figure 3.1. Middle to Late Devonian geological events……38

Figure 3.2. Woodford shale localities in South-central Oklahoma……..39

Figure 3.3a. Upper, middle and lower Woodford Shale subdivisions……42

Figure 3.3b. The F/F boundary in reference sections around the world ……42

Figure 3.4. Wyche-1 core subdivisions ……48

Figure 3.5. Borehole and core spectral gamma ray (GR) logs from the Wyche-1 core well……51

Figure 3.6. Powder X-ray diffraction (XRD) analysis from the Wyche-1 core well……..54

Figure 3.7. Nickel (Ni) and Cupper (Cu) concentrations from the Wyche-1 core well samples…....57

Figure 3.8. Scanning electron microscope (SEM) image, coupled with an energy dispersive X-Ray analyzer (EDX) showing the presence of sphalerite crystals (Zn,FeS) ……..58

Figure 3.9a. Hypothetical vertical and horizontal redox transitions in marine sedimentary basins. ……62

Figure 3.9b. Oxidation reactions of sedimentary organic matter in a vertical profile……62

Figure 3.10. Molybdenum (Mo) and Uranium (U) concentrations from the Wyche-1 core well samples……63

Figure 3.11. Manganese (Mn)/Iron (Fe) ratios and Fe normalized by Aluminum (Al) contents, from X-ray fluorescence (XRF) compositional analysis, Wyche-1 core well……..69

Figure 3.12a. Scanning electron microscope (SEM) images, coupled with an energy dispersive X-Ray analyzer (EDX) for two thin section Woodford Shale samples ……70

Figure 3.12b. SEM-EDX analyis from upper Woodford sample located 36.4 m (119’3”) depth. Syngenetic pyrite was characterized by pyrite framboids (Py) and tiny metallic particles were identified as ilmenite (IL) crystals (FeTiO3)……..70

Figure 3.13. Zirconium (Zr) and Titanium (Ti) element concentrations from X-ray fluorescence (XRF), Wyche-1 core well……72

Figure 3.14. Sequence Stratigraphic model for the Woodford Shale, Wyche-1 well Oklahoma…74

Figure 3.15. Sequence stratigraphy model and Woodford Shale well correlation in South Central Oklahoma ……..75

List of Tables

Table 2.1. Results of the anisotropy Thomsen's coefficient Epsilon (ε) and Gamma (γ) indexes calculated from UPV's analysis, Brittle compositional Index (Bi) from XRD analysis, Tensile Strength (*T*) and Fracture Toughness (K*ic*) tests from core lab test from Woodford shale samples……24

Table 2.2. Poroelasticity modulus, KVTI and KISO effective stress coefficients calculated from UPV's analysis……24

Table 3.1. Trace elements average values in shales and continental crust (After Taylor and McLennon 1985, Vine and Tourtelot 1970; Huyck 1990 and Tribovillard et al., 2006). Aluminum normalized and Element Factor (EF) average values from modern anoxic basin (From Calvert and Pedersen, 1993)……46

Table 3.2 Stable organic carbon isotopic analysis results……49

Table 3.3 X-ray diffraction (XRD) results for samples taken from Wyche -1 research core well…52

Abstract

The Woodford Shale (WDS) and the overlying Mississippian aged units are one of the most prolific unconventional reservoirs in the United States. Although the WDS extends to Texas, a total of 22 billion barrels of bitumen and 16 billion barrels of saturated hydrocarbons expelled from the Woodford have been calculated only from the central and southern areas in Oklahoma (Comer and Hinch, 1987). I included in this PhD dissertation three related studies that investigate the possible local and global controls on the distribution of the organic-rich Woodford Shale deposits, situated in the southcentral part of Oklahoma. The research presented here spans several years of study and publications, so that the three chapters are numbered and placed in historical perspective.

The first work dates to the end of 2014 (Molinares and Slatt, 2014), and was one of the first publications that described the importance of the paleo-topography as a critical factor in the exploitation of unconventional reservoirs. In the author's opinion, few workers had addressed the pre-Woodford sub-crop maps previous to this publication. Pre-Woodford Shale sub-crop maps provide a helpful guide for recognizing "sweet-spots" corridors associated with the accumulation of the Late Devonian - Early Mississippian rocks. In the Arkoma basin, synclinal structures cored by Hunton Group limestones could have been more resistant to erosion, whereas anticlinal structures, deeply eroded or cored by softer intervals (such as the Sylvan Shale), were more easily eroded and created narrow corridors where thicker and highly prospective Early-Mississippian coarse-grained sediments were accumulated. Other theses and publications (e.g. Althoff, 2012; McCullough 2014; Hasbrook, 2015; Infante et al., 2017; Torres et

al., 2017) have confirmed and supported the importance of the paleo-topography as key element in unconventional reservoir characterization.

The second chapter introduced the vertical anisotropy (bedding/layering), as another important element in the characterization of unconventional reservoirs (Molinares et al., 2016). The best areas for developing unconventional resources are normally characterized by a higher organic content, brittle lithofacies and high-pressured zones. However, vertical transverse isotropy (lamination/bedding) is not commonly included when defining intervals for hydraulic fracturing. In the second paper, Thomsen's coefficients epsilon (ε) and gamma (γ), values obtained from Ultra Pulse Velocities (UPV) analysis were used to quantify anisotropy and to explore their effect on rock brittleness. In fact, more laminae at brittle intervals possibly created planes of weakness that assist in reducing the effective minimum horizontal stress and break rock easier. Thomsen's ε and γ coefficients are proposed as proxies to estimate the effect of anisotropy on rock brittleness. Thomsen's coefficients have an advantage compared to other methods to determine vertical anisotropy because these coefficients may be applicable under a wide variety of observation scales, such as those recorded by 3D seismic surveys, borehole seismic, micro seismicity, sonic well logs and UPV core analysis.

The last chapter is a multiproxy research using a combination of stable carbon isotopes, spectral natural gamma-ray logs, scanning electron microscope images - coupled with an energy dispersive X-Ray analyzer (SEM-EDX), powder X-ray diffraction (XRD), X-ray fluorescence (XRF), and palynological analysis in samples from the Wyche-1 research well. This last work was presented at the GSA South-Central Section - 52nd Annual Meeting (2018) and awarded as the best PhD student oral presentation (Molinares et al., 2018).

The results confirm the age of the Woodford Shale (Late Devonian – Early Mississippian) and correlated a stable carbon isotopic curve obtained from Woodford Shale samples, with a series of positive Carbon excursion events associated with the Frasnian/Famennian (F/F) transition and the global extended Kellwasser events. The widespread occurrence of anoxic benthic conditions during the F/F boundary is poorly understood. However, the preservation of the OM in the Woodford Shale was the result of deep-water stagnation, low dilution rates, high salinity/dense vertical oceanic stratification, deep-water oxygen depletion, with no clear evidences of a shallow marginal sill southward. The preservation of organic matter in the Woodford Shale was largely influenced by relative sea level changes by controlling key primary productivity elements including: marine salinity, the influx of key nutrient (e.g. Fe-influx), water oxygenation, deep-water marine circulation and sedimentation/dilution rates.

References

Althoff, C.D., 2012, Characterization of depositional megacycles in the Woodford Trough of Central Oklahoma. [M.S. Thesis], University of Oklahoma. 99 p.

Comer, J.B., and Hinch, H.H., 1987, Recognizing and quantifying expulsion of oil from the Woodford Formation and age-equivalent rocks in Oklahoma and Arkansas: AAPG Bulletin, v. 71, no. 7.

Hasbrook, S., 2015, Geologic characterization of the Woodford Shale across the Arbuckle Uplift counties, south central Oklahoma: Norman, Oklahoma. [M.S. thesis], University of Oklahoma. 103 p.

Infante-Paez, L., L.-F. Cardona, B. McCullough, and R. Slatt, 2017, Seismic analysis of paleotopography and stratigraphic controls on total organic carbon: Rich sweet spot distribution in the Woodford Shale, Oklahoma, USA: Interpretation, v. 5, no. 1, p. T33-T47.

McCullough, B. J., 2014, Sequence Stratigraphic framework and characterization of the Woodford Shale on the southern Cherokee Platform of Central Oklahoma. [M.S. Thesis], University of Oklahoma. 212 p.

Molinares-Blanco, C.E., and R.M. Slatt, 2014, Thomas Amsden's pre-Woodford subcrop maps and the Late Devonian-Early Mississippian unconventional plays in the Arkoma Basin: Shale Shaker, v. 65, p. 212-219.

Molinares-Blanco, C.E., Sierra, R., and R.M. Slatt, 2016. Effect of anisotropy (lamination) on rock fracability for vertical transverse isotropic (VTI) unconventional reservoirs, a comparison between upper (Highstand system tract - HST) and middle (Transgressive system tract - TST) Woodford shale. SEG Technical Program Expanded Abstracts 2016: pp. 485-489.

Molinares-Blanco, C. E., Turner, B., and R. Slatt. 2018. Late Devonian organic-rich Woodford shale deposits and the Frasnian/Famennian (F/F) and DevonianCarboniferous (D/C) global anoxic events. 52nd Annual Meeting, GSA South-Central Section, 12–13 March 2018 | Little Rock, Arkansas.

Torres, E.J., R.M. Slatt, K.J. Marfurt, L.E. Infante, and L.A. Castillo, 2017, Identification of potential lacustrine stratigraphic intervals in the Woodford Shale, Oklahoma, using multi-attribute 3-D seismic displays and a supervised neural network: Unconventional Resources Technology Conference, URTeC 2692737, 13 p.

Chapter 1: Thomas Amsden's Pre-Woodford sub-crop maps and the Late Devonian - Early Mississippian unconventional plays in the Arkoma Basin

1. Introduction

Thanks to significant advances in horizontal drilling and multistage hydraulic fracturing, the Woodford Shale continues to attract interest in the U.S. unconventional-shale boom. Recently, two new play concepts have emerged. The first play has been named "SCOOP" or South-Central Oklahoma Oil Province, where operators to date focus on liquids-rich production (Fig. 1.1). It is a corridor several tens of miles wide and might be an extension of the Woodford-Cana play southward to the edge of the Anadarko Basin. The second is the "STACK" play. It is located west and northwest of Oklahoma City with targets associated with a combination of the Late Devonian - Early Mississippian Woodford Shale and Mississippian 'Lime' brittle units. These Mississippian beds lie directly above the Woodford Shale, with porosities comparable to the Woodford but with significantly better permeability (Brown, 2014). Thickness, porosity, depth, thermal maturity and overpressured zones have been considered as important driving factors for setting liquids-rich "sweet spots" in the Woodford Shale unconventional exploration (Andrews, 2009; Cardott, 2012; Curtis et al., 2012; Slatt et al., 2011, 2012). Little attention has been paid to pre-Woodford sub-crop maps, which are a key factor in the Late Devonian to Early Mississippian unconventional-plays distribution. However, after this publication other authors have confirmed and supported the importance of the paleo-topography as a key element in the unconventional reservoir characterization (e.g. McCullough 2014; Slatt et al., 2015; Hasbrook, 2015; Infante et al., 2017; Torres et al., 2017).

2. Importance of Thomas Amsden's Pre-Woodford sub-crop maps

In 1975 and 1980 the Oklahoma Geological Survey published the Bulletins 121 and 129 titled, respectively, "Hunton Group (Late Ordovician, Silurian and Early Devonian) in the Anadarko Basin of Oklahoma" and "Hunton Group (Late Ordovician, Silurian and Early Devonian) in the Arkoma Basin of Oklahoma", both authored by Thomas W. Amsden. In relationship to the Woodford Shale and overlying units, these bulletins include valuable information such as isopach and structure maps of the Woodford Shale, Hunton Group and Sylvan Shale (Amsden, 1975; Panels 1-4; Amsden, 1980; Panels 1-4). Additionally, these bulletins included two sub-crop maps supported by 136 cores (which cut some part of the Sylvan – Hunton – Woodford sequences), well cuttings descriptions from 117 wells and lithological descriptions of more than 800 thin sections.

A key observation made by Amsden and commented in these bulletins was that a period of uplift and erosion preceeded the deposition of the Late Devonian – Early Mississippian Woodford Shale (Amsden, 1980). This erosion created some fluvial drainage systems in the Anadarko (Amsden, 1975) and Arkoma Basins (Amsden, 1980, fig. 26) (Figures 1.2, 1.3a). In the Arkoma Basin, Woodford Shale thickness changes are principally related with the fact that the Woodford's basal and top surfaces are unconformities and may outline incised valleys and karst topography (Althoff, 2012; Molinares, 2013).

The Woodford Shale is generally 100 to 200 ft thick but thins to less than 50 ft northeast toward the Ozark Uplift, where the Misener and Sycamore Sandstones underlying the Woodford were accumulated periodically (Figure 1.2). The Misener is primarily a quartz sandstone cemented with crystalline dolomite that grades into a crystalline dolomite with scattered quartz

grains. These two end members are intimately associated, and the bedding commonly is defined by dolomite-rich layers alternating with quartz-rich layers (Amsden and Klapper, 1972). The Misener clearly overlies the pre-Woodford unconformity and locally is interbedded with Woodford-type shales (Amsden, 1980). The Sylamore Sandstone overlies the Hunton Group in eastern Oklahoma and grades upward into black shales of the Chattanooga Formation (Amsden, 1980). For these reasons, the Misener and Sylamore Sandstones are believed to be closely related in their depositional history to the Woodford Shale (Amsden and Klapper, 1972).

The Misener conodont faunas range in age from late Middle to Late Devonian (Givetian to early Famennian) and indicate that the Misener is correlative with part of the Woodford Shale in the region of the Arbuckle Mountains (Amsden and Klapper, 1972). There, the Woodford is thinner (<100 ft) but the Misener sandstones are not reported, possibly due to the absence of any substantial local source for such material (Amsden, 1960, p. 139-140).

In general, the Woodford Shale is thicker to the southwest in the Arkoma Basin, but this trend is interrupted in the center of the basin (Figure 1.2) where the Hunton Group is absent along some relatively narrow corridors (Figure 1.3a). Hunton Group erosion appears to be related to thicker overlying Mississippian intervals (Figure 1.4). Southwest of this central region, the Woodford thickness increases, following a trend that extends from northern Coal County northward through much of Hughes County, where most horizontal Woodford wells have been drilled. There, the Woodford Shale ranges from 7,000 to 10,500 ft deep and its thickness fluctuates between 100 and 200 ft (Figure 1.2).

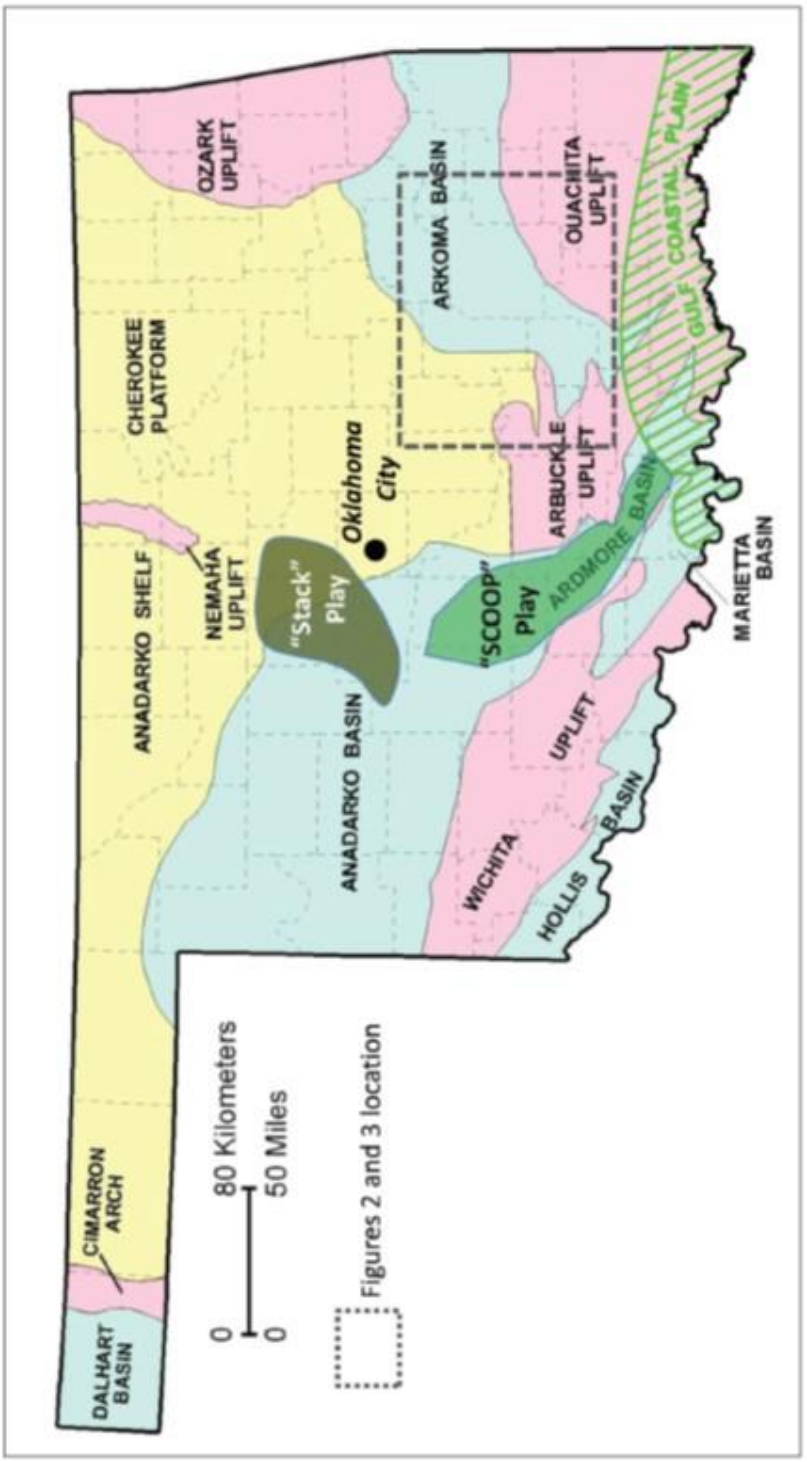

Figure 1.1. Location of "Stack" and "SCOOP" plays in the Oklahoma basins (After Cardott, 2012).

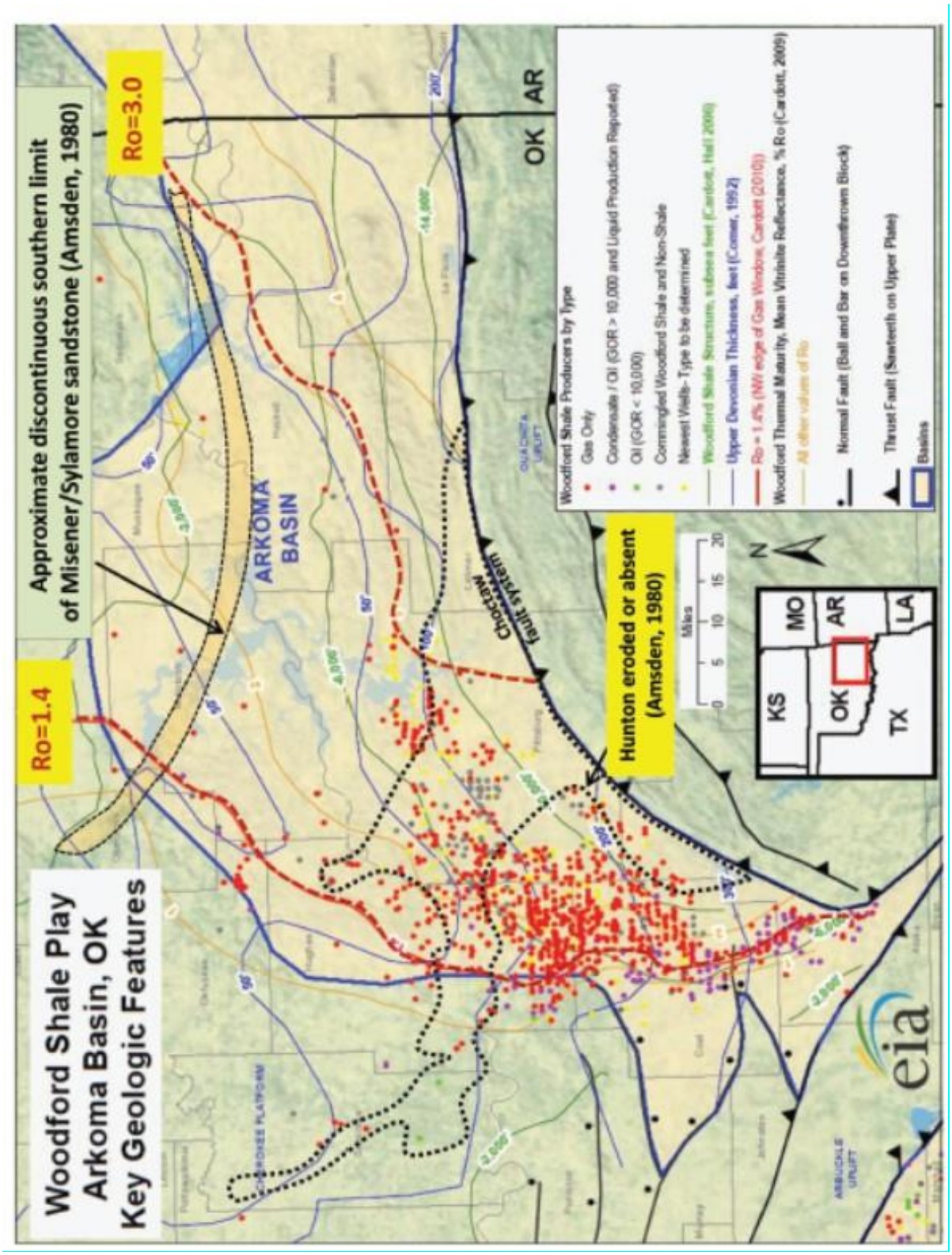

Figure 1.2. Woodford shale wells with first production from 01-01-2001 to 06-01-2011 (Modified from EIA 2012).

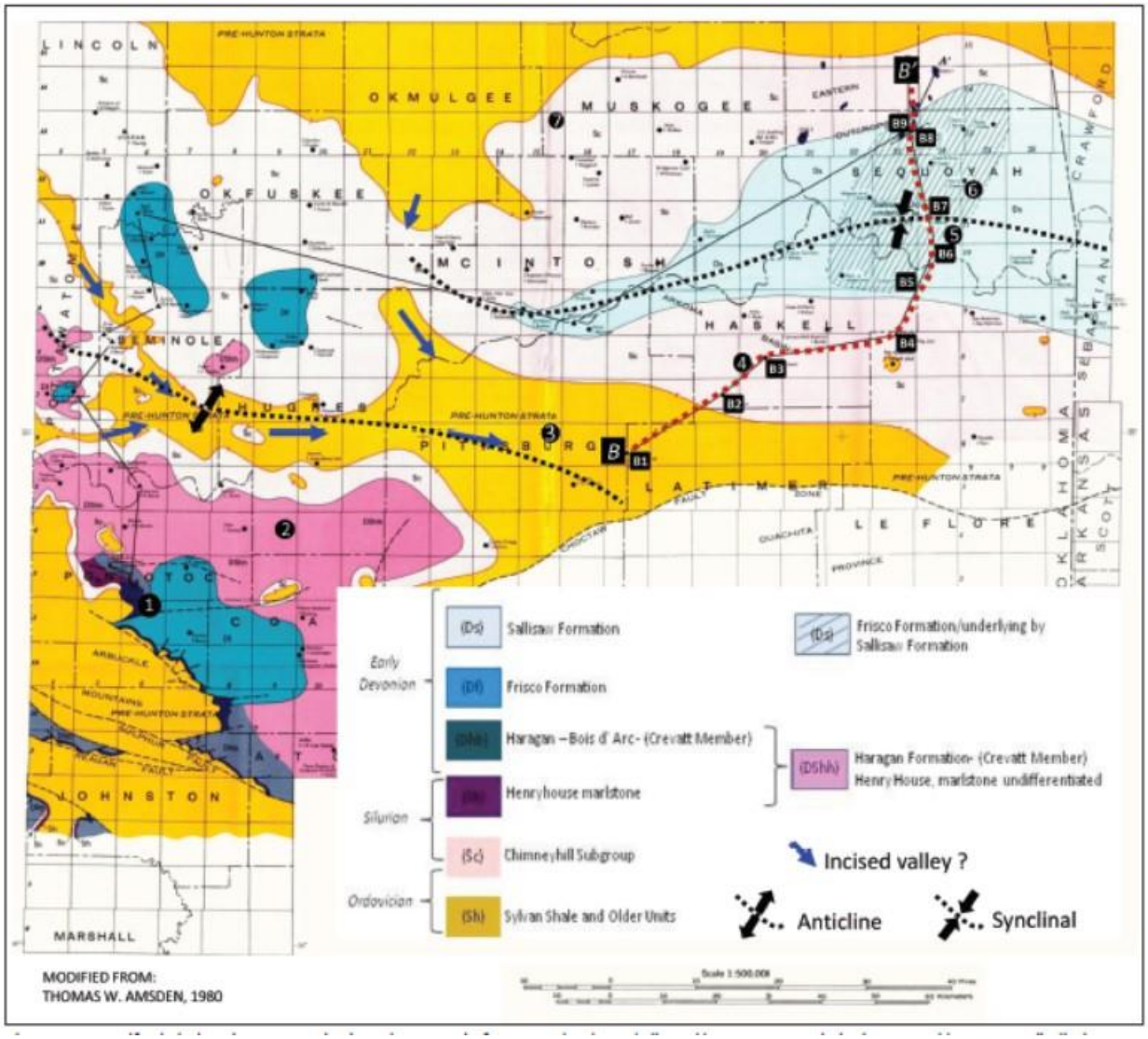

Figure 1.3a. Woodford Shale sub-crop map in the Arkoma Basin from Amsden (1980).

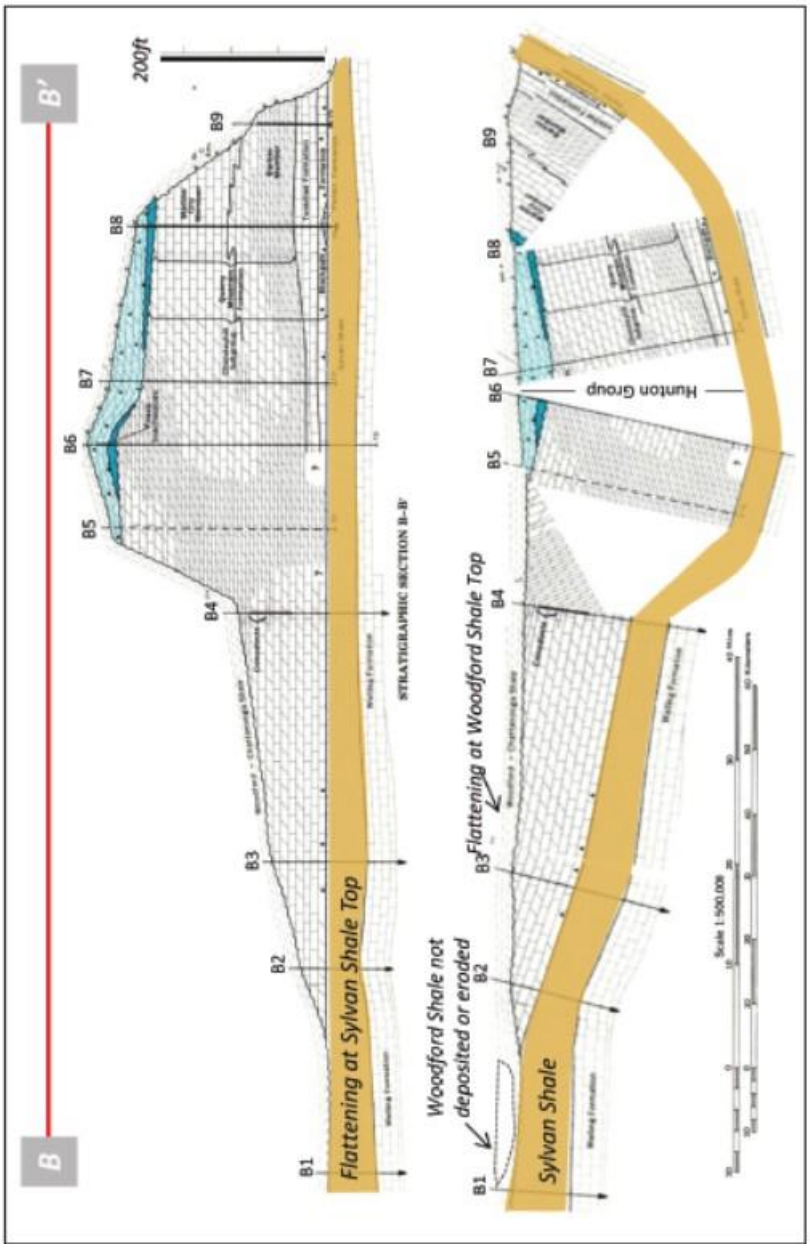

Figure 1.3b. Flattened section B-B' located northeast of the Arkoma Basin (see Figure 3a for cross section location). The thicknesses of the Sylvan Shale and older units are not to true vertical scale. Synclinal structures cored by the Hunton Group may have been more resistant to erosion, whereas anticlinal structures cored by the Sylvan Shale may have been less competent and easier to erode (modified from Amsden, 1980).

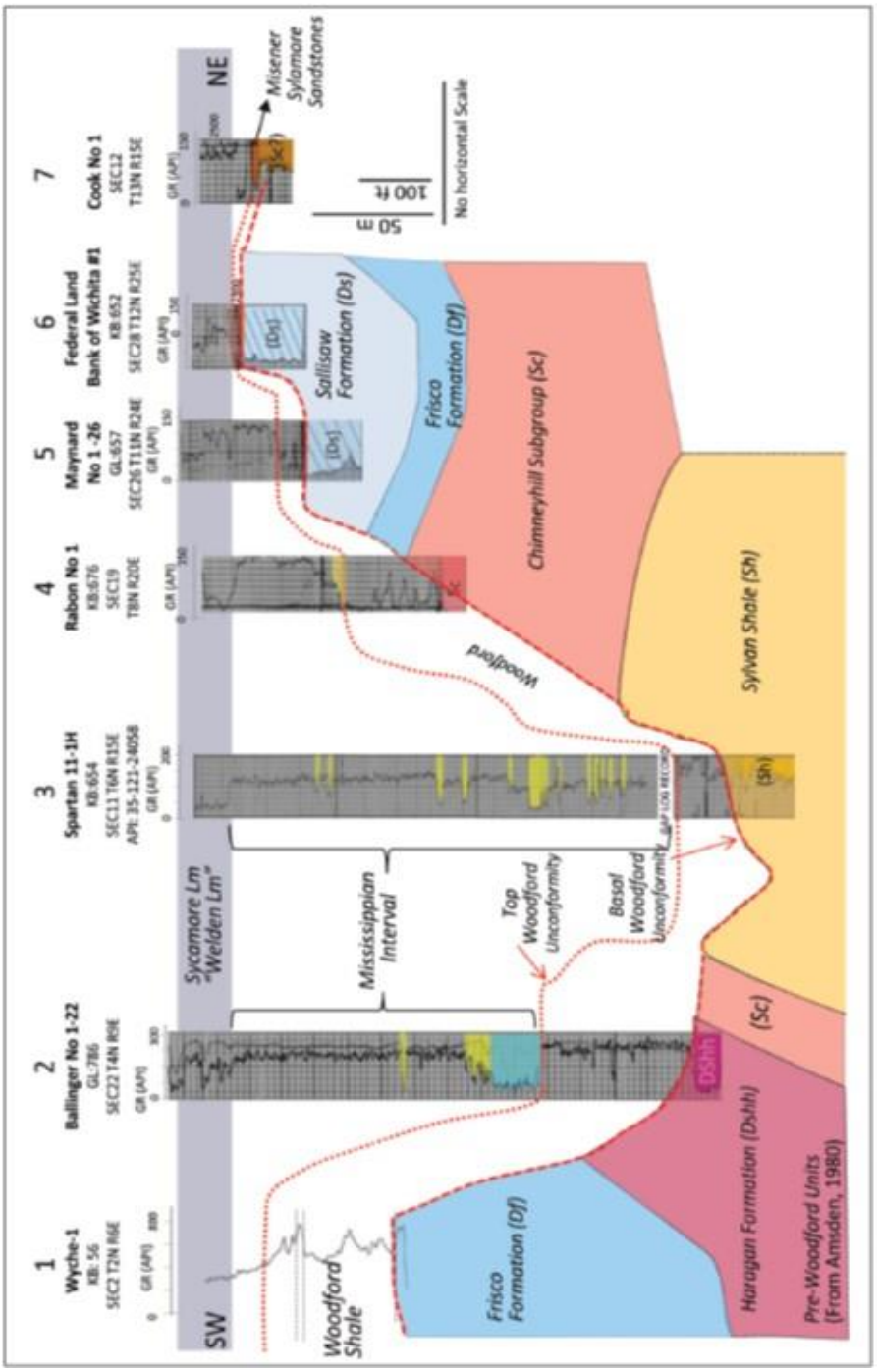

Figure 1.4. Well correlation in the Arkoma Basin. In general, the Woodford Shale is thicker to the southwest in the Arkoma Basin, but this trend is interrupted in the center of the basin where the Hunton Group is not present along some narrow corridors. The Hunton Group erosion appears to be related to thicker overlying Mississippian intervals. See Figure 1.3a for location of wells.

Furthermore, the liquids-rich corridor associated with the Woodford Shale in the Arkoma Basin seems to be interrupted where the Woodford is thinner or apparently absent (Figure 1.2), and the underlying Sylvan shale or the Woodford is in contact with an overlying thicker, coarser-grained Mississippian succession (Figure 1.4). The proximity with the Woodford Shale makes these Mississippian units highly prospective in the Arkoma Basin. Unfortunately, their distribution, composition and geomechanical properties have not been clearly determined and their reservoir potential has been overlooked.

3. Conclusions

In summary, the pre-Woodford Shale sub-crop maps presented by Amsden (1975, 1980) may provide a helpful guide for recognizing "sweet spots" corridors associated with the accumulation of Late Devonian - Early Mississippian rocks. The distribution of these units could have been controlled by the pre-Woodford topography and the competency of underlying units (Figures 1a, 1b). Synclinal structures cored by the Hunton Group and carbonate deposits could have been more resistant to erosion, whereas anticlinal structures cored by intervals such as the Sylvan Shale were more easily eroded and created narrow corridors where Early Mississippian coarse-grained sediments preferentially accumulated.

4. References

Althoff, C.D., 2012, Characterization of depositional megacycles in the Woodford Trough of central Oklahoma: Master's thesis, University of Oklahoma, Norman, Oklahoma, 101p.

Amsden, T.W., 1960, Hunton stratigraphy, part 6 of Stratigraphy and paleontology of the Hunton Group in the Arbuckle Mountain region: Oklahoma Geological Survey Bulletin 84, 311p.

Amsden, T.W., and G. Klapper, 1972, Misener sandstone (Middle-Upper Devonian), north-central Oklahoma: American Association of Petroleum Geologists Bulletin, v. 56, p. 2323-2334.

Amsden, T.W., 1975, Hunton Group (Late Ordovician, Silurian, and Early Devonian) in the Anadarko Basin of Oklahoma: Oklahoma Geological Survey Bulletin 121, 213p.

Amsden, T.W., 1980, Hunton Group (Late Ordovician, Silurian, and Early Devonian) in the Arkoma Basin of Oklahoma: Oklahoma Geological Survey Bulletin 129, 136p.

Andrews, R.D., 2009, Production decline curves and payout thresholds of horizontal Woodford well in the Arkoma Basin, Oklahoma: Shale Shake, v. 60, p. 103-112.

Brown, D., 2014, Oklahoma plays offer untapped potential: American Association of Petroleum Geologists Explorer, v. 35, no. 3, p. 8-10. (http://www.aapg.org/publications/news/explorer/2014/03mar#sthash.ONkmAPUG.dpuf)

Comer, J.B., 1992, Organic Geochemistry and Paleogeography of Upper Devonian Formations in Oklahoma and Northwestern Arkansas, in K.S. Johnson, and B.J. Cardott, eds., Source Rocks in the Southern Midcontinent, 1990 Symposium: OGS Circular, v. 93, p. 70-93.

Cardott, B.J., 2008, Overview of Woodford Gas-Shale Play of Oklahoma, U.S.A, 5 slides (Abstract-AAPG 2008, http://www.ogs.ou.edu/pdf/AAPG08woodford.pdf).

Cardott, B.J., 2009, Woodford gas-shale plays of Oklahoma: Louisiana Oil and Gas Symposium presentation (Generalized structure map of Woodford Shale, eastern Oklahoma, by R. Vance Hall 2006; http://www.ogs.ou.edu/fossilfuels/pdf/LAoilgas2009.pdf).

Cardott, B.J., 2010, Application of organic petrology to shale oil and gas potential of the Woodford Shale, Oklahoma, USA: TSOP Annual Meeting presentation, 50 slides (Vitrinite reflectance of Woodford Shale in southern Oklahoma on Woodford Shale structure map; http://www.ogs.ou.edu/fossilfuels/pdf/2011TSOPOrganicPetGS.pdf)

Cardott, B.J., 2012, Thermal maturity of Woodford Shale gas and oil plays, Oklahoma, USA: Journal of Coal Geology, v. 103, p. 109-119.

Curtis, M.E., B.J. Cardott, C.H. Sondergeld, and C.S. Rai, 2012, Development of organic porosity in the Woodford Shale with increasing thermal maturity: International Journal of Coal Geology, v. 103, p. 26-31.

EIA, 2012, http://www.eia.gov/oil_gas/rpd/shaleusa6.pdf.

Hasbrook, S., 2015, Geologic characterization of the Woodford Shale across the Arbuckle Uplift counties, south central Oklahoma: Norman, Oklahoma. [M.S. thesis], University of Oklahoma. 103 p.

Infante-Paez, L., L.-F. Cardona, B. McCullough, and R. Slatt, 2017, Seismic analysis of paleotopography and stratigraphic controls on total organic carbon: Rich sweet spot distribution in the Woodford Shale, Oklahoma, USA: Interpretation, v. 5, no. 1, p. T33-T47.

McCullough, B. J., 2014, Sequence Stratigraphic framework and characterization of the Woodford Shale on the southern Cherokee Platform of Central Oklahoma. [M.S. Thesis], University of Oklahoma. 212 p.

Molinares, C. E., 2013, Stratigraphy and palynomorphs composition of the Woodford Shale in the Wyche Farm shale pit, Pontotoc County, Oklahoma: Master's thesis, University of Oklahoma, Norman, Oklahoma, 89p.

Slatt, R. M., and N.R. O'Brien, 2011, Pore types in the Barnett and Woodford gas shales: Contribution to understanding gas storage and migration pathways in fine-grained rocks: American Associaiton of Petroleum Geologists Bulletin, v.95, p. 2017-2030.

Slatt, R. M., N. Buckner, Y. Abousleiman, R. Sierra, P. Philp, A. Miceli-Romero, R. Portas, N.O'Brien, M. Tran, R. Davis, and T. Wawrzyniec, 2012, Outcrop/behind outcrop (quarry), multiscale characterization of the Woodford gas shale, Oklahoma, in J. Breyer, ed., Shale Reservoirs – Giant Resources for the 21st Century: American Association of Petroleum Geologists Memoir 97, p. 382-402.

Torres, E.J., R.M. Slatt, K.J. Marfurt, L.E. Infante, and L.A. Castillo, 2017, Identification of potential lacustrine stratigraphic intervals in the Woodford Shale, Oklahoma, using multi-attribute 3-D seismic displays and a supervised neural network: Unconventional Resources Technology Conference, URTeC 2692737, 13 p.

Chapter 2: The effect of anisotropy (lamination/bedding) on shale brittleness in the Woodford Shale Unconventional deposits, Oklahoma.

Contributing Authors:

C. E. Molinares-Blanco[1, 2], R. Sierra[2] and R. M. Slatt[1]

Authors Affiliation:

[1] Institute of Reservoir Characterization, School of Geosciences, the University of Oklahoma. Norman, Oklahoma, U.S.A.

[2] Oxy - Bogota, Colombia.

Presented at SEG Annual Convention, Technical Program Expanded Abstracts 2016
https://library.seg.org/doi/10.1190/segam2016-13868486.1

Key Points:

• The Woodford Shale like many other unconventional reservoir rocks is evidently anisotropic or classed as vertical transverse isotropy (VTI). But, VTI (lamination/bedding) is not routinely included when defining intervals for hydraulic fracturing.

• Thomsen's coefficients ε and γ obtained from Ultra Pulse Velocities analysis were used to quantify anisotropy and to explore their potential effects on rock brittleness using Tensile Strength (T) and Fracture Toughness (K_{ic}) core analysis.

• More laminae at middle Woodford intervals create planes of weakness that assist in reducing the effective minimum horizontal principal stress during hydraulic fracturing.

Abstract

The Woodford Shale as other unconventional shale reservoirs is evidently anisotropic. However, vertical transverse anisotropy (lamination/bedding) is not routinely included when defining intervals for hydraulic fracturing. Thomsen's coefficients Epsilon (ε) and Gamma (γ), obtained from Ultra Pulse Velocities (UPV) analysis were used to quantify anisotropy and to explore their effect on rock brittleness. The intervals with more laminae are characterized by higher ε and γ coefficients, and by less Tensile Strength (T) and Fracture Toughness (K_{ic}). Formation micro-resistivity logs and thin sections help to support the idea that the differences in acoustic anisotropy between the upper Woodford Shale and the middle Woodford shale samples are due to lamination/bedding. This work illustrates that neglecting anisotropy in unconventional reservoirs may lead to an incorrect estimate of the minimum horizontal stress and that more laminae at brittle intervals may create planes of weakness that assist in reducing the effective minimum horizontal stress.

1. Introduction

The Woodford Shale (WDS) is one of the most important unconventional shale resources in the USA and an excellent hydrocarbon source rock with high TOC (total organic carbon) values ranging from 3.47 to 16.90 wt.% with mainly Type II kerogen (Miceli-Romero and Philp, 2012). The WDS is also brittle due to biogenic quartz rich siliceous and cherty intervals composed of silicified *Tasmanites* and quartz derived from radiolarian and sponge spicules (Kirkland et al., 1992). The WDS has been one of the most competitive lower 48 unconventional play areas in term of persistent rig count, possibly due to its oil-rich production and competitive pre-Tax rate of return (ROR%). Oil and gas companies have significantly reduced operational costs and they are more efficient in terms of drilling and completion times. However, one of the most common optimization problems that companies are facing is to select the best intervals for setting ("landing") their horizontal wells, because more than one brittle interval may be characterized before drilling by similar geomechanical rock properties, such as the Young's modulus (E) and the Poisson ratio (υ) calculated from well logs (Fig. 2.1).

Brittle rock intervals based only on geomechanic (dynamic) properties calculated from well logs and mineralogic analysis from cores or logs may respond differently to hydraulic fracturing because that approach habitually ignores the rock anisotropy on defining rock brittleness (Sayers et al., 2015). In fact, most of the unconventional reservoirs may be described as Vertical Transverse Isotropic (VTI) under the absence of significant vertical discontinuities (i.e. fractures, faults, cracks, etc). VTI implies that shale rocks are isotropic within a plane but exhibit different properties perpendicular to this plane (Sondergeld and Rai 2011).

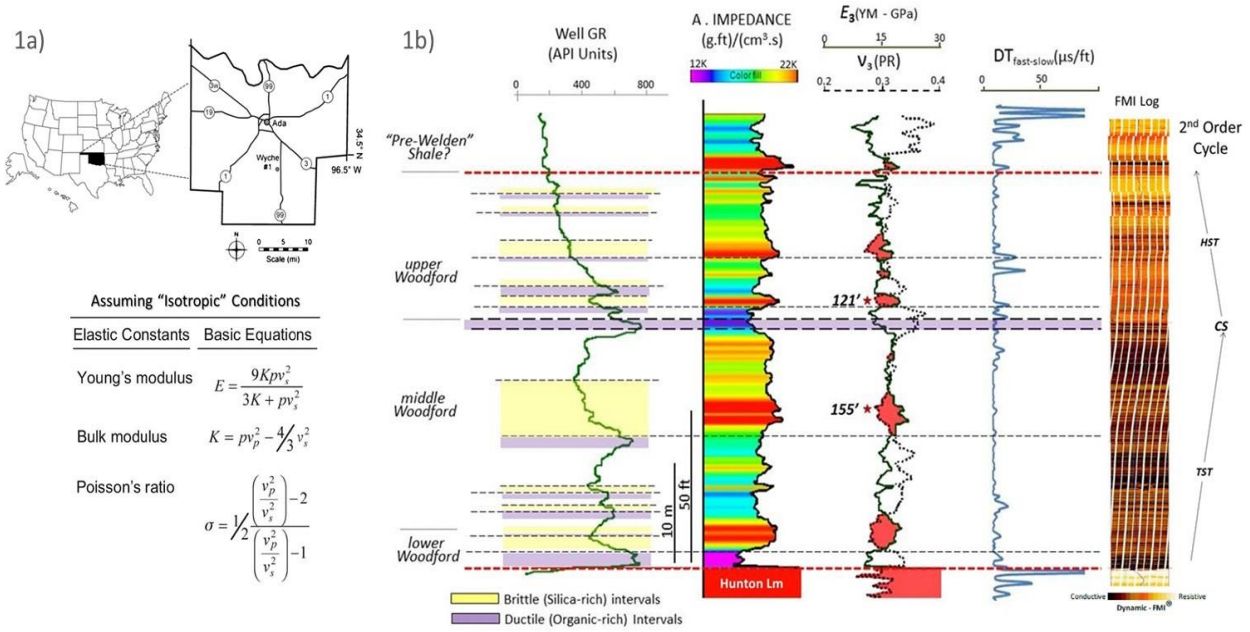

Fig 2.1a) The Wyche-1 core well was a research well drilled, cored and logged about 100ft. behind an active quarry in the Wyche shale pit, Pontotoc County, Oklahoma. **b)** The Wyche-1 core well Gamma Ray (GR) quartz-rich brittle intervals (yellow areas) and organic-rich ductile intervals (purple areas) compared with the Acoustic (A) Impedance, Young's modulus (E3) and the Poisson's ratio (v3) calculated from sonic and density well logs. These calculations assumed isotropic conditions. The Woodford brittle intervals are characterized by high acoustic impedances and the highest E and the lowest v, define areas of intersection crossover. The differences between fast and slow velocities (DT fast-slow track) are indicating a marked horizontal anisotropy for the Hunton and Pre-Welden Shale intervals. Micro-resistivity well (FMI®) log shows almost horizontal bedding and the absence of fractures. Red Stars highlight two samples located at 121 feet and 155 feet. (After Molinares-Blanco, 2013).

The anisotropy in organic-rich shale reservoir rocks is observed from different scales (Fig. 2.2): The finest vertical isotropy is associated with plate shaped clay particles, typically oriented parallel to each other and observed in scanning electron microscope (SEM) captures (Sayers, 2005; Slatt and O'Brien, 2011). The VTI is also observed in thin sections and at an even higher scale related to bedding or layering on Woodford Shale outcrops (e.g. Slatt et al., 2012). The

anisotropy may be quantified by the number of individual laminae (<1 cm thick) and/or beds (>1 cm thick). But it is a really complicated and subjective exercise that involves some bias and may be limited by tools resolution when borehole logs are involved. Thomsen's coefficients Epsilon (ε) and Gamma (γ) (Thomsen, 1986,) are related to the differences of the P- and S- wave velocities parallel and perpendicular to lamination/bedding and are proposed here as a proxy for determining anisotropy (lamination/bedding). P- and S- acoustic waves propagate faster in a direction parallel to the anisotropy plane but, propagate slower and as a function of the anisotropy, in a direction perpendicular to the anisotropy planes (e.g. Vernik and Landis, 1996; Wang 2002).

Tensile Strength (*T*) is the maximum stress or energy that a material can withhold while being stretched or pulled before breaking. Brazilian Test is a lab test for quantifying the tensile strength of rocks and is expressed in stress units (Pa or N/m^2). Fracture Toughness (K_{ic}) is a property which describes the ability of a material containing a crack to resist fracture aperture propagation. *T* is one of the most important properties for well and hydraulic fracturing design applications and is defined as the energy required to grow a thin crack expressed in MPa $m^{1/2}$ or MN/ $m^{1/2}$. The subscript $_{ic}$ after the K letter means crack opening under a normal tensile stress perpendicular to the crack, since the material can also be shear (mode ii) or tear (mode iii) stress modeled (Scholz, 2002). Brittle compositional (Bi) index is another common measurement to estimate rock brittleness (e.g. Jarvie et al., 2007; Wang and Gale, 2009). However, unconventional reservoir rocks with similar mineralogical composition and characterized by the same values of Bi may display different values of Young modulus (*E*) and Poisson ratio (υ) (Wang and Gale, 2009). Anisotropy (lamination/bedding) may be associated with the fact that rocks with

the same Bi mineralogical composition, but different values of E and υ may respond completely different under hydraulic stimulation (Herwanger et al., 2015).

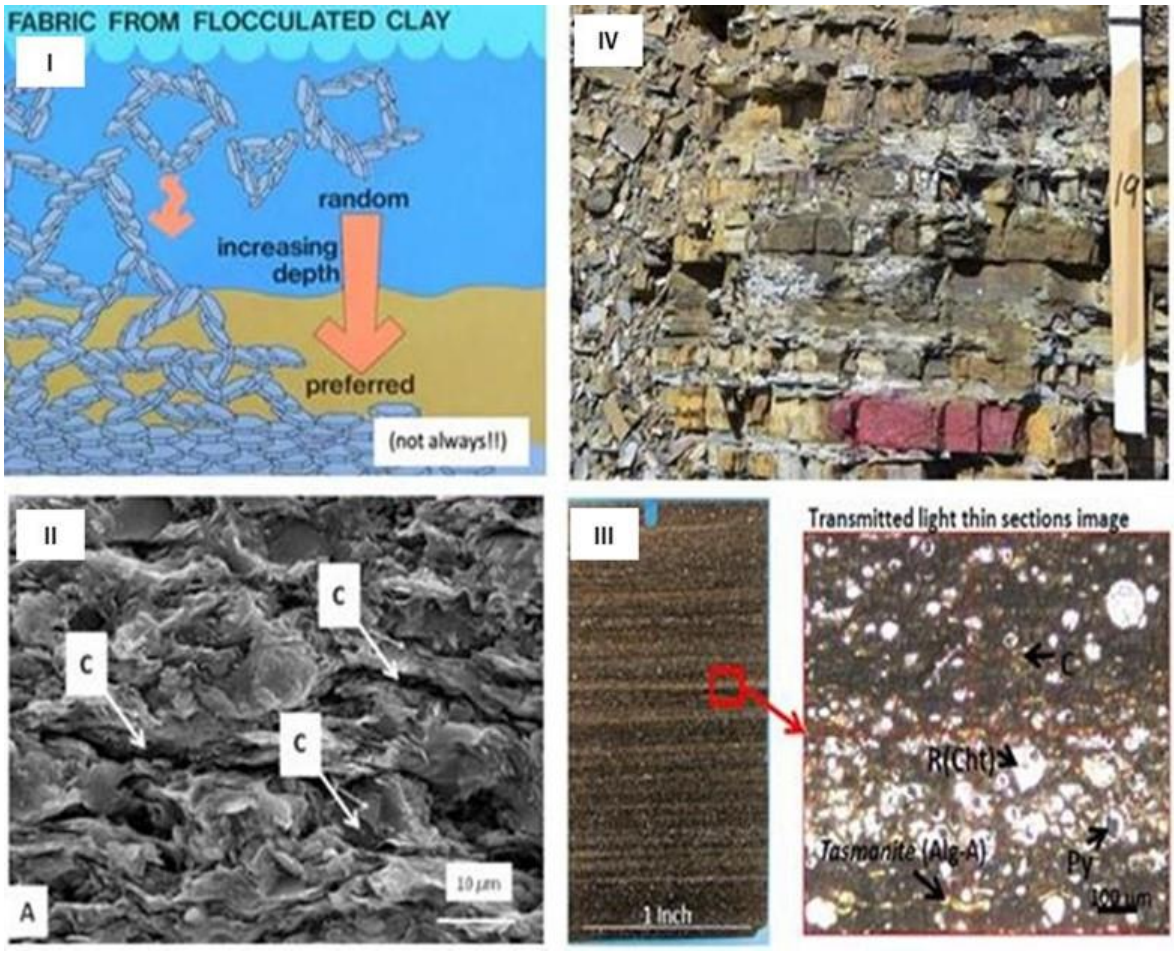

Fig 2.2. The Vertical Transverse Isotropy can be generated from nanno- to meso- scales in organic-rich, self-storage unconventional deposits: I) The finest intrinsic anisotropy is due to the constituent plate-shaped clay particles, normally oriented parallel to each other (Sayers, 2005; Slatt and O'Brien, 2011); the transverse isotropy associated with the small-scale lamination is commonly observed in (II) SEM, where letter C represents micro-porosity channels. (III) lamination in Woodford Shale thin sections showing radiolarian (R) chert particles, Tasmanites (Alg-A), Pyrite (Py) and organic stringers (c). (IV) in the horizontal bedding or layering, typically perceived at outcrop scale (after, Slatt and Abousleiman, 2011).

This work has as objective to compare the K_{ic} and T in some Woodford shale brittle intervals associated with organic and quartz rich clay deposits, characterized by significant differences on lamination/layering (anisotropy) and described previously as Highstand System Tract (Lower/Middle Woodford Shale) and Transgressive System Tract (Upper Woodford Shale) deposits (Slatt et al., 2012). The goal is to support the idea that in brittle mudstone intervals more laminae in the middle Woodford might assist in reducing the effective minimum horizontal principal stress (Slatt and Abousleiman, 2011). This is because under classic Griffth's crack theory, laminae rather than being physio-chemically bonded are geomechanical discontinuities, that can act as planes of weakness or flaws during hydraulic fracturing.

2. Materials and Methods

The analysis was run on core samples from a behind outcrop well core, drilled in the Wyche shale pit, Pontotoc County, Oklahoma (Portas, 2009; Molinares-Blanco, 2013) A complete set of well logs are available and detailed lithofacies descriptions and reservoir properties have been reported in some previous publications (e.g. Abousleiman et al., 2007; Slatt et al., 2012; Miceli-Romero and Philp, 2012; Molinares-Blanco, 2013). The Woodford Shale in this core is approximately 120 feet (~40 m) long and delimited at the top by some organic-poor shale units named "pre-Welden" shale and overlies mainly Hunton Group's carbonate rocks (Fig. 2.1). The total core was described and stored at the Reservoir Characterization Institute (RCI) of the University of Oklahoma. Some core pieces were immersed and preserved in mineral oil PG1 at the well site for later geomechanical studies (Abousleiman et al., 2007; 2009; Sierra et al., 2010).

The VTI rock modeling incorporates the Young's modulus (E), Poisson's ratio (υ) and the Shear modulus (μ) in directions parallel (subscripts 1) and perpendicular (subscripts 3) to the anisotropy planes (Fig. 2.3). The five independent elastic constants (C_{11}, $C_{12} = C_{13}$, C_{33}, C_{44}, C_{66}) needed to fully describe the stiffness in a VTI modeling were obtained by measuring P- and S-wave velocities from core plugs parallel, perpendicular, and ± 45° to the laminae plane. The equations which relate the elastic properties parallel and perpendicular to the anisotropy plane and the five stiffness coefficients are expressed as follow:

$$E_1 = \frac{(C_{11} - C_{12})(C_{11}C_{33} - 2C_{13}^2 + C_{12}C_{33})}{C_{11}C_{33} - C_{13}^2}, \quad (1)$$

$$E_3 = C_{33} - 2\frac{C_{13}^2}{C_{11} + C_{12}}, \quad (2)$$

$$\upsilon_1 = \frac{(C_{33}C_{12} - C_{13}^2)}{C_{11}C_{33} - C_{13}^2}, \quad (3)$$

$$\upsilon_3 = \frac{C_{13}}{C_{11} + C_{12}}, \quad (4)$$

$$\mu_1 = C_{66} = \frac{E}{2(1+\nu)}, \quad \text{and} \quad (5)$$

$$\mu_3 = C_{44}. \quad (6)$$

Thomsen's anisotropy coefficients ε and γ were calculated based on the elastic constants obtained from UPV core analysis. Epsilon coefficient (ε) illustrates the fractional difference between horizontal and vertical P-waves, while Gamma coefficient (γ) measures the same characteristic but for S-waves:

$$\varepsilon = \frac{C_{11} - C_{33}}{2C_{33}} = \frac{V_p^2(90°) - V_p^2(0°)}{2V_p^2(0°)}, \text{ and} \quad (7)$$

$$\gamma = \frac{C_{66} - C_{44}}{2C_{44}} = \frac{V_s^2(90°) - V_s^2(0°)}{2V_s^2(0°)}. \quad (8)$$

Brazilian Test was completed for measuring the Tensile Strength (*T*). *T* from five core samples were calculated as $T = 2P/(\pi DL)$. Where P corresponds with the applied load, D the diameter of the sample (D=2R) and L the length of the sample (see Sierra et al., 2010). The Chevron Notch Semicircular Specimen (CNSCB) test was chosen for estimating the Fracture Toughness of the rocks. The notch was cut at 90 degrees with respect to the base of the specimen for mode-I fracture modeling. The compositional Brittleness indexes (Bi) proposed before by Jarvie et al., (2007) and modified later by Wang and Gale (2009) were calculated based on X-ray diffraction analysis (XRD). A detailed description and the original results for the geomechanical analysis here analyzed were reported before by Abousleiman et al., (2007; 2009) and Sierra et al., (2010).

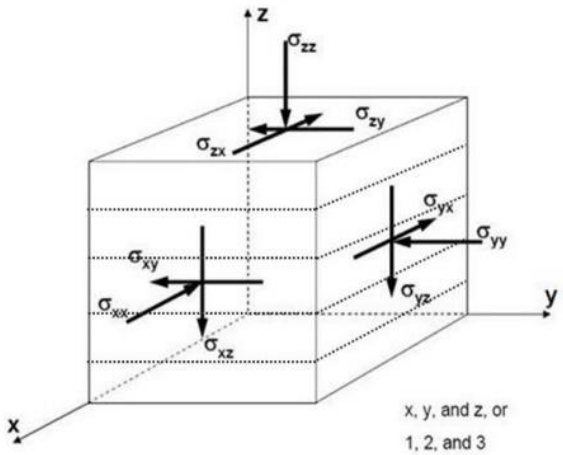

$$\begin{bmatrix} \varepsilon_x \\ \varepsilon_y \\ \varepsilon_z \\ \gamma_{xz} \\ \gamma_{yz} \\ \gamma_{xy} \end{bmatrix} = \begin{bmatrix} 1/E & -\nu/E & -\nu'/E' & 0 & 0 & 0 \\ -\nu/E & 1/E & -\nu'/E' & 0 & 0 & 0 \\ -\nu'/E' & -\nu'/E' & 1/E' & 0 & 0 & 0 \\ 0 & 0 & 0 & \mu' & 0 & 0 \\ 0 & 0 & 0 & 0 & \mu' & 0 \\ 0 & 0 & 0 & 0 & 0 & \mu \end{bmatrix} \begin{bmatrix} \sigma_x \\ \sigma_y \\ \sigma_z \\ \tau_{xz} \\ \tau_{yz} \\ \tau_{xy} \end{bmatrix}$$

Fig 2.3. The elastic compliance matrix for the Vertical Transverse Isotropy (VTI) cases expressed in terms of the Young's modulus (*E*), Poisson's ratio (*v*) and the Shear modulus (μ), along the symmetry axis (*E*, *v* and μ) and perpendicular (*E', v'* and μ').

3. Results

Table 2.1 and figure 2.4 display the different relationships and cross-plots between the geomechanical properties *T* and *Kic* versus the Bi and the Thomsen's ε and γ anisotropy coefficients for the five Woodford shale core samples. First, it is highlighted that the shale composition based on XRD analysis does not explain completely the rock brittleness because samples with similar Brittleness Index (Bi), one from the upper Woodford (111 ft) and the other from the middle Woodford (136 ft), display different values of K_{ic} and *T* (Fig. 2.4). That means that rocks with similar composition may crack or propagates fractures at different values of

applied load. This confirmed from the lab tests the reasonable assumption that Woodford Shale samples are easier to break parallel (II) than perpendicular (T) to the lamination.

Although the number of samples is limited, it is observed that the middle Woodford Shale samples exhibit more anisotropy characterized by higher ε and γ Thomsen's coefficients, while the samples from the upper Woodford interval are marked by less anisotropy, because of lower values of ε and γ coefficients (Table 2.1). The dynamic-FMI® micro-resistivity well log (Fig 2.1) confirms the idea that the upper Woodford Shale is characterized by less anisotropy (laminations), in comparison with the middle Woodford Shale interval, which is also supported by core and thin section inspection (Fig. 2.5).

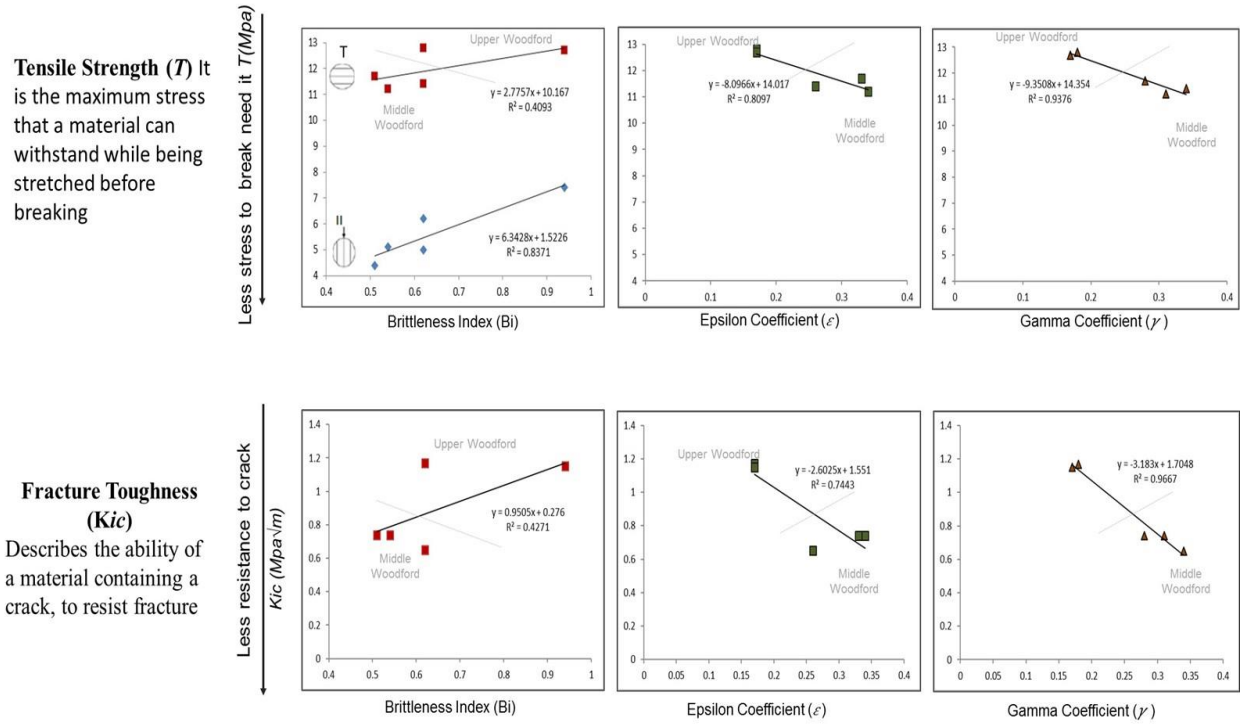

Fig 2.4. Cross plot between the Tensile Strength (*T*) and Fracture Toughness (K*ic*) versus compositional brittle index (Bi), Epsilon (ε) and Gamma (γ) anisotropy coefficients calculated

from UPV analysis for the upper and middle Woodford samples. The Woodford Shale core samples are easier to break parallel (II) than perpendicular (T) to the lamination. Notice that the correlation is better for the Epsilon (ε) and Gamma (γ) cross-plots and higher anisotropy is associated with lower values of Tensile Strength (*T*) and Fracture Toughness (K*ic*).

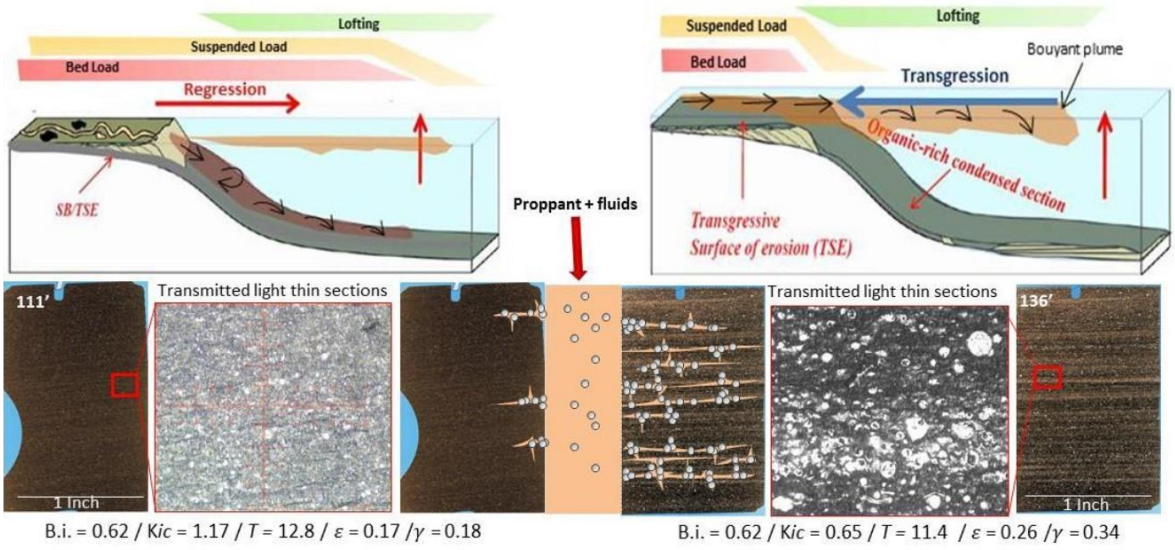

Fig 2.5. VTI differences between the Upper Woodford (HST - right) and middle Woodford (TST - left) shale deposits. The sample with fewer laminae (left figure) corresponds with HST upper Woodford interval (111 ft) and the interval of more laminae with the TST middle Woodford (136 ft). This scheme also illustrates the hypothetical response during hydraulic stimulation that will depend on the local stress field, rock, and fluid properties. However, laminae can act as weakness planes to propagate or create induced hydraulic fractures. Figures also illustrating the changes between lofting, suspended load and bed load transport mechanisms after Zavala et al., (2011) and Slatt et al., (2012).

	Depth (ft)	Ten Strength T (Mpa)	Ten Strength ll (Mpa)	K*ic*	ε	γ	Bi
Upper Woodford	111	12.8	6.2	1.17	0.17	0.18	0.62
	121	12.7	7.4	1.15	0.17	0.17	0.94
middle Woodford	136	11.4	5	0.65	0.26	0.34	0.62
	145	11.2	5.1	0.74	0.34	0.31	0.54
	166	11.7	4.4	0.74	0.33	0.28	0.51

Table 2.1 Results of the anisotropy Thomsen's coefficient Epsilon (ε) and Gamma (γ) indexes calculated from UPV's analysis, Brittle compositional Index (Bi) from XRD analysis, Tensile Strength (*T*) and Fracture Toughness (K*ic*) tests from core lab test of Woodford shale samples (Data from Sierra et al., 2010).

	Depth (ft)	E_{11}	E_{33}	V_{11}	V_{33}	G_{11}	G_{33}	α_{11}	α_{33}	K_{VTI}	K_{ISO}	$K_{ISO} - K_{VTI}$
upper Woodford	111	20.3	15.8	0.157	0.2	7.8	5.7	0.67	0.74	0.30	0.19	-0.12
	121	18.8	13.8	0.159	0.25	7.5	5.5	0.67	0.73	0.41	0.19	-0.22
middle Woodford	136	22.2	13.5	0.139	0.26	9.3	5.5	0.62	0.7	0.50	0.16	-0.34
	145	19.6	10.4	0.121	0.25	8.4	5	0.67	0.75	0.54	0.14	-0.40
	166	19.5	10.9	0.133	0.26	8.8	5.3	0.7	0.76	0.54	0.15	-0.38

Table 2.2. Poroelasticity modulus, KVTI and KISO effective stress coefficients calculated from UPV's analysis.

3.1 Effects of anisotropy (VTI) on the rock brittleness

According to the poro-elasticity theory (Biot, 1941) and assuming that shales are isotropic bodies, the minimum horizontal stress (σ_{hmin}) required to create or to propagate a fracture in a normal stress domain might be defined as:

$$\sigma_{hmin} = \alpha p + K_{\mathrm{ISO}}\,(\sigma_v - p);\;\; K_{\mathrm{ISO}} = \frac{v}{1-v} = \frac{\sigma_{min}}{\sigma_v}$$

Where α is the Biot's poro-elastic coefficient, that is related to the solid grain compressibility and to the bulk rock compressibility and generally is assumed equal to 1 (Hubbert and Rubey, 1959); p is the pore pressure; σ_v is the vertical stress, v is the Poisson' ratio and K_o is the effective stress coefficient originally established by Mathew and Kelly (1967) as the ratio between the minimum effective in-situ stress and the overburden stress. K_o might be empirically calculated from the Poisson's ratio values or derived from formation evaluation leak-off (LOT) test and locality established depending on stress field regions.

In compacted shales and when α=1, the mineral skeleton of shales is inferred to have a compressibility equal (or negligible) compared to the bulk rock compressibility. However, there are geological evidences, such as horizontal stress distribution profiles, that support the idea that Biot's coefficient values are lower than 1 (see Burrus et al., 1998 for a detailed discussion) and even limited in number, there are direct lab measurements which also confirm that α is reasonably less than one and decreasing in value with increment of the pressure applied (e.g. Abousleiman et al., 2007). In addition to the fact that α values are probably lesser than one, maybe σ_{hmin} is not reduced in shales because they are anisotropic and to avoid shale anisotropy

may lead to an incorrect estimate of minimum horizontal stress (Sayers, 2015). For a VTI medium, the minimum horizontal stress is better defined as:

$$\sigma_{hmin} = \alpha_h p + K_{VTI}\,(\sigma_v - \alpha_v p);\;\; K_{VTI} = \frac{C_{13}}{C_{33}} = \frac{E_{11}\,v_{33}}{E_{33}\,(1 - v_{11})}$$

Where, α_h and α_v are the Biot's poro-elastic coefficients horizontally and vertically oriented to respect the anisotropy planes; E_{11} and E_{33} are the horizontal and vertical Young's modulus; and υ_{33} and υ_{11} are the Poisson's ratios that quantify the horizontal strain resulting from vertical and horizontal stresses (Sayers et al., 2010). Assuming isotropic conditions, the upper Woodford samples are characterized by higher values of effective stress coefficient (K_{ISO}) in comparison with the middle Woodford Shale samples (Table 2.2). However, when the VTI (anisotropy) is incorporated into the modeling, the middle Woodford Shale samples were characterized by a higher effective stress coefficient (K_{VTI}), in comparison with the upper Woodford Shale samples (Table 2.2). A higher value of effective stress coefficient (K_o) will be associated with a higher minimum horizontal stress value and rocks are more brittle (easy to break or to propagate a fracture) when the minimum horizontal stress is lower. The anisotropy modeling increased the K_{VTI} values for the middle Woodford in comparison with the upper Woodford, but their behavior was more brittle during the geomechanic lab tests (Fig. 2.4). These results bring new questions about the role of Biot's poro-elastic coefficients, their changes under variable confining pressure conditions and the suitability of using poroelasticity modulus (*E* and *v*) to calculate the effective stress coefficients under isotropic and anisotropic (VTI) scenarios (Sayers, 2010).

3.2 Rock brittleness, lamination and Sequence Stratigraphy

The middle Woodford is more anisotropic than the upper Woodford and the differences in the anisotropy are related to the sedimentary process prevailing during the accumulation of these intervals. Additionally, to relate geomechanical properties to sequence stratigraphy models has practical implications for regional mapping because sequence stratigraphy subunits such as systems tracts and parasequences are commonly mappeable from 3D seismic volumes and well log correlations (Slatt and Abousleiman, 2011).

The most laterally continuous and frequent lamination associated with the Transgressive System Tract (TST) of the lower and middle Woodford may be due to a rise in base (sea) level, so, the shoreline is translated landward (i.e. transgression). Consequently, deposition may be dominated by buoyant plumes and lofting depositional processes, which could be affected by seasonal upwelling and/or iron rich wind fertilization processes that in recent times bring continental nutrients to offshore areas and create periodic algae blooms (Fig. 2.5). On the other hand, during Highstand System Tract (HST) regressive periods, the seaward movement of the shoreline creates less accommodation space on the continental shelf areas and the shoreline is displaced (i.e. progrades) seaward (Slatt et al., 2012). As a result, offshore accumulation might be affected by the transfer and accumulation of continental sediments, commonly characterized by thicker laminated or less structured bodies (Fig. 2.5), where some sedimentary features (structures), sensitive to the contemporaneous subaqueous topography and associated with small increments in traction bottom-energy current are also commonly observed (Slatt and

O’Brien, 2011). For that reason, TST organic-rich shale deposits probably tend to be more laminae/layered, than HST shale deposits.

4. Conclusions

Unconventional reservoirs can be described as Vertical Transverse Isotropic (VTI) under the absence of significant vertical discontinuities (i.e. fractures, faults, cracks, etc). To ignore that condition may lead to an incorrect estimate of the minimum horizontal stress (Shmin). Rocks more laminated are characterized by being more acoustic anisotropic in term of Thomsen's coefficients Ɛ and ɣ. More laminae at brittle intervals possibly created planes of weakness that assist in reducing the effective minimum horizontal stress and break rock easier.

This observation can be useful in unconventional reservoir characterization and reservoir optimization processes because rock intervals marked by a higher acoustic anisotropy (more laminae/bedding) could be related to a lower minimum horizontal stress. However, the K_{VTI} values calculated for the middle Woodford Shale samples were higher, in comparison with the upper Woodford samples. A lower K_{VTI} value would produce a reduction in the minimum effective horizontal stress, but it also depends on Biot's poro-elastic coefficients, pore pressure and the local stress field. Thomsen's ε and γ acoustic anisotropic coefficients proposed here as proxies to estimate the effect of anisotropy on rock brittleness have an advantage compared to other methods because these coefficients may be applicable under a wide variety of observation scales (P and S-wave frequencies) such as those recorded by 3D seismic, borehole seismic, micro seismicity, sonic well logs and UPV's core analysis.

5. References

Abousleiman, Y.N., M.H. Tran, S.K. Hoang, 2007. Geomechanics field and lab characterization of Woodford shale: the next gas play. SPE paper 110120. SPE Annual Technical Conference, Anaheim, Nov. 11-14, 2007.

Abousleiman, Y.N., M.H. Tran, S.K. Hoang, 2009. GeoMechanics Field Characterization of the Two Prolific U.S. Mid-West Gas Plays with Advanced Wire-Line Logging Tools. SPE paper 124428. SPE Annual Technical Conference, New Orleans, Oct. 4-7, 2009.

Biot, M. A., 1941. General theory of three-dimensional consolidation: Journal of Applied Physics, 12, p. 155–164.

Burrus, J., 1998. Overpressures models for clastic rocks: their relation to hydrocarbon expulsion: a critical reevaluation. In: Law, B.E., G.F. Ulmishek, and V.I. Slavin eds., Abnormal pressures in hydrocarbon environments: AAPG Memoir 70, p. 35–63.

Herwanger, J. V., A. D., Botrill, and Mildren, S.D., 2015. Uses and Abuses of the Brittleness Index with Applications to Hydraulic Stimulation. Unconventional Resources Technology Conference (URTeC paper: 2172545), San Antonio, Texas, USA, 20-22 July 2015.

Hubbert, M. King, and Rubey, W. W., 1959, Role of Fluid Pressure. In: Mechanics of overthrust Faulting, Part 1 Geological Society of America GSA Bulletin, February 1959, p. 70.

Jarvie, D. M., Hill, R. J., Ruble, T. E., and Pollastro, R. M., 2007. Unconventional shale-gas systems: the Mississippian Barnett Shale of North-Central Texas as one model for thermogenic shale-gas assessment: AAPG Bulletin, v. 91, p. 475 – 499.

Kirkland, D. W., R. E. Denison, D. M. Summers, and J. R. Gormly, 1992, Geology and organic geochemistry of the Woodford Shale in the Criner Hills and western Arbuckle Mountains, Oklahoma, in K. S. Johnson and B. J. Cardott, eds., Source rocks in the southern mid-continent: 1990 Symposium: OGS Circular 9, p. 38–69.

Matthews, W.R., Kelly, J., 1967. How to predict formation pressure and fracture gradient. Oil Gas J. 780 65, p. 92-106.

Miceli-Romero, A., and R. P. Philp, 2012, Organic geochemistry of the Woodford Shale, southeastern Oklahoma: How variable can shales be?: AAPG Bulletin, 96, p. 493–517.

Molinares-Blanco, C.E., 2013, Stratigraphy and palynomorphs composition of the WoodfordShale in the Wyche Farm Shale Pit, Pontotoc County, Oklahoma: [M.S. Thesis], University of Oklahoma, 90 p.

Portas-Arroyal, R.M., 2009, Characterization and origin of fracture patterns in the Woodford Shale in southeastern Oklahoma for application to exploration and development. [M.S. Thesis], University of Oklahoma. 110 p.

Sayers, C. M., 2005, Seismic anisotropy of shales: Geophysical Prospecting, v. 53, p. 667-676.

Sayers, C. M., 2010, Geophysics under stress: Geomechanical applications of seismic and borehole acoustic waves: SEG Distinguished Instructor Series No. 13.

Sayers, C.M., L. den Boer, S. Dasgupta, and B. Goodway, 2015, Anisotropy estimate for the Horn River Basin from sonic logs in vertical and deviated wells: The Leading Edge, 34, p. 296–306.

Scholz, C., 2002, The Mechanics of Earthquakes and Faulting, 2 ed. Cambridge: Cambridge University Press.

Sierra et al., 2010 Sierra, R., M. H. Tran, Y. N. Abousleiman, and R. M. Slatt, 2010. Woodford Shale mechanical properties and impacts of lithofacies: 44th U.S. Rock Mechanics Symposium, Salt Lake City (ARMA 10-461).

Slatt, R. M., and Y. Abousleiman, 2011. Merging sequence stratigraphy and geomechanics for unconventional gas shales: The Leading Edge, v. 30, p. 274-282.

Slatt, R. M., and N.R. O'Brien, 2011. Pore Types in the Barnett and Woodford gas shales: Contribution to understanding gas storage and migration pathways in fine-grained rocks: AAPG Bulletin, v. 95, n 12, p. 2017-2030.

Slatt, R. M., N. Buckner, Y. Abousleiman, R. Sierra, P. Philp, A. Miceli-Romero, R. Portas, N.O'Brien, M. Tran, R. Davis, and T. Wawrzyniec, 2012. Outcrop/behind outcrop (quarry), multiscale characterization of the Woodford Gas Shale, Oklahoma. In: J. Breyer, eds., Shale reservoirs—Giant resources for the 21st century: AAPG Memoir 97, p. 382-402.

Sondergeld, C.H. and C.S., Rai, 2011. Elastic anisotropy of shales. The Leading Edge, v. 30, p. 324–331.

Thomsen, L., 1986. Weak elastic anisotropy, Geophysics, v. 51, n 10, p. 1954-1966.

Vernik, L., and C., Landis, 1996. Elastic anisotropy of source rocks: Implications for hydrocarbon generation and primary migration, AAPG Bulletin, 80, p. 531–544.

Wang, F.P., and Gale, J. F. W., 2009, Screening criteria for shale-gas systems: Gulf Coast Association of Geological Societies Transactions, v. 59, p. 779-793.

Wang, Z., 2002. Seismic anisotropy in sedimentary rocks: Part 2 – Laboratory data. Geophysics 67, p. 1423–1440.

Zavala, C., M. Arcuri, H. Gamero, C. Contreras and M. D., Meglio, 2011. A genetic facies tract for the analysis of sustained hyperpycnal flow deposits. In: R. M. Slatt and C. Zavala (eds), Sediment transfer from shelf to deep water—Revisiting the delivery system, AAPG Studies in Geology 61: 31–51.

Chapter 3: The Frasnian/Famennian (F/F) transition in the Woodford Shale, South Central Oklahoma – A Multiproxy Approach

Contributing Authors:

MOLINARES BLANCO, Carlos E.[1], SLATT, Roger M.[1], KOZIK, Nevin P.[2], YOUNG, Seth A.[2], PHILP, Richard P.[1], and MICELI-ROMERO, Andrea[3]

Authors Affiliation:

1 School of Geoscience, the University of Oklahoma. Norman, Oklahoma, U.S.A.

2 Department of Earth, Ocean, and Atmospheric Sciences, Florida State University, National High Magnetic Field Laboratory, Tallahassee, FL 32306

3 Department of Geology and Geophysics, Texas A&M University, College Station, TX 77843

It was presented at the GSA South-Central Section - 52nd Annual Meeting – 2018 and it was prized as the best PhD student oral presentation.

https://gsa.confex.com/gsa/2018SC/webprogram/Paper310250.html

Abstract

The Late Devonian Frasnian/Famennian (F/F) stages transition was recorded in an organic-rich black shale interval, equivalent to the Woodford Shale and logged in the Wyche-1 near-surface research core-well, located in the Lawrence Uplift, South-central Oklahoma. The total studied stratigraphic section includes approximately 54 m (~180 ft.), from the unconformable Woodford Shale contact with Early Devonian limestones, equivalent to the Hunton Group, to the gradual upward transition with the Early Carboniferous and organic-poor, light gray colored, pre-Walden Shales. The Woodford has been subdivided into the lower, middle and upper Woodford Shale intervals and two positive $\delta^{13}C$ isotopic excursion events identified in the middle Woodford were correlative with the Upper (UK) and Lower (LK) Kellwasser global anoxic (extinction) events. Thorium/uranium (Th/U) ratios from spectral gamma-ray logs, evidenced oxic to suboxic conditions during the accumulation of the pre-Walden Shale and predominantly anoxic-bottom water conditions during the Woodford Shale deposition. Thorium/potassium (Th/K) ratios displayed clay mineralogical compositional changes, principally associated with illite contents variations, which were confirmed in powder X-ray diffraction (XRD) compositional analysis. Aluminum normalized enrichment factor (EF), contents of nickel (Ni), copper (Cu), molybdenum (Mo), uranium (U), iron (Fe), zirconium (Zr) and titanium (Ti) were obtained from X-ray fluorescence (XRF) elemental compositional analysis. Low Ni and Cu normalized EF values were associated with low marine (organic -C sink) productivity, during the accumulation of the middle Woodford and pre-Walden Shales intervals. High to moderate marine productivity was interpreted during the accumulation of the lower and middle Woodford Shale intervals, based on higher EF Ni and EF Cu concentrations. Mo and U contents and Mo/U ratios were used to

establish paleo-redox conditions. The EF Mo and EF U values were equivalent or higher than the average values reported from the modern Black Sea and Framvaren Fjord anoxic basins. In contrast, the middle Woodford was characterized by low Mo and low Mo/U ratios (~0.1x), compared with the seawater actual oceanic averages. Low Mo/U ratios were related to euxinia (anoxia + high sulfidic) and highly isolated stagnant bottom-water conditions, confirmed by the presence of C_{40} carotenoids biomarkers. High Zr/Al and Ti/Al contents characterized the upper Woodford and the end of the euxinic conditions. Higher Zr/Al and Ti/Al ratios were also related to higher terrestrial palynomorphs (spores) contents and higher Fe/Al normalized ratios and characterized by a higher ilmenite detrital mineral content, confirmed in scanning electron microscope images, coupled with an energy dispersive X-Ray analyzer (SEM-EDX). The regressive cycle identified in the upper Woodford corresponds with a sea level drop, which might coincide with the onset of the first Late Devonian glacial events reported from South America localities.

1. Introduction

The Late Devonian Frasnian/Famennian (F/F) transition is characterized by one of the most severe biological crises during Phanerozoic time recorded in both terrestrial and marine ecosystems (Raup and Sepkoski, 1982; Copper, 1986; McGhee, 1996; Walliser, 1995; Racki, 2005; Bond and Grasby, 2017). In the terrestrial realm, the Late Devonian is characterized by important evolutive plant changes, such as larger root plant systems, first seed plants, the spread of vascular plants into dry uplands, the appearance of arborescence habit (*Progymnosperms*) and possibly the first forests on earth (Algeo et al., 1995). In the marine realm, the F/F boundary was marked by a significant diversity loss, particularly in shallow/tropical seas and affected by the massive extinction of stromatoporoid and reef-building organisms (Sandberg et al., 2002; Copper 2002; Racki 2005) (Fig 3.1). The F/F extinctions were apparently more drastic on equatorial marine regions than high latitude environments (McGhee, 1996) but, the F/F localities described around the world are mainly located within the paleo-equatorial belt, with scarce reports from paleo-high latitudes and deep offshore waters (Racki, 2005). In fact, some authors describe the F/F crisis as an event associated with a significant decrease of new species origination rates, rather than a raise on extinction rates (McGhee, 1996).

The Lower (LK) and Upper Kellwasser (UK) are two anoxic/extinction events associated with the F/F boundary and named after two bituminous limestone layers described at Lower Saxony, Steinbruch Schmidt (Kellerwald), Germany (Buggisch 1991; Schindler, 1993). The LK and UK strata have been described worldwide and they are characterized by two organic rich layers and positive stable carbon excursions correlative within those layers (e.g. Buggisch, 1991; Schindler, 1993; Joachimski and Buggisch, 1993; Joachimski et al., 2001; 2002; Filipiak, 2002;

Bond et al., 2004; Saltzman, 2005; Buggisch and Joachimski 2006; Van Geldern et al., 2006; Hillbun et al., 2015). The F/F extinction triggering mechanism remains debated (e.g. Bond and Grasby, 2017), they include single or interactions between multiple-causality scenarios such as, bolide extraterrestrial impact(s) (Claeys et al., 1992; Wang, 1992; McGhee, 1996) and large igneous province volcanism (McGuee, 1996; Bond and Grasby, 2017) and factors related with plant evolution (Algeo et al., 1995; 2001). The F/F extinction events are closely related to permanent anoxic conditions and for that reason, anoxia have been proposed as the main cause for the F/F marine extinctions (Joachimski and Buggisch, 1993; Algeo et al., 1995; McGhee, 1996; Bond and Wignall, 2008). In fact, in some localities these anoxic conditions were in addition euxinic, which means a high presence of free H_2S dissolved in the oceanic water that affected deeply the marine ecosystems (Joachimski et al., 2001; Meyer and Kump, 2008).

However, anoxic conditions were apparently not well developed in shallow-water locations and therefore, it could not be responsible for the decease of shallow-water taxa, principally stromatoporoid and coral reef-builder populations (McGuee, 1996; Copper, 2002; Bond et al., 2004; Racki, 2005). Some authors consider that the most reasonable explanation for the F/F reef-builders collapse seems to be a global sea-level drop (Johnson et al., 1985; Savoy and Mountjoy 1995; Joachimski et al., 2002; Bond and Wignall, 2008), as the consequence of combined effects of cooling and decreasing atmospheric CO_2 levels (Berner and Kothavala, 2001; Rothman 2002), and that eustatic sea level drop, possibly was related to the first Late Devonian low latitude mountain glacial events (Copper 1986; Isaacson et al., 1999; Streel et al., 2000a; Soreghan et al., 2008).

The Woodford is an organic-rich black shale, Late Devonian to early Mississippian in age, and one of the most prolific oil and gas source rocks in Oklahoma, USA (Comer and Hinch, 1987; Cardott, 2012). This study documents the oceanic productivity and oxygenation changes during the accumulation of the Woodford Shale in South-central Oklahoma, using a combination of bulk organic matter stable carbon isotopes ($\delta^{13}C_{org}$), spectral natural gamma-ray logs, scanning electron microscope images coupled with an energy dispersive X-Ray analyzer (SEM-EDX), powder X-ray diffraction (XRD), X-ray fluorescence (XRF), and palynological analysis. This work includes rock samples from intervals near some localities where previous studies have identified the F/F transition based on conodonts (Over and Barrick 1990; Over, 1992a; 1992b; Over 2002) and magnetostratigraphy analysis (Crick et al., 2002; Fig 3.2).

The goals of this study include: 1) to confirm that the F/F transition is located within the middle Woodford Shale deposits, based on paleontological reports and stable isotopic analysis; 2) to identify possible anoxic (euxinic) conditions and how those anoxic intervals were related to oceanic productivity (organic C sinking flux) and 3) to analyze how the anoxic and paleo-productivity changes could have been associated with variations on weathering/river nutrient influx input, apparently controlled by global transgressive/regressive sea level cycles.

Carb
Trns
Late Devonian
Famennian
Frasnian
Middle Devonian
Givetian
Eifelian
duplicata
sulcata
praesulcata
expansa
postera
trachytera
marginifera
rhomboidea
crepida
triangularis
linguiformis
rhenana
lamieae
hassi
punctata
transitans
falsiovalis
disparilis
herm.-crist.
varcus
hemiansatus
ensensis
kockelianus
australis
costatus
partitus
Sea Level
Fall
Rise
Algeo et al., 2007
D-C
Hangenberg event
IIf
Savoy and Mountjoy 1995
IIe
Microtektites (Belgium)
Johnson et al., 1985
UK
LK
IId
IIc
IIb
IIa
If
Meteoric impacts
Alamo
Slijan
Flynn Creek
δ13C (PDB)
+1
+2
+3
rCO2 level
6
8
10
12
eolian and dust from arid areas
Increased dispersion of weathering products
Low sea level
Calcimicrobial
Renalcis, Rothpletzella, Epiphyton
Reef caps and karst
- LOWSTAND CONDITIONS -
Little dispersion of weathering products
High sea level
Coral-Stromatoporid
Patch reef builders
- HIGHSTAND CONDITIONS -
Archaeopteris
1st Seed Plants
Evieux
Hampshire
Oswayo
Baggy
South Am. Glaciation
D/C Glacial
FAD progymnosperms
2nd Cortex
Max. tree height (m)
1
10
30
1
3

Fig. 3.1. Middle to Late Devonian geological events. The UK and LK correspond with the Upper and Lower Kellwasser events. Sea level curves after Johnson et al., 1985; Mountjoy 1995 and Algeo et al., 2007. Meteoric impacts and crater compiled by McGuee, 1996 and microtektites reported by Claeys et al., 1991. CO_2 and $\delta^{13}C$ curves compiled from Saltzman, 2005; Buggisch and Joachimski 2006. CO_2 decreasing values are coincident with a greenhouse to icehouse earth transition and the first Late Devonian South American glacial events (Copper, 1986; Isaacson et al., 1999; Streel et al., 2000; Soreghan et al., 2008).

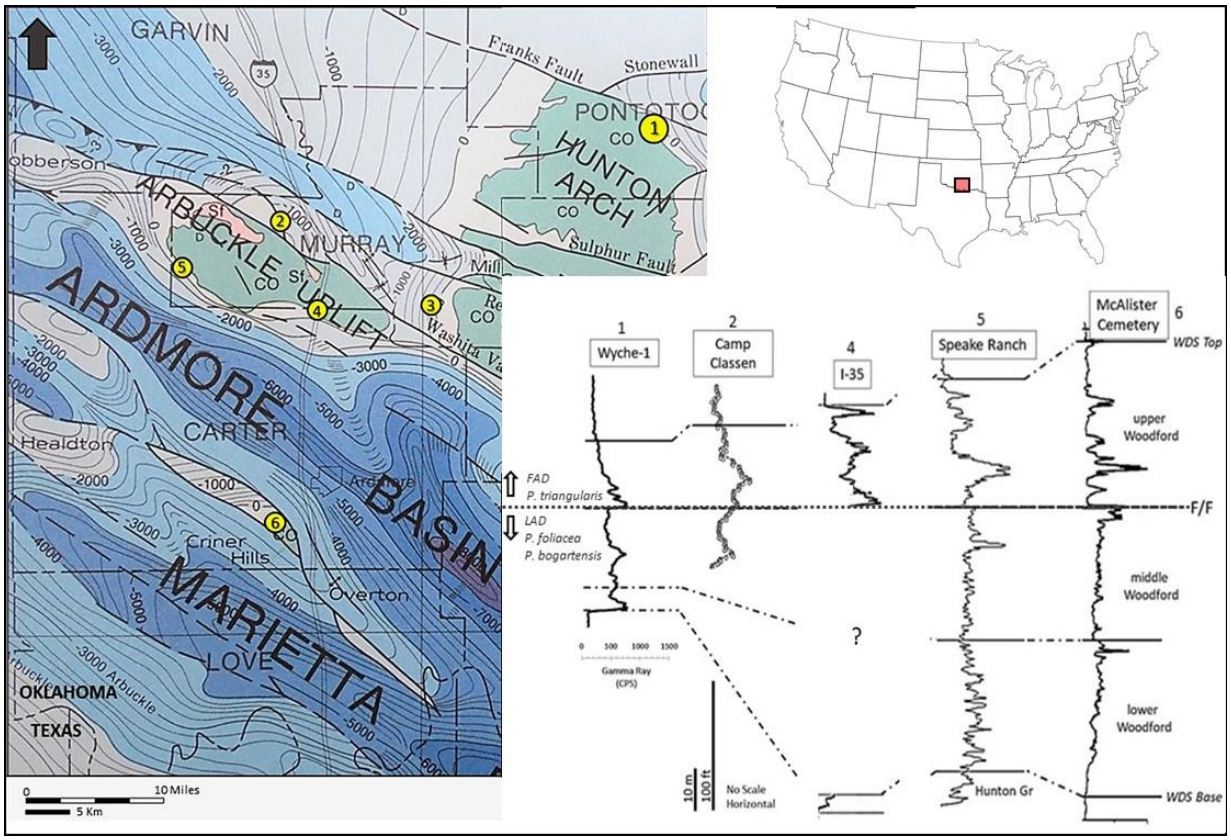

Fig 3.2. Woodford shale localities in South-central Oklahoma. 1) Wyche-1 well, Lawrence Uplift (Slatt et al., 2012); 2) YMCA Camp Classen section (Over, 2002; Crick et al., 2002); 3) Hunton Anticline section (Turner and Slatt, 2016; Turner et al., 2016); 4) I-35 road cut outcrop (Becerra et al., 2018); 5) Speake Ranch outcrop (Galvis et al., 2018); 6) McAlister Cemetery Quarry (Kirkland et al., 1992; Serna-Bernal, 2013; Ekwunife 2017). Co=Cambro-Ordovician strata; C=Gneiss-Granite; SG=Tishomingo Granite; SF=Felsic Rocks. Contours represent thickness in meter from Arbuckle group to surface (Modified from Tectonic Map of Texas, Ewing et al., 1991).

2. Stratigraphic Framework

In the Arbuckle Mountains and Lawrence Uplift region, the Woodford Shale is Late Devonian to Lower Mississippian in age, principally based on conodonts and palynological contents (Kondas et al., 2018). The Woodford lies unconformably on Silurian to Lower Devonian limestones of the Hunton Group and is limited at the top by organic-poor shales and/or limestones of early Mississippian age (Over and Barrick, 1990; Over, 1992a; Over 2002). The Woodford Shale has been subdivided by several authors into three units from bottom to top described as, lower, middle and upper member (Fig 3.3). This subdivision has been based on: palynomorph distributions (Urban, 1960), geochemistry (Slatt et al., 2011; 2012; Miceli-Romero and Philp, 2012; Wang, 2016; Torres-Parada, 2017), gamma ray log character (Northcutt et al., 2001), and recognized in outcrops, thanks to their lithological differences (e.g. Kirkland et al., 1992; Cardott and Chaplin, 1993; Treanton, 2014; McCullough, 2014; Bontempi, 2015; Becerra et al., 2018; Galvis et al., 2018; Ghosh et al., 2018).

The lower Woodford is composed of dark gray siliceous shale and fissile shales, interbedded with highly silicified and massive cherts (Fig 3.3), some thickest and most complete sections contain a basal transgressive sandstone, interbedded with siltstones and greenish shales characterized by a poor organic content (Galvis et al., 2018). That lower interval could be stratigraphically equivalent to the Middle to Late Devonian Misener Formation (Amsden, 1980), which contains conodonts fossils and lies conformably under the Woodford Shale (Amsden and Klapper, 1972). The middle interval is mainly composed of black to dark gray siliceous mudstones and organic rich fissile shales, characterized by a frequent odor of petroleum in outcrops (Fig 3.3). The middle Woodford member has the highest gamma ray values and total organic Carbon (TOC)

content (Slatt et al., 2012; Miceli-Romero and Philp, 2012), and evidently has a lower quartz content, non-calcareous matrix and clay mineral fraction dominated by illite. The upper Woodford is similar to the lower interval, but it is distinguished by the presence of dolomitic mudstones and normally a higher content of phosphate nodules, interbedding with siliceous mudstones (Kirkland et al., 1992; Slatt et al., 2012).

Phosphate nodules in the upper Woodford are particularly abundant in the upper 50 ft. of the McAlester Cemetery Quarry (Kirkland et al., 1992; Serna-Bernal, 2013; Ekwunife, 2017; Klockow, 2017). They are also common in other Woodford localities including the Henry House Fall Quarry (Turner et al., 2015) and the I-35 road cut (Becerra et al., 2018). The phosphates are spherical to slightly flattened parallel to the bedding and composed of collophane (microcrystalline apatite), with variable amounts of carbonate replacing phosphate. The quartz content in these nodules is roughly 10%, probably derived from biogenic silica. It is common that nodules have a nucleus associated with thin and elongated fragments of crustacean and ammonoids shells (Kirkland et al., 1992). The upper Woodford is also characterized by the presence of petrified logs (Fig 3.3), commonly associated with the genus *Archaeopteris* (Kirkland et al., 1992; Johnson and Cardott 1992; Slatt et al., 2012). The *Archaeopteris* was the most abundant and diverse arborescent *Progymnosperm* plant during Late Devonian times (Algeo et al., 2001). These trees expanded from tropical to boreal paleo-latitudes and were characterized by having trunks thicker than ~1.5 m (5 ft.) in diameter and heights exceeding ~30 m (100 ft.) (Fig 3.1). The presence of the petrified logs (sizes) might indicates that the locus of deposition was located not too far from the Late Devonian *Archaeopteris* first forests, unless the log had traveled a long distant from a land mass.

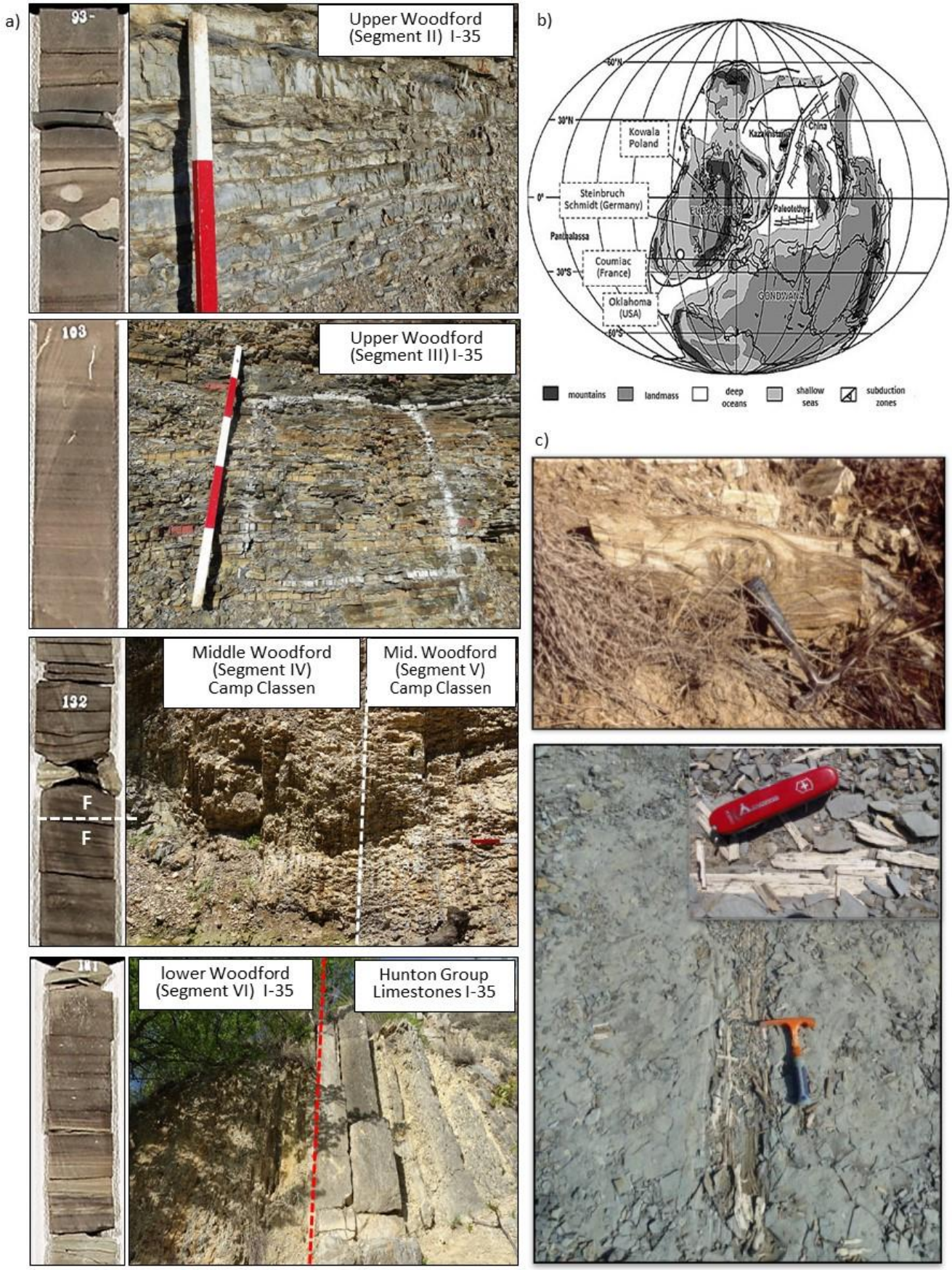
a)
93
Upper Woodford
(Segment II) I-35
103
Upper Woodford
(Segment III) I-35
132
F
F
Middle Woodford
(Segment IV)
Camp Classen
Mid. Woodford
(Segment V)
Camp Classen
111
lower Woodford
(Segment VI) I-35
Hunton Group
Limestones I-35
b)
60°N
30°N
0°
30°S
60°S
Kowala
Poland
Steinbruch
Schmidt (Germany)
Coumiac
(France)
Oklahoma
(USA)
Panthalassa
Paleotethys
GONDWANA
China
mountains
landmass
deep
oceans
shallow
seas
subduction
zones
c)

Fig 3.3 a) Upper, middle and lower Woodford Shale subdivisions. Core photos represent 6 in. (~15 cm) of rock. Upper Woodford is characterized by the presence of phosphate nodules (segment II) and natural fractures (segment III), and photos from I-35 road cut outcrop. The Frasnian/Famennian (F/F) boundary was identified in the middle Woodford Shale, characterized by organic rich black shales (segments IV and V), photo from the YMCA Camp Classen Section. In the lower Woodford phosphate nodules are not common. Lower Woodford is unconformably over Hunton Limestones and/or some basal gray to greenish shales to fine-grained sandstones. **b**) The F/F boundary in reference section located in Steinbruch Schmidt (Kellerwald), Germany (Buggisch, 1991; Schindler, 1993); F/F global stratotype at Coumiac, Montagne Noire, France (Klapper et al., 1994); Poland, Kowala section (Filipiak, 2002) and the Oklahoma, YMCA Camp Classen section (After Crick et al., 2002). **c**) Petrified logs commonly associated with the genus *Archaeopteris spp.* from Oklahoma outcrops (Photos courtesy Brian Cardott and Roger Slatt).

The Wyche-1 research core well was subdivided from top to bottom into six segments and described next: The first segment (I) is characterized by light gray siliceous shales, with poor organic contents, low gamma-ray values and correlative with the pre-Welden Shale (Over and Barrick, 1990; Over, 1992a; 1992b). The segments II and III are equivalents to Upper Woodford Shale. The segment II corresponds with organic mudstones interbedding with siliceous mudstones and abundant phosphate nodules. Segment III corresponds with siliceous mudstones, hard, compacted and visibly affected by natural fractures (Fig 3.3). The segment IV and V are organic-richer intervals, characterized by the higher gamma-ray values and interpreted as the middle Woodford. The segment VI was correlated with the lower Woodford Shale and is distinguished from the upper Woodford by decreasing or complete absence of phosphate nodules. The segment VI tends to be more organic-richer than the upper Woodford, particularly some basal shales accumulated on top of some limestone equivalent to the Hunton group (Fig 3.3). The total 54 m (~180 ft.) were described and preserved at the University of Oklahoma, except by a sampling gap preserved in mineral oil for geomechanic studies (Abousleiman et al., 2007; Sierra et al., 2010; Slatt and Abousleiman, 2011; Slatt et al., 2012).

3. Methods

For the stable organic carbon isotopic analysis, 33 samples were selected and from approximately 10 grams of core samples, the carbonate contents were first removed by standard acidification and centrifugation methods. After this process, the CO_2 from the total combustion of the organic matter was analyzed using a Carlo Erba Elemental Analyzer coupled to a ThermoFinnigan Delta Plus XP IRM, located in the National High Magnetic Field Lab (MagLab), at Florida State University (FSU). The results are reported in the standard $\delta^{13}C$ notation relative to the V-PDB (Vienna Pee Dee Belemnite) standard, with an analytical precision of +0.2 ‰ (1σ). Sample precision and calibration of data were performed during routine analysis of laboratory standards that are calibrated against IAEA (International Atomic Energy Agency) standards. Internal FSU standards include Acetanilide (-29.2‰), Urea-2 (-8.13‰) and WYSTD (-12.7‰) (Kozik et al., 2019). The Total organic carbon (TOC) content was determined by a comparison of voltages for the CO_2^+ ion bean intensity of masses 44, 45 and 46 between unknown samples and known wt% carbon of the gravimetric standard Acetanilide, which was analyzed during the same sequence (Table 3.1).

Spectral natural gamma-ray logs were used to determine the contribution of gamma radiation in the Woodford Shale caused by absorption of thorium (Th), reactive potassium (K_{40}), and the uranium (U) (Adams and Weaver, 1958; Luening and Kolonic, 2003). Th/U ratios were used as a paleo-redox proxy and Th/K ratios as clay compositional variation proxy (e.g. Adams and Weaver, 1958). These ratios were analyzed parallel with 22 X-ray diffraction (XRD) sample analyses to check potential changes in clay mineral compositional trends. The XRD analyses were performed using a Rigaku Ultima IV diffractometer™, using a curved-graphite diffracted-beam monochromator detector and applying the standard Bragg-Brentano method. The XRD analysis

was completed using the Jade^{TM} software and compared with the ICDD (International Centre for Diffraction Data) PDF^{4+} database, in the X-ray diffraction lab, School of Geology and Geophysics, University of Oklahoma.

Trace and major element compositions analysis were collected using a Bruker Tracer IV–SD, X-ray fluorescent spectrometer, available in the IRC, University of Oklahoma. Samples from well cores were scanned every 2 inches with a minimum of 2 torr vacuum and every point was scanned during 60 seconds at 40 kV for trace elements and during 90 seconds at 15 kV for the major elements. Details of the analytical methodology, including data quality, detection limits and calibration can be found in Rowe et al., (2012) and Turner et al., (2015). Aluminum (Al) was used as a normalization concentration factor to reduce the effects of the detrital and authigenic dilution (Calvert and Pederson, 1993; Tribovillard et al., 2006). Al normalized values of trace elements are usually given as $x10^{-4}$ notation and it was applicable in this case, because Al resides principally within the detrital clay fraction and has not shown evidence of significant remobilizing during diagenesis (Elmore et al., 2016). The Aluminum normalized concentration was used to calculate the enrichment factors (EF) plots:

$$EF_{\text{element X}} = [X]/Al_{\text{sample}} / [X]/Al_{\text{average shale}}$$

The EF compares the elemental concentration of the analyzed sample in terms of international standards and values greater than one mean enrichments of trace element respect to standards and values less than one are associated with depletions, corresponding with international average values for the upper continental crust compiled by Tribovillard et al., (2006). The complete XRF raw data are available from the first author upon request.

The Average EF from four modern anoxic basin analogues (i.e. Black Sea, Cariaco, Framvaren Fjord and Saanich Inlet basins) were also compilated and used for paleo-environmental comparison (Table 3.1).

Table 3.1. Trace elements average values in shales and continental crust (Compiled by Tribovillard et al., 2006). Aluminum normalized and enrichment factor (EF) average values from modern anoxic basin. NA = Not Available (From Calvert and Pedersen, 1993).

			Black Sea		Saanich Inlet		Framvaren		Cariaco Trench	
	Average Shale	Average Continental Crust	X/Al (10^4)	EF	X/Al (10^4)	EF	X/Al (10^4)	EF	X/Al (10^4)	EF
Cu	45.0	25.0	7.1	1.4	12.3	2.4	37.5	7.3	5.3	1.0
Mn	850.0	600.0	132.6	1.4	106.3	1.1	160.0	1.7	31.2	0.3
Mo	1.3	1.5	4.3	14.3	18.0	60.0	100.0	33.3	11.1	37.0
Ni	68.0	44.0	19.8	2.6	7.4	1.0	90.6	11.8	5.8	0.8
U	3.0	2.8	3.3	8.2	1.4	3.5	8.1	20.2	2.2	5.5
Ti	2000	5700	NA	NA	NA	NA	NA	NA	NA	NA
Zr	70	165	NA	NA	NA	NA	NA	NA	NA	NA
Al	88,900	80,400	NA	NA	NA	NA	NA	NA	NA	NA

Thirty-eight (38) rock thin sections were examined using a Zeiss Axio Imager Z1m optical microscope and SEM/EDX analysis using a FEI Quanta 250 Scanning Electron Microscope located in the Devon Energy SEM Lab, University of Oklahoma. SEM shales samples were prepared following the methodology proposed by O'Brien and Slatt, 1990; Slatt and O'Brien, 2011, and analyzed on the SEM equipped with an energy dispersive spectroscopy (EDX) detector, operating at acceleration voltages between 5 and 15 KeV. Sampling was completed taking account those intervals affected by fractures and/or fluid mineralization and by examining in detail thin sections, particularly those related within the natural fractured intervals. Additionally, 22 samples were also subjected to standard palynological preparation and at least one complete oxidized slide per sample was scanned under a 40x objective. 300 Palynomorphs per slide were categorized into three groups: Pollen and pteridophyte spores, tasmanites and acritarch cysts. These morphogroups were used also to recognize transgressive/regressive cycles.

4. Results

4.1 Chronostratigraphic framework

Reference sections equivalent in age to the Woodford Shale contain a series of positive $\delta^{13}C$ isotopic excursions associated with the Kellwasser events (e.g. Buggisch, 1991; Buggisch and Joachimski, 2006; Hillbun et al., 2015). To define the chronostratigraphic framework, the carbon isotopic curve obtained was used as a correlation tool, in combination with conodont biostratigraphy (Over and Barrick 1990; Over 1992a; 1992b; Over, 2002) and palynological reports from nearby Woodford Shale localities (Urban, 1960; Molinares-Blanco, 2013; Kondas et al., 2018). In the Wyche-core, within the middle Woodford interval a series of positive $\delta^{13}C$ isotopic excursions correlative with the global UK and LK events were identified (Saltzman, 2005; Buggisch and Joachimski, 2006). These isotopic excursions coincide with the top of the presence of a permanent zone of euxinia (PZE), previously reported by Miceli-Romero and Philp (2012) and Connock et al., (2018), and based on aryl-isoprenoids and C_{40} aromatic Carotenoid biomarkers contents (Fig 3.4; Table 3.2).

In the Lawrence Uplift, the uppermost Woodford Shale contains a well-preserved and diverse conodont fauna which represent the Late Famennian - early Mississippian boundary (Over and Barrick, 1990; Over, 1992). The Late Devonian fauna that occur near the top of the Woodford Shale is characterized by the conodont fossil assemblage: *Pseudopolygnathus marburgensis trigonicus*, *Palmatolepis gracilis gracilis*, and *Pelekysgnathus guizhouensis*.

The *Pseudopolygnathus marburgensis trigonicus* ranges from the Upper *P. expansa* biozone through Middle *P. praesulcata* biozone and represents the older Late Famennian strata. The *P. sulcata* biozone is the lowest Carboniferous biozone and was identified at the Lawrence Uplift by

the first occurrence of *Siphonodella duplicata* (Over and Barrick, 1990; Over, 1992). This boundary agrees with a positive isotopic excursion localized at the top of the Wyche section between the segments I and II and interpreted here as the Devonian/Carboniferous (D/C) boundary (Fig. 3.4). This event is correlative with another anoxic global event named the Hangenberg event, which strongly affected ammonoids, trilobites, conodonts, pelagic ostracods, corals and bivalves (e.g. Racki, 2005; Buggisch and Joachimski, 2006; McGhee 1996).

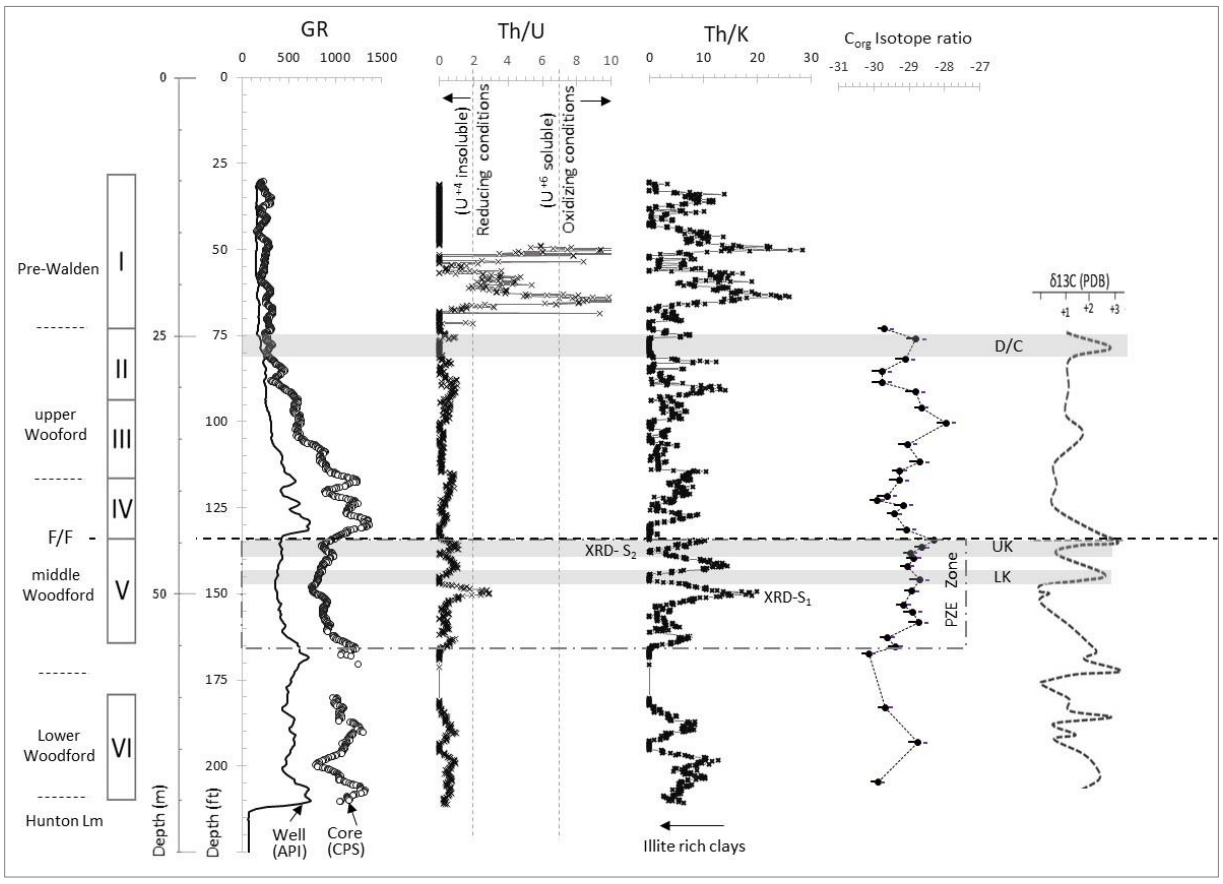

Fig. 3.4. Wyche-1 core subdivision. PWS= Pre-Walden Shales, UW = Upper Woodford, MW = Middle Woodford and LW = Lower Woodford. F/F corresponds with the Frasnian/Famennian boundary. Gamma-ray (GR) borehole in standard API units and core-gamma in counts per second (CPS). Th/U and Th/K ratios calculated from the spectral gamma-ray log. D/C = Devonian/Carboniferous boundary. UK and LK are equivalent to the Upper and Lower Kellwasser events. PZE = persistent zone of euxinia by Connock et al., 2018. Stable isotopic curve obtained in this study, compared with the global reference by Buggisch and Joachimski, 2006.

Table 3.2 Stable organic carbon isotopic analysis results. Gamma ray in count per seconds (CPS), E_TOC = estimated total organic carbon contents and C_{org} $\delta^{13}C$ ratios relative to the V-PDB.

Depth (ft)	Sample Weight (g)	Gamma Ray (CPS)	E_TOC	C_{org} $\delta^{13}C$	Stdv
70.60	10.11	278.4637	3.31	-29.72296607	0.16
73.60	9.966	292.5626	3.43	-28.80645544	0.16
79.60	10.062	NA	NA	-29.11653051	0.16
83.01	10.048	NA	NA	-29.77830167	0.16
86.20	10.041	413.0471	4.44	-29.77830167	0.16
89.01	10.132	381.1029	4.17	-28.82308332	0.16
93.60	10.054	583.2921	5.87	-28.65217367	0.09
98.00	10.053	627.3852	6.24	-27.94475972	0.16
104.20	9.979	609.9711	6.10	-29.04331940	0.16
109.40	10.086	870.3672	8.28	-28.71306685	0.16
111.90	12.2	851.6807	8.13	-29.27057327	0.09
114.80	10.085	954.159	8.99	-29.28891552	0.16
119.30	10.045	1014.896	9.50	-29.63785287	0.16
120.59	9.99	898.5272	8.52	-29.91324287	0.09
122.05	9.956	1036.137	9.68	-29.15631787	0.16
124.60	10.02	NA	NA	-29.42153267	0.09
129.10	9.91	1316.45	12.03	-29.08211803	0.16
132.10	9.975	1135.079	10.51	-28.29785584	0.16
134.30	10.073	958.1967	9.02	-28.65023207	0.09
136.01	10.11	850.8541	8.12	-28.97011067	0.09
137.40	10.105	897.095	8.51	-28.87739927	0.09
139.80	10.815	936.8934	8.84	-29.05845347	0.09
143.80	9.948	837.3372	8.01	-28.71049818	0.16
147.10	9.96	790.7692	7.61	-28.93564727	0.09
151.01	10.093	875.8711	8.33	-29.15310647	0.09
153.20	10.056	906.4922	8.59	-28.90139936	0.16
156.30	10.088	871.4694	8.29	-28.73583189	0.16
160.50	9.98	910.4667	8.62	-29.62297367	0.09
163.20	10.065	1002.788	9.40	-29.38949627	0.09
165.20	10.047	1192.335	10.99	-30.15060347	0.09
181.00	9.993	1023.838	9.57	-29.67151367	0.09
191.20	10.02	1179.286	10.88	-28.75575152	0.16
202.70	9.12	1041.114	9.72	-29.89285607	0.09

4.2 Natural gamma-ray spectrometry analysis

Thorium (Th) / Uranium (U) ratios were used as a paleo-redox proxy (Fig 3.4). Th/U ratios less than two were associated with an environment under reducing (anoxic) conditions, which apparently were predominant during the accumulation of the whole Woodford Shale interval. In contrast, Th/U values greater than seven were observed at the top of the core, within the pre-Walden Shale and were related to U mobilization and therefore, oxidizing conditions. (Fig 3.4).

The contributions of the elements U, Th and K to the total gamma-ray radiation were obtained throughout a spectral gamma-ray core log (Fig 3.5). Th has a single insoluble tetravalent valency (Th^{+4}), which is useful for redox comparisons (Adams and Weaver, 1958). In contrast, U has two oxidation states which are controlled by redox conditions (Calvert and Pedersen, 1993; Algeo and Maynard, 2004; Tribovillard et al., 2006). U has a soluble hexavalent state (U^{+6}) which is in solution under oxic conditions, but that state is transformed to the insoluble tetravalent state (U^{+4}), which is precipitated under reducing (anoxic) conditions.

However, instead of being entirely authigenic (U_{auth}), a portion of U can also be detrital (U_{det}) and often associated with detrital U-bearing minerals (e.g. zircon) (Fig 3.5). The average amount of Th present within the detrital U-bearing mineral fraction is often assumed to be three times higher than the concentration of U. For that reason, the U_{auth} fraction from the total uranium (U_{tot}) in ppm was calculated using the expression proposed by Wignall and Myers, (1988): $U_{auth} = U_{tot} – (Th/3)$

The U_{det} dominates the pre-Walden Shale section (segment I) and the U_{auth} fraction dominates the Woodford Shale interval (segments II to VI), except for a more detrital rich interval

around 45.8 m (~150 ft.) depth, accumulated right before the positive isotopic excursion associated with the onset of the LK anoxic event (Fig 3.5).

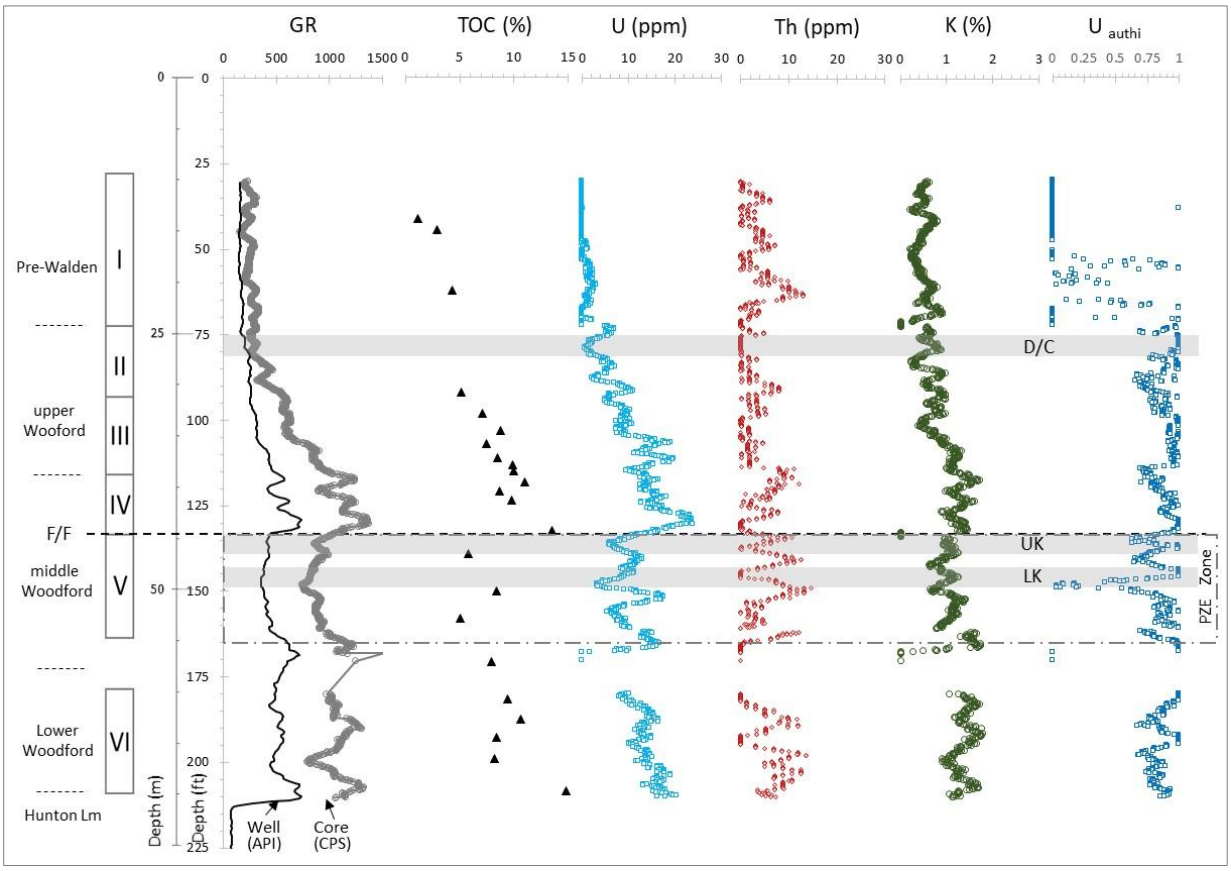

Fig 3.5. Borehole and core spectral gamma ray (GR) logs from the Wyche-1 core well. The core GR unit in counts per second (CPS) was used to tie the core to the well with the gamma ray from borehole. UK and LK correspond with the Upper and Lower Kellwasser events, D/C with the Devonian/Carboniferous boundary and the PZE = persistent zone of euxinia reported by Connock et al., 2018. The GR is dominate by the U contribution, over Th and Potassium and K contents. Uranium and total organic carbon (TOC) have a good positive correlation, but that correlation decreases in the intervals affected by the presence of permanent euxinic conditions.

Th/K ratios were used as a guide to recognize geochemical facies and particularly changes in clay compositions (Adams and Weaver, 1958). XRD compositional analysis from Wyche core samples with low Th/K ratios are likely related to more potassium in the clay fraction, possibly

associated with higher illite contents in the mixed illite-smectite (I/S) clay fractions, but further analysis are required to verify this idea (Table 3.3).

Table 3.3. X-ray diffraction (XRD) results for samples taken from Wyche -1 research core well.

Depth(ft.)	quartz	I/S mixed	chlorite	kaolinite	pyrite	dolomite	ankerite	gypsum	muscovite	oligoclase	albite	K-feldspar	jarosite
66'2"	70	29.4			0.6								
76'0"	33.8	20.6		0.4	0.9	36.5	7.8						
84'0"	81.5	16.1			0.3				2.1			2.1	
87'1"	32.1	18			0.5	47.9						1.5	
104'2"	85.7	13.7			0.6								
123'"	69.7	23.2			2.8								4.3
123'"	72.8	24.2			3								
127'"	55	37.3			2.3								5.4
127'"	58.1	39.4			2.5								
131'"	51.3	32.7		0.3	2.4			7.9			3.3		2.1
136'"	43.1	37		0.8	6.7	2.4	5.7	1.8			2.5		
137'"	47.7	37			3.1	6.4	5.8						
139'8"	41.6	37.9	0.6		3.2	16.7							
143'5"	50.2	40	0.2	0.5	2.9	6.2							
143'5"	50	40.2		0.7	2.9	6.2							
147'10"	45.8	40			3.1	11.1							
149'5"	44.3	33.8	0.9		2.4	14.7					1.4	2.4	
153'2"	54.7	33.1	0.6		4.2	7.4							
158'4"	43.4	29.6		0.7	2.4	15.8				8.1			
158'4"	46.7	33.4		0.3	2.4	17.2							
186'8"	56.7	41	0.5	0.2	1.6								
191'7"	48.3	41.6	0.3	1.4	2.1	4.1					2.2		

Chlorite, k-feldspar and kaolinite were also commonly reported from low Th/K intervals and as traces in the high Th/K intervals. Kaolinite is often associated to soils produced by alteration of biotite and plagioclase feldspar, normally favored by wet and humid tropical conditions (Potter et al., 2005). This observation might support the idea that the UK and LK anoxic events are related to short-term changes in weathering rates, which have been related to the spread of vascular land plants during the Late Devonian (Algeo et al., 1995).

Illite $(K,H_3O)(Al,Mg,Fe)_2(Si,Al)_4O_{10}[(OH)_2,(H_2O)]$ can be formed by a diagenetic process from smectite $[(Na,Ca)_{0.33}(Al,Mg)_2(Si_4O_{10})(OH)_2{\cdot}nH_2O]$, in a process denominated as I/S transformation (Potter et al., 2005). This process occurs at depths around 2-3 km and temperatures between 120-140°C degrees (Bruce 1984; Pollastro, 1993; O'Brien and Slatt, 1990). However, these diagenetic transformations was discarded because maximum temperature

reached by this section was probably less than 80°C degrees and organic matter reported from Wyche-1 core sample has been classified as thermally immature, based on vitrine reflectance (R_0 = 0.55) and biomarkers analysis (Cardott and Lambert, 1985; Cardott, 2012; Miceli-Romero and Philp, 2012; Connock et al., 2018).

Higher weathering and iron detrital input apparently occurred during the UK and LK events and possibly stopped, at least temporarily, the permanent high reducing and euxinic conditions associated with the prevalent sulphate bacteria activity during the accumulation of the middle Woodford Shale deposits (Connock et al., 2018). During the UK and LK accumulation, Fe_20_3 and SO_3 ratios were higher than the Pyrite stoichiometric ratio of 0,5 and thank that surplus in Fe contents, authigenic Fe-rich carbonate (i.e. Ankerite) minerals were precipitated (Fig 3.6; Table 3.3). Moreover, during the Late Devonian glacial stages, clay contents were characterized by low Th/K ratios, drier and cooler conditions were prevalent and possibly physical weathering was favored over chemical reactions. In contrast, during interglacial stages, more humid climatic conditions facilitated the chemical weathering, where K and U cations removed from source areas helped to form authigenic phases enriched in these two elements, with the corresponding Th enrichment in the residual soils and high Th/K ratios observed in the Woodford shale clays.

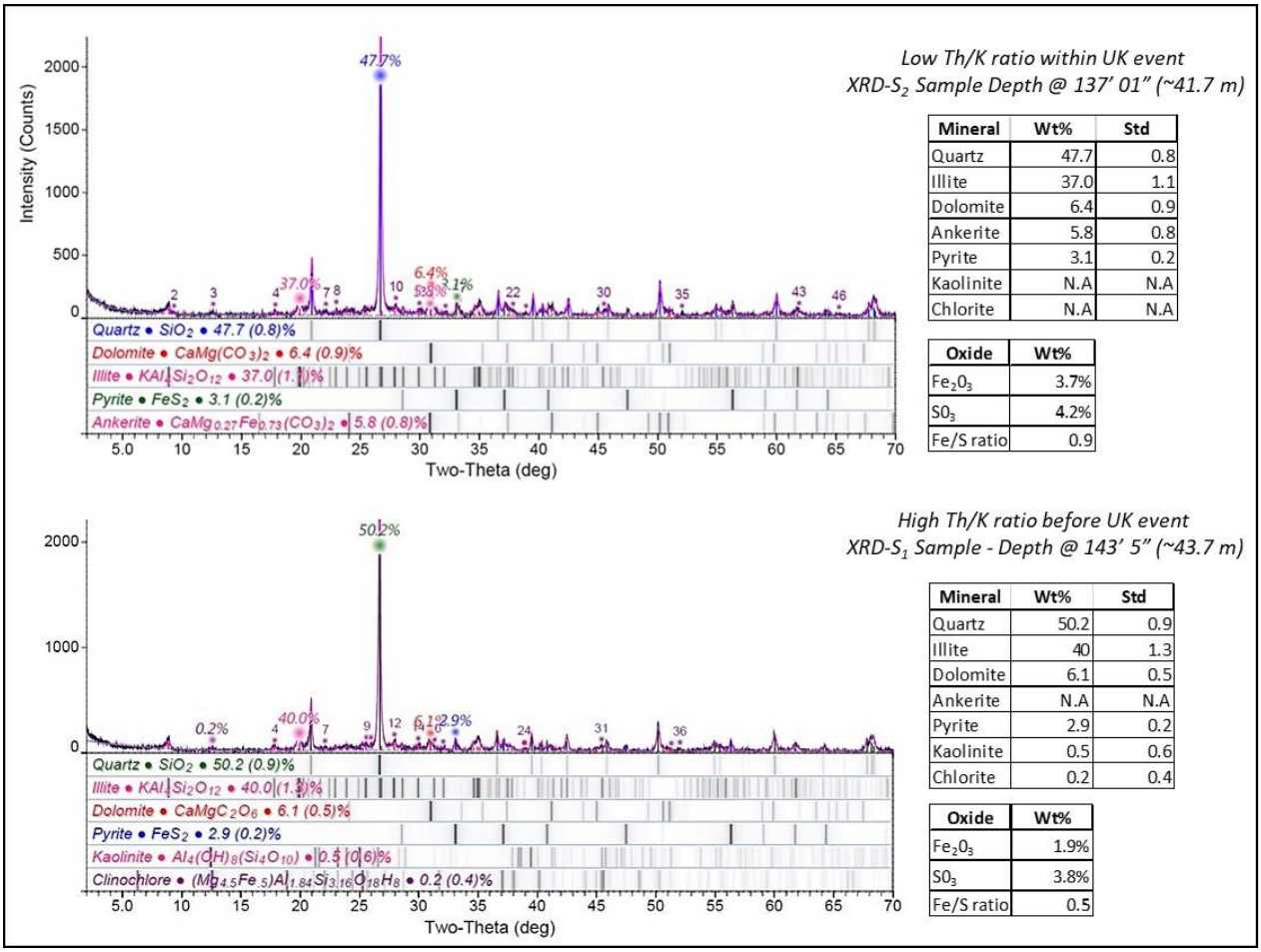

Fig 3.6. Powder X-ray diffraction (XRD) analysis. The first sample was characterized by low Thorium/Potassium (Th/K) ratios, typical from intervals associated with the Upper (UK) and Lower Kellwasser (LK) events. The second sample was characterized by higher Th/K ratios and higher Illite clay contents, but iron limited contents (See Fig. 1.4 for samples location in the stratigraphic column).

4.3 Major and trace element concentrations

Major and trace elements are subdivided into two different categories according with their behavior under oxic, anoxic and euxinic conditions (Calvert and Pederson, 1993; Algeo and Maynard, 2004; Tribovillard et al., 2006; Algeo and Tribovillard, 2009). The first group includes the elements whose valency does not change with redox conditions and/or form highly insoluble sulphide phases under euxinic conditions, such as nickel (Ni) and copper (Cu). The second group

embrace the elements which valency varies with the redox potential and highly soluble anionic species in oxic waters which are reduced to reactive or insoluble species of lower valency under anoxic (euxinic) conditions: included in this group are the elements molybdenum (Mo) and uranium (U). The distribution and concentration of these trace elements were compared with previous publications (e.g. Calvert and Pederson, 1993; Algeo and Maynard, 2004; Algeo and Lyons, 2006; Tribovillard et al., 2006; Algeo et al., 2007; Algeo and Tribovillard, 2009; Algeo and Rowe, 2012; Turner et al., 2015; Turner and Slatt, 2016), and used to determine how paleo-productivity rates and paleo-redox controlled the accumulation and preservation of the organic-rich Woodford Shale lithofacies.

The final concentration of organic matter in the sediment below the water column depends on the interaction of several processes including: the organic matter production (Pederson and Calvert, 1990), degradation of organic matter by oxidation (Demaison and Moore, 1980), as well as dilution controlled by weathering/sedimentation rates (Canfield, 1994; Bohacs et al., 2005) and after deposition, by diagenetic factors and hydrocarbon migration (Tourtelot, 1979). High organic content in fine-grained marine rocks is favored by high to moderate rates of primary organic productivity, and low to moderate rates of oxidation and dilution (Bohacs et al., 2015). The contribution of these processes in the accumulation of the organic rich intervals in the Woodford Shale will be discussed in the next paragraphs.

4.3.1 Organic matter production

The organic matter (OM) and Marine productivity is largely controlled by the levels of nutrients available in the photic zone and they are generally proportional to the organic carbon

sinking flux to the sea floor, which is frequently correlative to the total concentration of Ni and Cu in fine-grained rocks (Canfield, 1994; Tribovillard et al., 2006). Ni and Cu element contents identified in the Wyche-1 core samples in more than 95% of the cases were higher than their X-ray fluorescence, lower detections measurements (LDM); therefore, these values were valid and used as productivity proxies in the analysis (Fig 3.7). The Lowest Ni and Cu values were identified in the upper pre-Walden Shales (segment I) and the middle Woodford Shale (segment V), which indicates that organic carbon flux and marine productivity were lower during the accumulation of these two segments. In contrast, higher Ni and Cu contents were noticed for the other Woodford shale segments, which were also characterized by higher total organic contents (TOC) and correlative higher gamma ray values (Fig 3.7).

Thin section samples from segments II and III were characterized by SEM-EDX microscopic analysis (Fig 3.8). These images confirmed the presence of post-diagenetic pyrite (FeS) and sphalerite (Zn,FeS) crystals filling the microfractures but, chalcopyrite crystals ($CuFeS_2$) were not detected in the mineral paragenesis. Mineralized microfractures from Woodford Shale samples frequently contain other sulfidic minerals such as celestine ($SrSO_4$), barite ($BaSO_4$) and non-framboid pyrite crystals (FeS), which were not here identified. Chalcopyrite ($CuFeS_2$) in the Woodford Shale fractures was not identified, and it is not reported in other Woodford Shale diagenetic studies (Elmore et al., 2016).

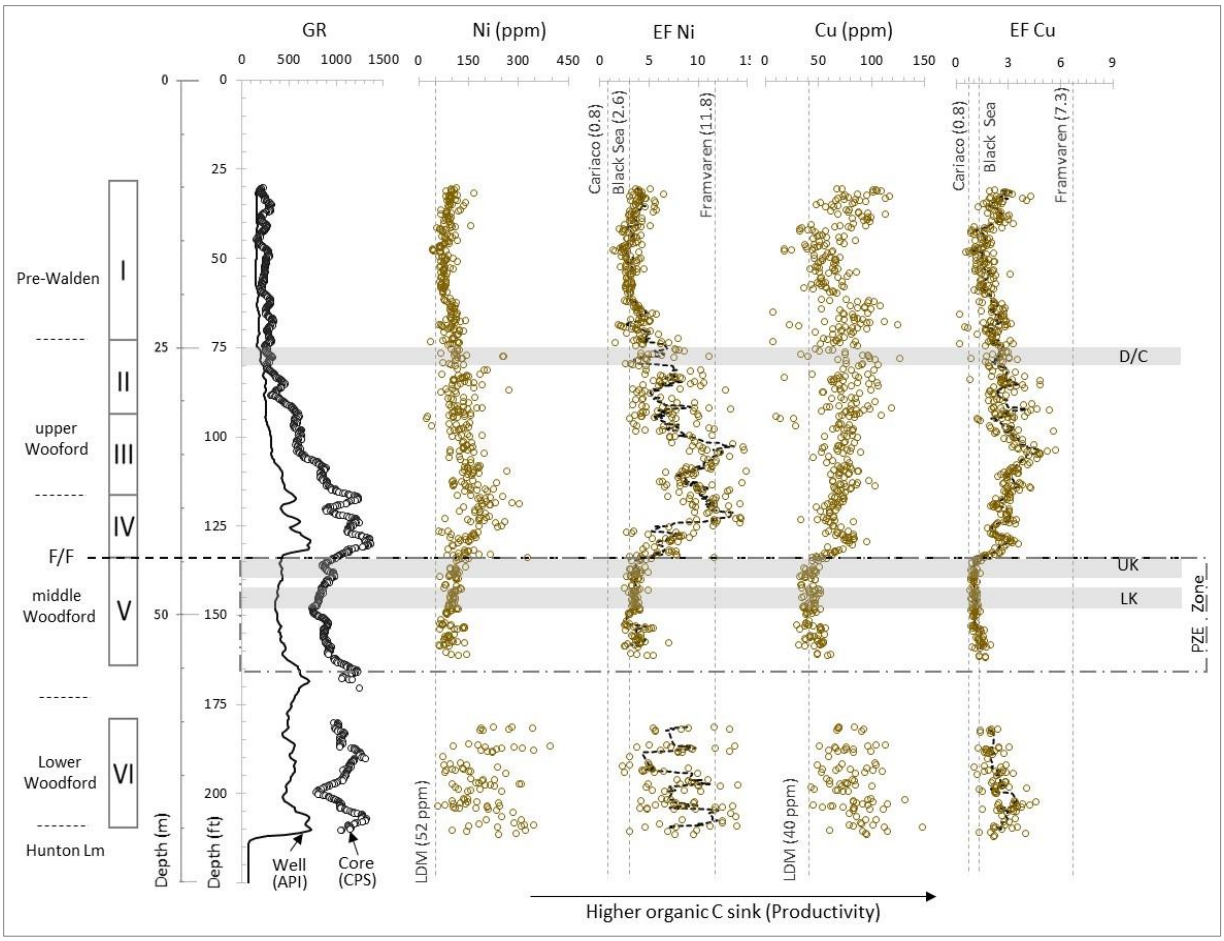

Fig 3.7. Nickel (Ni) and Cupper (Cu) concentration in part per million (ppm), for the Wyche-1 core well (After Turner et al., 2015 and Turner and Slatt, 2016). LDM corresponds with lower detection limits. Dotted lines represent six point moving average values. The EF Ni and Cu average values from modern analogues basins after Calvert and Pederson, 1993. UK and LK correspond with the Upper and Lower Kellwasser events, D/C = Devonian/Carboniferous boundary and the PZE = Persistent zone of euxinia interval reported by Connock et al., (2018).

Furthermore, Cu and Ni values after normalization by aluminum (i.e. EF normalization), confirm that Cu variability could be in fact due to the effect of bedding between organic-rich mudstones (shales) and siliciclastic mudstones (cherts), instead of originating by the natural microfractures. More frequent lamination/bedding in the upper and lower Woodford than the middle Woodford interval have been identified in wells based on higher resolution, formation

micro-resistivity well logs and this feature produced a significant change in geomechanical properties, including their ability to create or propagate fractures (Slatt and Abousleiman, 2011).

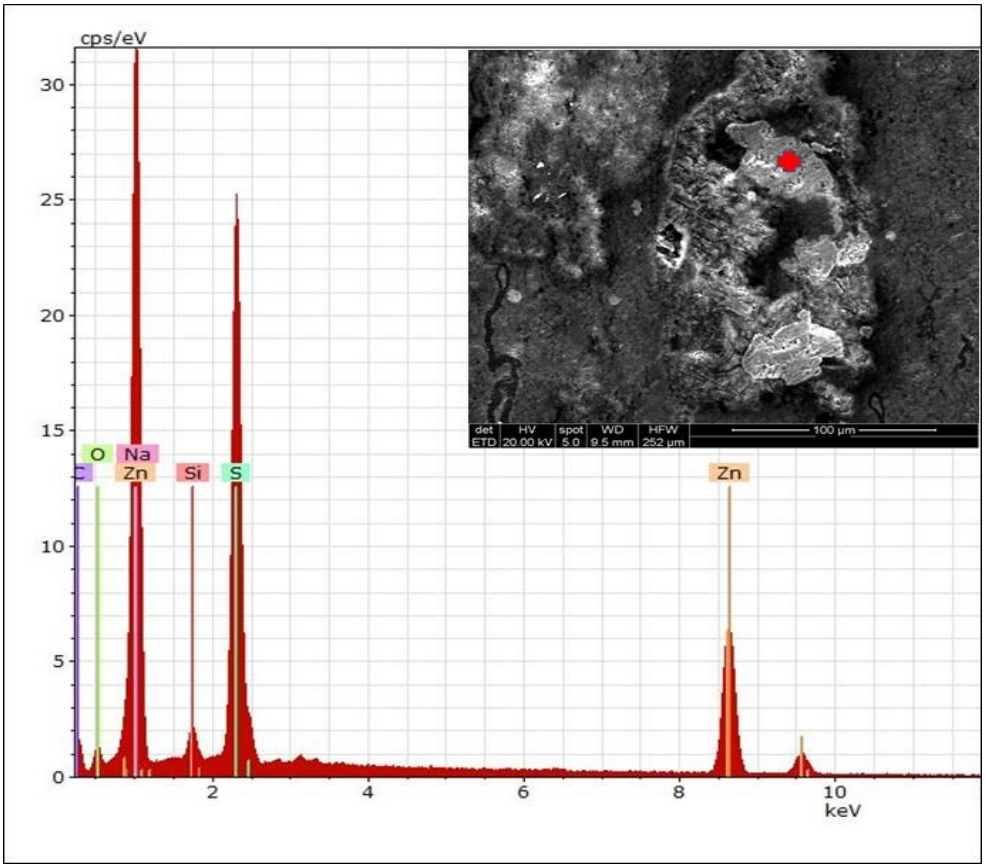

Fig. 3.8 Scanning electron microscope (SEM) image, coupled with an energy dispersive X-Ray analyzer (EDX) showing the presence of sphalerite crystals (Zn,FeS), filling some microfractures, upper Woodford segment III, Wyche-1 core well.

In the Wyche well, Ni and Cu values indicate that marine productivity during the accumulation of the Woodford was equivalent to the Black Sea and Framvaren Fjord basins and probably more intense during the accumulation of segments III and IV. The Black Sea is the largest (~423,000 km^2) modern euxinic marine basin, characterized by low sedimentation (10 – 200 g m^{-2} yr^{-1}) and organic carbon accumulation rates (~ 1- 10 g m^{-2} yr^{-1}), and separated from oxygenated open marine oceanic waters by a sill of ~ 33 m depth, located in the Bosporus Strait (Algeo and

Lyons, 2006). Framvaren is a relatively small Fjord (5,8 km^2) located in southern Norway, separated from the North Sea by a shallower sill of 2.5 m depth, and characterized by low bulk sedimentation (50 - 120 g m^{-2} yr^{-1}) rates, but higher organic accumulation (12-24 g m^{-2} yr^{-1}) rates, mostly of terrigenous origin (Algeo and Lyons, 2006). The Cariaco basin is the second largest (~7,000 km^2) modern anoxic basin analogue, located on the north Venezuela continental shelf, and it is separated from the Caribbean Sea by a series of deep sills on its western margin, which controls the surface and intermediate water fluxes. Cariaco basin is characterized by moderate bulk sedimentation (80-250 g m^{-2} yr^{-1}) and organic carbon accumulation (10-60 g m^{-2} yr^{-1}) rates, mostly marine in origin (Algeo and Lyons 2006). Ni and Cu were preferred as proxies for organic C sinking flux (productivity) rather than other elements such as barium (Ba) and phosphorous (P), because Ni and Cu are less soluble under reducing (anoxic) conditions, particularly during the early diagenesis phases (Algeo and Maynard, 2004; Tribovillard et al., 2006). Under reducing (anoxic) conditions, Ni can be preserved in organic-rich facies as Ni- porphyrins (Lewan, 1984) and the amounts of Ni in porphyrin structures are apparently controlled by the presence of a persistent open shale systems, which allows the diffusion of Ni from the overlying water body to the upper sediment layers (Lewan and Maynard, 1982). Ni is also chalcophile (having affinity for sulfur) and Ni can be included into pyrite structure or forms its own sulfide phases under reducing conditions similar to the Cu, which under anoxic conditions is reduced from Cu^{2+} to Cu^{+} and incorporated to porphyrins or to sulfidic structures (Tribovillard et al., 2006).

In contrast, under sulfidic (euxinic) conditions the authigenic phosphates and barite ($BaSO_4$) mineral precipitation is mainly controlled by the Iron (Fe) and Manganese (Mn) redox oxyhydroxides solubility (Jarvis et al., 1994). Fe(Mn)-oxyhydroxides can cap P and Ba on their

molecular structures, but when Fe(Mn)-oxyhydroxides are dissolved, reactive P and Ba diffuse out of the sediments, reducing the chance of these elements be trapped (Algeo and Ingall, 2007; Tribovillard et al., 2006). In fact, the P cycling is very efficient and thanks to this process, approximately 99% of organic phosphorous trapped in sediments is recycled, diffusing upward to the water column and used again in biological processes (Algeo and Ingall, 2007). In consequence, phosphate deposits are frequently associated with upwelling and high productivity zones, high phosphate accumulations are not necessarily always indicative of a high OM flux, because P and Ba may be enriched efficiently in sediments associated with the precipitation of Fe(Mn)-oxyhydroxides, even under the absence of high productivity in shallow marine waters (Jarvis et al., 1994; Tribovillard et al., 2006). Furthermore, the presence of phosphate nodules can also cause distortion in paleo-environmental interpretations (Turner et al., 2015), because trace elements can be incorporated in the phosphate nodules structures, replacing the PO_4, Ca and F (Jarvis et al., 1994; Tribovillard et al., 2006), but those types of variations are frequently very spatially restricted and related to local disturbances with a very limited correlative value.

4.3.2. Oxygenation and redox proxies

The contact between oxygenated and oxygen free zones may be either above the sediment-water interface or below the sediment-water interface (Fig 3.9a and 3.9b). Inside the water column, anoxia may be developed in stagnant or confined water masses where there is not enough O_2 circulation or in places where intense organic matter degradation consumes O_2 faster than it is replaced (Canfield, 1994). In this situation, the sediment-water interfaces are anoxic themselves, so that the consumption of dissolved oxygen exceeds the rates of oxygenation

renewal by turbiditic or other bottom currents (Calvert and Pedersen, 1993). In the second scenario, when anoxia is located below the sediment-water interface, the amount of oxygen in pores regulate the OM degradation and important features such as the benthic fossil content, lamination (bioturbation), rock color and pyrite content (Potter et al., 2005). However, marine sediments become anoxic at variable depths below the sediment/water interface and that occurs when the rate of burial of particulate organic matter exceeds the rates of degradation by oxygen or other secondary oxidant agents (Froelich et al., 1979).

These anaerobic oxidizing agents are in order of decreasing energy: 1) nitrate reduction, 2) manganese reduction from valence IV to II, 3) iron reduction from valence III to II, and 4) sulfate reduction (Fig 3.9b). In fact, fully anoxic conditions are certainly established only when all these oxidant agents have been depleted and the concentrations of H_2S produced by sulfate-reducing bacteria is high enough that it can ultimately auto-inhibit their activity (Froelich et al., 1979; Calvert and Pedersen 1993; Tribovillard et al., 2006). Redfield stoichiometric proportions are commonly used to illustrate the classical sequence of equations, and how heterotrophic bacterial activity consumes organic matter, using various electron acceptors after oxygen consumption (e.g. Froelich et al., 1979; Tribovillard et al., 2006). Mo and U have been used widely as a paleo-redox proxy, with higher concentrations interpreted to reflect lower redox potential (Tribovillard et al., 2006). EF values > 3 corresponds with enriched reducing environments and EF > 10 are typically related to highly enriched authigenic deposits (Algeo and Maynard, 2004; Algeo and Lyons, 2006; Tribovillard et al., 2006).

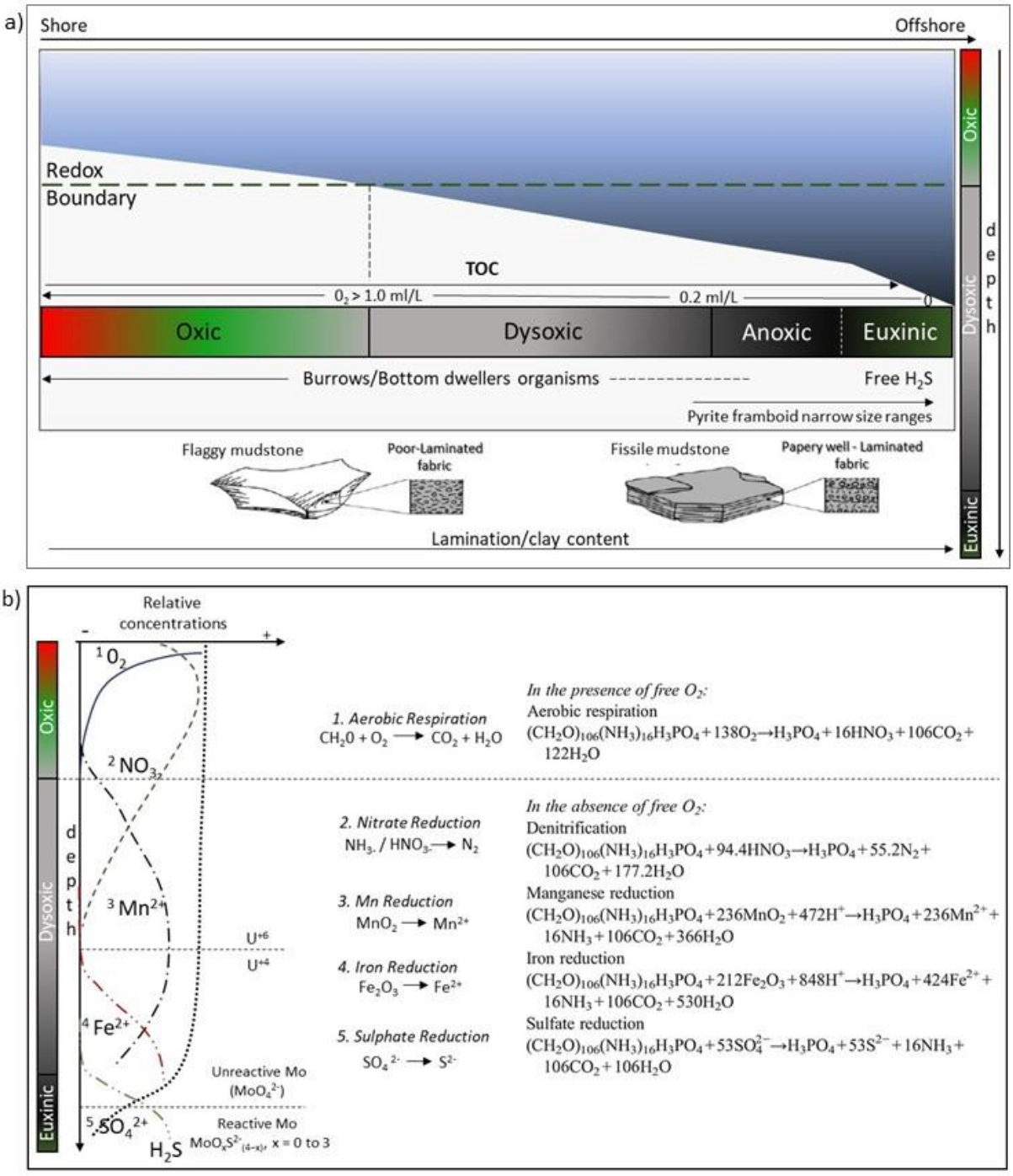

Fig 3.9 a) Hypothetical vertical and horizontal redox transitions in marine sedimentary basins. **b**) Oxidation reactions of sedimentary organic matter in a vertical profile. Redfield stoichiometric proportions are used. See text for further explanation. (After Froelich et al., 1979; Tribovillard et al., 2006; Calver and Pedersen 1993; Algeo and Tribovillard, 2009).

Mo and U were used to determine oxic, suboxic and euxinic conditions during the accumulation of the pre-Walden and Woodford Shale deposits and they were compared with modern anoxic reference basins (Table 3.1; Fig 3.10). Molybdenum $(Mo)_{aq}$ and Uranium $(U)_{aq}$ aqueous phases are uniformly present in low concentrations in seawater globally (Mo/U ~7.5-7.9 molar ratio) and, due to their long residence times in seawater (~780 and 450 kyr, respectively), it seems unlikely that they varied much through time. (Tribovillard et al., 2006; Algeo and Tribovillard, 2009).

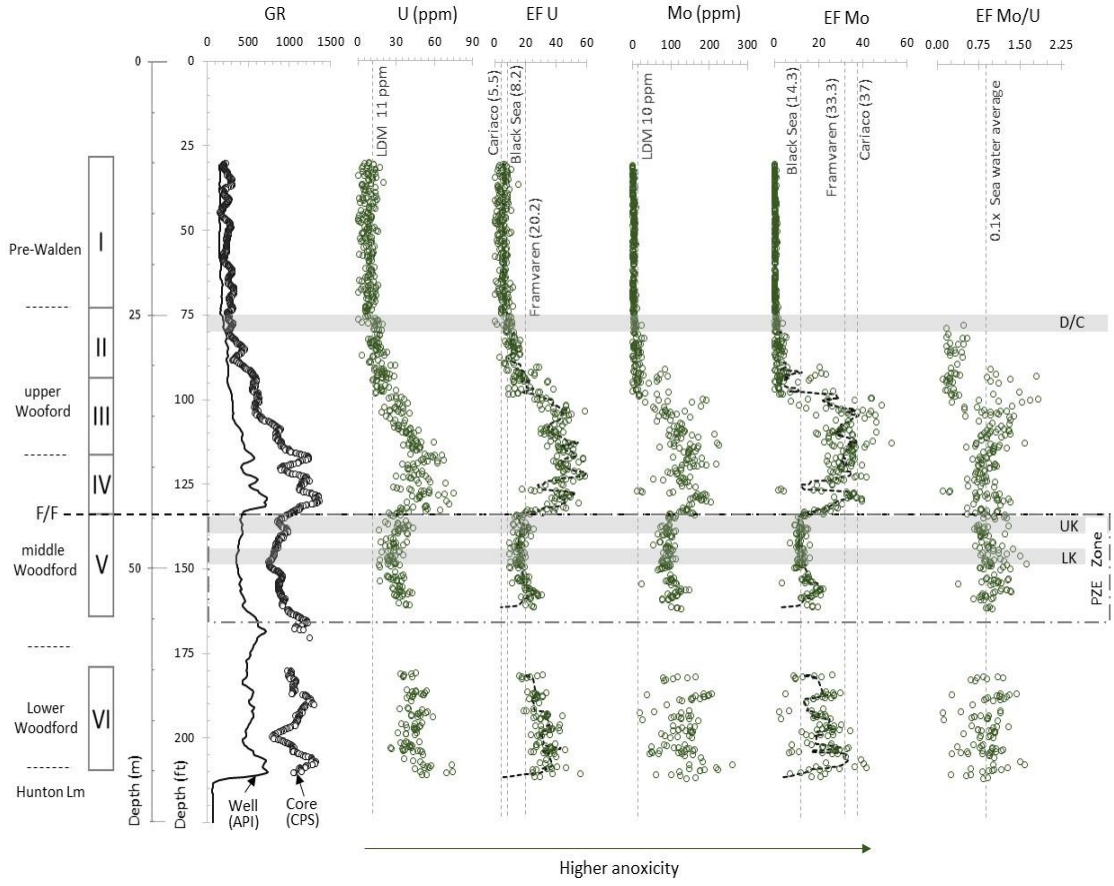

Fig. 3.10. Molybdenum (Mo) and Uranium (U) concentrations in part per million (ppm), from the Wyche-1 core well. (After Turner et al., 2015 and Turner and Slatt, 2016). Dotted black lines represent six point moving average values. LDM = XRF lower detection limits. UK and LK correspond with the Upper and Lower Kellwasser events, D/C with the Devonian/Carboniferous boundary and the PZE = persistent zone of euxinia reported by Connock et al., 2018. Modern anoxic basins analogues values from Calvert and Pederson, 1993; Algeo and Tribovillard, 2009.

The marine geochemistry of Mo and U under oxic to suboxic reducing conditions are similar, but they have some differences under highly reducing (sulfidic) conditions, which are useful to determine redox variations within sediment during accumulation (Algeo and Lyons, 2006). The first difference is that authigenic uranium (U_{auth}) uptake commences at the Fe^{+3}/Fe^{+2} redox boundary and earlier than authigenic molybdenum (Mo_{auth}) reduction. U reduction from U^{+6} to U^{+4} occurs preferably within the sediment (not in the water column) and possibly catalyzed by enzymes produced by iron and sulfate-reducing bacteria (Fig 3.9b). On the other hand, Mo requires the presence of H_2S for starting uptake (Algeo and Tribovillard, 2009). Under oxic conditions, Mo is largely present as unreactive molybdate oxyanion and under a critical concentration of hydrogen sulfide (a_{HS}-= $10^{-3.6}$ to $10^{-4.3}$, equivalent to ~50–250 µMHS^-), Mo start conversion from molybdate oxyanion (MoO_4^{2-}) to the reactive thiomolybdates form ($MoO_xS^{2-}_{(4-x)}$, x = 0 to 3), which can be adsorbed either into humic organic substances or throughout Fe(Mn) oxyhydroxides (Algeo and Maynard, 2004; Algeo and Lyons, 2006). The second difference is that Mo_{auth} transferred to sediments is accelerated by the presence of Fe(Mn)-oxyhydroxide shuttle particles, whereas U_{auth} is not affected by this process (Algeo and Lyons, 2006). The Fe(Mn)-oxyhydroxide formed at the chemocline and can adsorb molybdate oxyanions during transit through the water column. Once they reach the sediment/water interface, these “shuttle” particles are reductively dissolved, releasing molybdate ions that either diffuse back into the water column or can be scavenged by other mineral phases within the sediment (Algeo and Tribovillard, 2009). In this way, changes of Mo/U element ratios in marine sediments can provide information about benthic redox conditions and the evolution of water-mass chemistry in anoxic basins.

Mo/U ratios were significant lower (~0.1x) than the seawater global average during the accumulation of the Middle and Lower Woodford shale intervals (Fig 3.10). The lower Mo concentration and Mo/U ratios observed during the accumulation of the middle Woodford (segment V) were associated with bottom waters of silled euxinic basins, when Oklahoman basins were more sulfide-rich, and Mo was continuously depleted. Even Mo rarely shows significant covariation with pyrite, or total S in sediments (Algeo and Maynard, 2004), normally it is inversely related to deep water $(H_2S)_{aq}$ in modern silled basins, because of drawdown of deepwater $(Mo)_{aq}$ under more stagnant conditions (Algeo and Lyons, 2006; Turner and Slatt, 2016). In fact, if Fe is strongly limited or H_2S concentrations influences Mo accumulation by acting as a "switch" to transform molybdate (non-reactive) to thiomolybdates (reactive), lower Mo concentrations and decreased burial fluxes at higher aqueous sulfide concentrations are expected (Algeo and Lyons, 2006). For example, the Cariaco basin has an Mo/U ratio (~6.7) which is slightly less than actual seawater average (~7.5-7.9), due to comparatively short renewal times ~100-125 yr in deep-waters (Algeo and Lyons, 2006; Algeo and Rowe, 2012), while in the Black Sea (characterized by more prolonged renewal times of 650 ± 125 yr, the elevated rates of Mo removal to the sediment, without compensatory resupply produces a lesser degree of enrichment of Mo_{auth} relative to U_{auth} and much lower Mo/U ratios than actual seawater averages.

This observation agrees with the restricted and sulfidic conditions based on biomarkers (Connock et al., 2018). A suite of a special group of aromatic organic compounds known as C_{40} carotenoids have been identified recently in samples from the interval corresponding with the Woodford Shale segment V analyzed here (Fig 3.10). C_{40} Carotenoids biomarkers have been used for showing the presence of euxinic conditions in the photic zone during the time of accumulation

of organic-rich mudstones in phanerozoic global extinctions (e.g. Meyer and Kump, 2008). Based on these biomarkers, the lower and upper Woodford intervals were characterized by isolated pulses of euxinia, while a portion of the middle Woodford was associated to persistent euxinic conditions and coincided with higher values of gamacerane indices, indicating hypersaline conditions, shallowing chemocline and poorly ventilated waters (Miceli-Romero and Philp, 2012; Connock et al., 2018). The decrease of the chemocline apparently increased the competition for nutrient resources and produced a microbial community shift, from photosynthetic algae to more abundant sulphate reduction bacteria populations, which is coincident also with the low Mo and Mo/U ratios observed for this interval (Fig 3.10).

Low Mo/U ratios were also observed in the pre-Walden and the uppermost Woodford Shale (Fig 3.10). However, these lower Mo/U ratios can be explained in a different way, because upper Woodford low Mo/U ratios are more related to oxic conditions and high phosphatic intervals could be associated with upwelling zones (Algeo and Tribovillard, 2009; Turner and Slatt, 2016). In open marine anoxic facies associated with upwelling zones, Mo uptake is limited due the fact $[H_2S]_{aq}$ that concentrations at the sediment-water interface are below the critical threshold for conversion of unreactive molybdate to the reactive thiomolybdate (Fig 3.9b). That means that water mass exchange was probably faster than H_2S diffusing out of the sediments, as it now is in some eastern tropical Pacific continental margins (e.g. Algeo and Tribovillard, 2009). Mo and U contents were under or close to detection limits for pre-Walden, but the Th/U ratios and bioturbation structures confirm that oxidant water/bottom conditions were prevalent during their accumulation (Slatt et al., 2012) and low C_{40} Carotenoid concentrations (Connock et al.,

2018), confirm also the idea that the low Mo/U ratios observed in the upper Woodford are associated more to low H_2S concentrations and oxic/suboxic conditions.

Mo and U concentrations vs TOC tend to significantly fluctuate and decrease under highly sulfidic (euxinic) conditions (Algeo and Maynard, 2004; Tribovillard et al., 2006). However, Ni and Cu are less affected by euxinic conditions and based on these contrasting behaviors, it was possible to distinguish the circumstances when high TOC were associated with high primary productivity and the presence of low sulfidic conditions, as was the case for the upper Woodford (segments II and III) and lower Woodford Shale (segment VI) intervals, from those periods when sulfidic conditions were established and sedimentary OM flux was reduced, and high TOC was more related with a low dilution and high preservation potential, as was identified for the Woodford segment V.

Mn/Fe ratios were used also as a paleo-redox proxy and an important change in the concentration of iron was detected at the top of the middle Woodford segment V, coinciding with the end of euxinic conditions (Fig 3.11). Redox sensitive behavior of Mn and Fe has been well documented by many authors (e.g. Froelich et al., 1979; Calvert and Pederson 1993; Tribovillard et al., 2006). Mn tends to be reduced first and shallower within water/sediment depths than Fe (Fig 3.9b). Fe(Mn)oxyhydroxides redox cycling is in fact an important factor controlling the preservation of phosphatic rich facies and probably can help to explain why phosphatic nodules are preferably accumulated in the Upper Woodford shale instead of the less oxygenated middle/lower Woodford segments.

In bottom waters with Fe(Mn)oxyhydroxides available (i.e. upper Woodford shale), the Fe(Mn)oxyhydroxides particles within the sediments can facilitate retention of organic (reactive)

P and it is adsorbed into authigenic carbonate fluorapatite phases as Ca^{2+} and F^{-}, which diffuse within the sediments (Fig 3.11). In contrast, under reducing (euxinic) bottom waters (i.e. during lower and middle Woodford shales), the lack of ferric iron phases allows most re-mineralized P to diffuse out of the sediment–water interface (e.g. Algeo and Ingall, 2007). Euxinic basins characterized by free H_2S in the water tends to produce pyrite framboids (small raspberry-shaped clusters of pyrite crystals), characterized by a narrow size range, whereas non-sulfidic anoxic environments have larger and broader pyrite framboid size ranges (Wignall and Newton 1998). SEM-EDX thin section from the middle Woodford, associated with the permanent sulfidic conditions (segment V), were related to higher Mn/Fe ratios and low Fe concentrations, which were also characterized by tiny (less than 10 μm) authigenic and narrower pyrite framboid size distribution ranges (Fig 3.12). Diagenetic pyrite formation is limited by deficiencies in organic carbon, sulfate and reactive Fe (Raiswell and Berner, 1985), but high concentration of organic carbon and permanent sulfidic conditions from the middle Woodford shales provide evidence that these two factors were not a limiting aspect, and probably during the accumulation of middle Woodford shale deposits, the authigenic pyrite formation was limited by the Fe contents, as previously purposed by authors based on C-S-Fe ternary plots (i.e. Roberts and Mitterer, 1991).

In general, Late Devonian oceans were characterized by Nitrogen (N) inventory depletion, because of denitrification during permanent greenhouse-anoxic conditions (Saltzman, 2015). These conditions normally persist on geological time scales, only if Fe and Mo company anoxic conditions as bio-limiting nutrients (Falkowski, 1997). The Woodford Shale significant Fe concentrations increments coinciding with the end of euxinic conditions and the onset of marine productivity and may help to support the idea that changes in Fe (and possible Mo) contents

during the F/F transition, affected the oceanic bottom-water redox conditions, marine productivity and increased the organic matter potential that could be preserved.

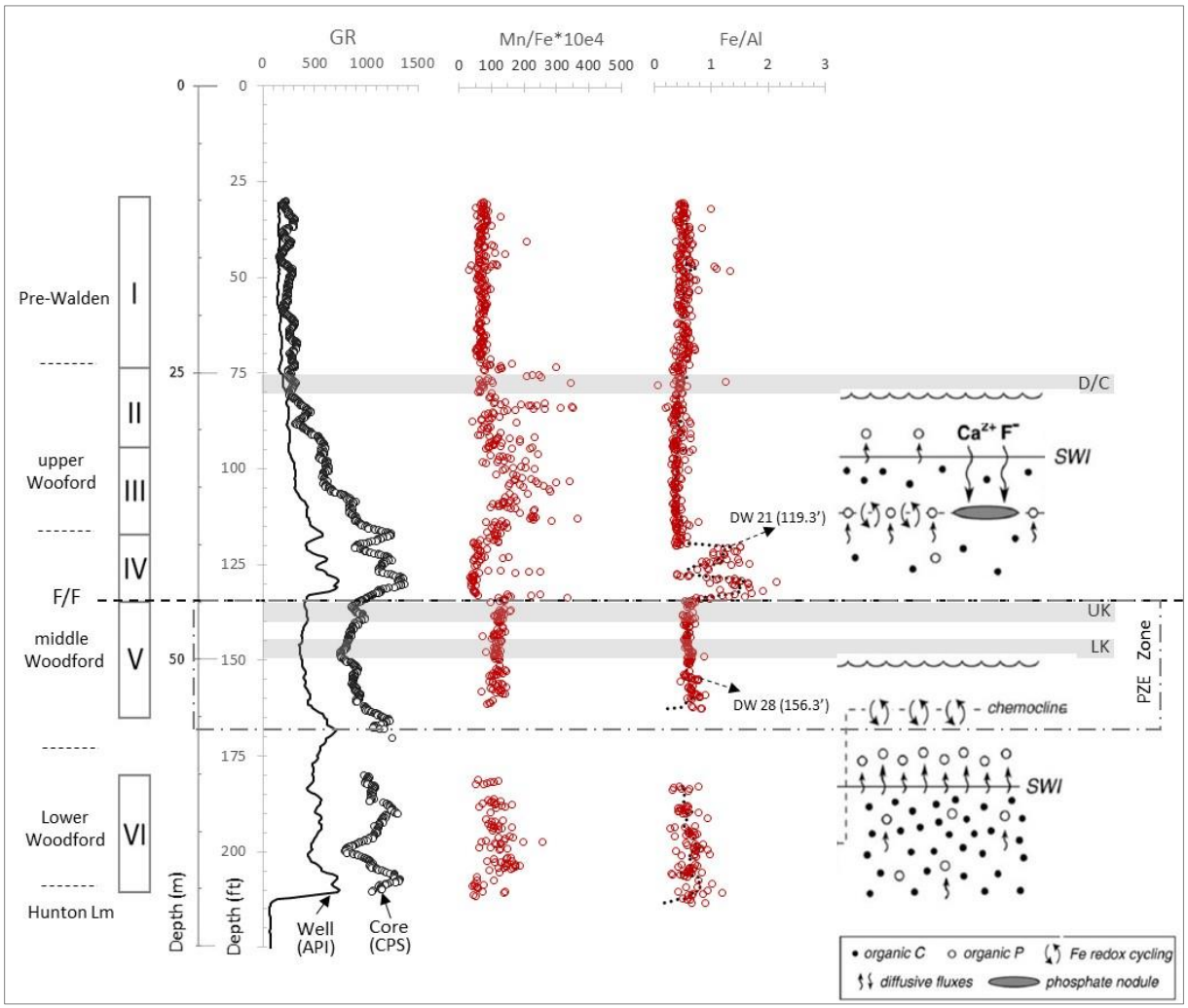

Fig 3.11. Manganese (Mn)/Iron (Fe) ratios and Fe normalized by Aluminum (Al) contents, from X-ray fluorescence (XRF) compositional analysis, Wyche-1 core well (After Turner et al., 2015 and Turner and Slatt, 2016). DW 21 and DW 28 correspond with two thin section samples with high and low Fe contents, analyzed under scanning electron microscope (SEM), and coupled with an energy dispersive X-Ray analyzer (EDX) (See Fig 1.14). Under oxic bottom-waters (upper section), redox cycling of Fe within the sediment facilitates retention of organic phosphorous (P) in the upper Woodford. Under anoxic (reducing) bottom-waters (lower section), the lack of ferric iron phases, favored that P diffused out of the sediments. SWI = sediment water interface, PZE = permanent zone of euxinia. Modified from Algeo and Ingall, 2007.

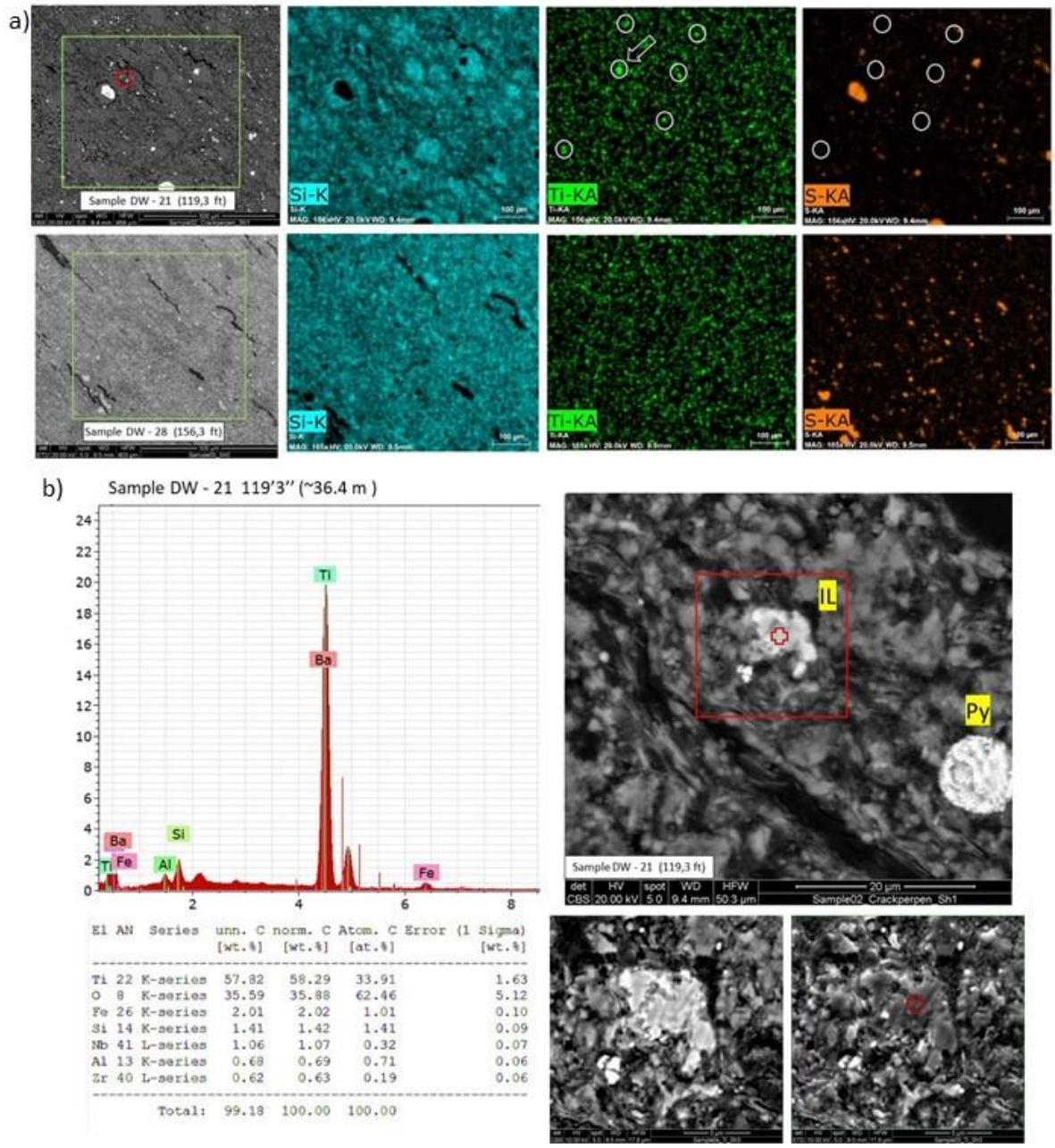

El	AN	Series	unn. C [wt.%]	norm. C [wt.%]	Atom. C [at.%]	Error (1 Sigma) [wt.%]
Ti	22	K-series	57.82	58.29	33.91	1.63
O	8	K-series	35.59	35.88	62.46	5.12
Fe	26	K-series	2.01	2.02	1.01	0.10
Si	14	K-series	1.41	1.42	1.41	0.09
Nb	41	L-series	1.06	1.07	0.32	0.07
Al	13	K-series	0.68	0.69	0.71	0.06
Zr	40	L-series	0.62	0.63	0.19	0.06
		Total:	99.18	100.00	100.00	

Fig 3.12a) Scanning electron microscope (SEM) images, coupled with an energy dispersive X-Ray analyzer (EDX) for two thin section Woodford Shale samples. The lower sample (DW 28 @ 156'3" ft) was characterized by low iron and detrital contents (lower images). The second sample (DW 21 @ 119'3") was marked by higher Fe and detrital contents with abundant ilmenite. Ilmenite crystals were distinguished from other metallic phases, such as pyrite, because high titanium (Ti) and low sulphur (S) on SEM-EDX images. **b**) SEM-EDX analyis from upper Woodford sample located 36.4 m (119'3") depth. Syngenetic pyrite was characterized by pyrite framboids (Py) and tiny metallic particles were identified as ilmenite (IL) crystals ($FeTiO_3$).

4.3.3. **Weathering and dilution**

Chemical weathering could be monitored based on the principle that large cation elements (e.g. Al, Ti, Si) remain relatively fixed, whereas smaller cation elements (e.g. K, Na, Ca) are removed first during weathering alteration (Potter et al., 2005). Oxides calculated from rock compositional analysis are often used to quantify weathering applying some ratios, such as the chemical index of alteration (CIA) (Nesbitt and Young, 1982). However, CIA as a weathering proxies is not directly applicable to fine-grained marine sediments, because deep-sea sediments commonly experience hydraulic sorting and other complications associated with the difficulty of separating individual mineral phases in major oxide phases (Potter et al., 2005; Lupker et al., 2013).

As alternative, Al normalized concentration of Titanium (Ti) and Zirconium (Zr) were preferred as proxies for determining variation on intensity in weathering (and erosion) from source areas (e.g. Lash and Engelder, 2011; Lash, 2017). These ratios seem to support the idea that the main source of Fe immediately after the Woodford Shale euxinic conditions was related to an increased detrital continental influx (Fig 3.13). Ti/Al and Zr/Al ratios are frequently used to evaluate weathering changes on continental land masses and Ti and Zr trace elements are comparatively non-mobile element with Ti-bearing minerals (e.g., ilmenite, rutile, anatase) and Zr-bearing minerals (e.g. Zircons), characterized by being typically present in coarser siliciclastic fractions (Algeo and Rowe 2012; Tribovillard et al., 2006; Turner et al., 2015).

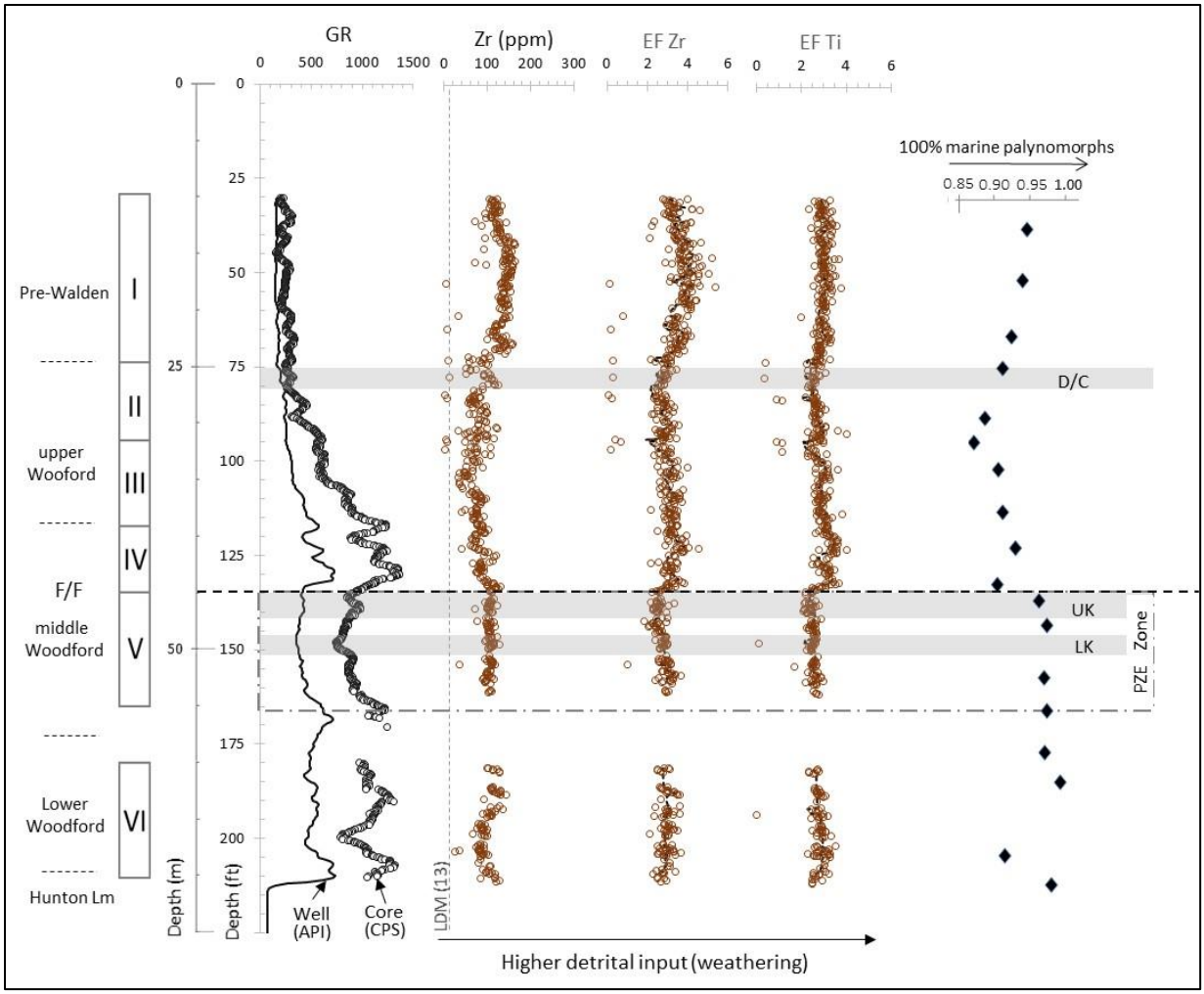

Fig 3.13. Zirconium (Zr) and Titanium (Ti) element concentrations from X-ray fluorescence (XRF), Wyche-1 core well (After Turner et al., 2015 and Turner and Slatt, 2016). Higher detrital contents correlate with higher continental (spores) palynomorphs contents. UK and LK correspond with the Upper and Lower Kellwasser events, D/C with the Devonian/Carboniferous boundary and the permanent zone of euxinia (PZE).

Furthermore, Woodford Shale SEM-EDX compositional analysis revealed the presence of tiny metallic detrital fragments, which were characterized by being Fe- and Ti-rich mineral phases associated with detrital ilmenite (Fig 3.12b). The presence of multiple grain sizes could be associated to different sources and/or transportation mechanisms, but it must to be confirmed.

The ilmenite and Fe-oxides occurrence help to support the idea of a higher detrital continental input and Fe transported from continental areas, in part responsible for ending the permanent euxinic conditions. Late Devonian seas have been characterized by low nitrogen inventories and intense denitrification oceanic conditions (Saltzman, 2005). Denitrification is frequently caused (or enhanced) by iron-limited marine conditions (Falkowski, 1997). More humid conditions associated with more mature soils and evolutionary plant changes, in combination with high continental detrital fluxes (Algeo et al., 1995; 2001), possibly facilitated a higher Fe detrital input to the North America epicontinental seas and consequently, all these combined effects increased the sedimentation rates and the primary marine productivity, which facilitated a higher organic carbon sink and changed the redox conditions during the F/F transition.

4.3 Sequence Stratigraphy Analysis

The elemental gamma-ray (GR) spectroscopy, palynology and XRF elemental compositional analysis were used in order to identify the major flooding surfaces in the Woodford Shale. A total of 14 of flooding surfaces were inferred, correlated and defined. Based on that third-order sequences stacking patterns, a higher second-order cycle was established (Fig 3.14). The sequence stratigraphy model has been based on previously reported Woodford Shale (Portas 2009; Slatt et al., 2011; Amorocho-Sanchez, 2012; Althoff, 2012; Chain, 2012; Serna-Bernal, 2013; Molinares-Blanco, 2013; McCullough, 2014; Treanton, 2014; Cardona-Valencia, 2014; Ali, 2015; Infante-Paez, 2015; Zhang, 2016; Maynard, 2016; Tuner et al., 2015; 2016; Jones, 2017; Ekwunide, 2017; Becerra et al., 2018; Galvis et al., 2018), principally by identifying oscillations in

GR well logs, and throughout the identification of GR stacking patterns (GRP). As a result, some laterally continuous and mappable units were identified (Fig 3.15).

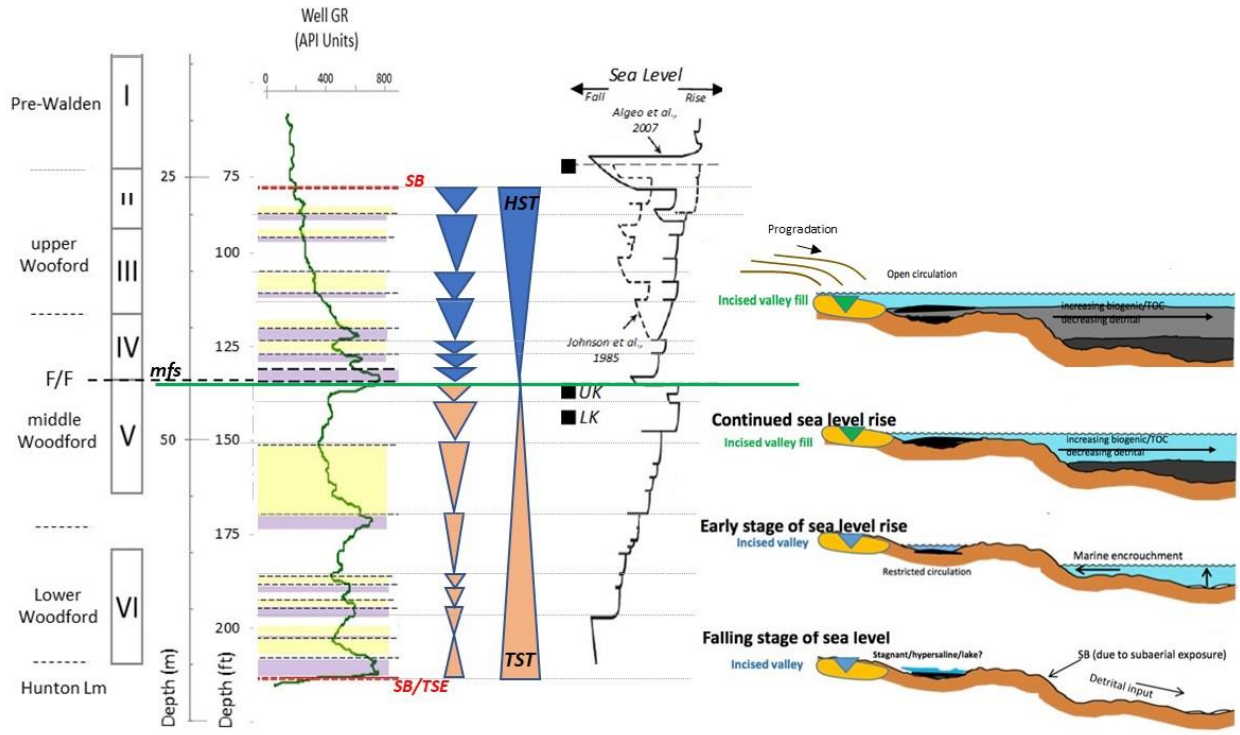

Fig 3.14. Sequence Stratigraphic model for the Woodford Shale, Wyche-1 well Oklahoma. Sea level curve after Algeo et al., 2007. UK and LK correspond to the Upper and Lower Kellwasser events. HST = High Stand System Tract; TST = Transgressive System Tract; *mfs* = Maximum flooding Surface. Woodford Shale depositional model after Slatt et al., 2011; Infante-Paez et al., 2017; Torres-Parada et al., 2017.

Frequently, the basal Woodford shale is characterized by being deposited unconformably above the Hunton limestones. After Hunton group accumulation, a sea level drop allowed the development of an erosional topography that lead to the accumulation of hypersaline lacustrine settings and ticker and more TOC-rich intervals (e.g. Infante et al., 2017; Torres-Parada et al., 2017). In the lower and middle Woodford interval, flooding surfaces were easier to correlate and relative continuous, while the continuity in the upper Woodford interval and overlying units were

more uncertain (Fig 3.15). The difficulty on identifying the flooding surfaces in the upper Woodford and differences with previous interpretations can be explained as the result of the second order regressive pattern and/or lateral discontinuities, characterized by the possible presence of hiatus.

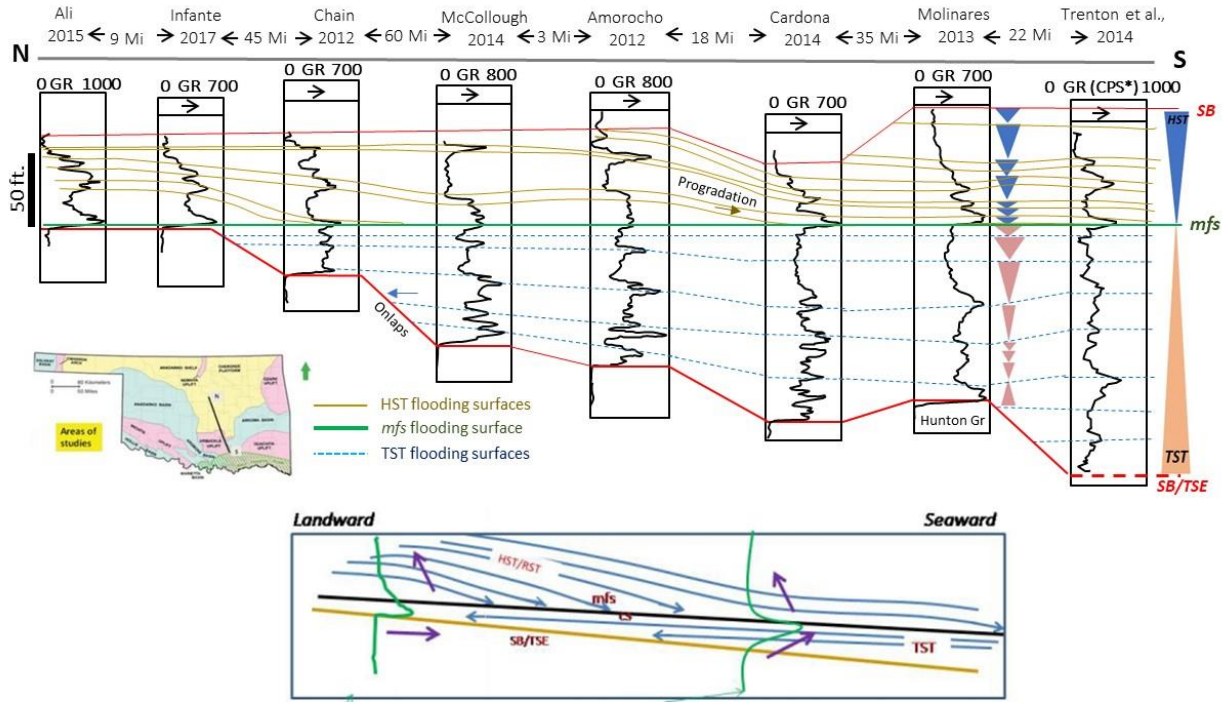

Fig 3.15. Sequence stratigraphy model and Woodford Shale well correlation in South Central Oklahoma. HST = High Stand System Tract; TST = Transgressive System Tract; *mfs* = maximum flooding surface; SB = Sequence Boundary; SB/TSE = Sequence boundary or transgressive surface of erosion (After, Slatt et al., 2012; Infante et al., 2017).

The second-order Transgressive System Tract (TST) is characterized by flooding surfaces with GR and TOC values that progressively rise to the highest values in correspondence of the maximum flooding surface (*mfs*). Underlying this surface, the shales were characterized by homogenous and the finely laminated organic-richest mudstones (Fig 3.14). Transgressive-regressive hemicycles were recognized based on the GR well log shape and supported by the comparison with detailed facies descriptions, palynology, mineralogy and composition from the

XRF and XRD analysis. The transgressive hemicycles are characterized by sharp base or lower GR values, more detrital-silica richer lithofacies and associated with low TOC contents. The regressive hemicycles were characterized by decreasing upward GR and TOC values, with the corresponding more marine, and higher TOC and GR values at the flooding surfaces.

The second-order regressive pattern was associated with the Highstand System Tract (HST) and characterized by increments in the detrital components, higher Ti, Zr and Fe contents, higher terrestrial palynomorphs (Urban, 1960; Molinares-Blanco 2013; Turner et al., 2015; Kondas et al., 2018). The HST was also characterized by the progressive decrease on the anoxic conditions and the end of the permanent zone of the euxinia (PZE) and more oxygenated open marine circulation by the end of the Late Devonian (Fig 3.14). The HST regressive pattern might be associated with the onset of the Late Devonian, early Famennian glacial events (Copper, 1986; Isaacson et al., 1999; Streel et al., 2000; Soreghan et al., 2008), which apparently induced a global sea level drop and regression in the North American platform (Johnson et al., 1985; Joachimski et al., 2002; Bond et al., 2004; Bond and Wignall, 2008; Bond et al., 2013). The third-order flooding surfaces within the HST were characterized also by decreasing upward GR values and respectively lower TOC contents.

5. Conclusions

A multiproxy analysis from Woodford Shale samples in the research Wyche-1 core well recorded the depositional changes associated with the Frasnian and Famennian (F/F) transition in South-central Oklahoma. The Woodford Shale accumulated unconformably over early Devonian limestones, equivalent to the Hunton group, and was delimited at the top by organic-poor mudstones, equivalent to the pre-Walden Shale. The Woodford was subdivided into the lower, middle and upper intervals. The middle interval was organic-richer than the upper and lower Woodford and accumulated under the presence of permanent euxinic conditions. The upper Woodford was characterized by oxic to suboxic redox conditions, the abundant presence of phosphatic nodules, a higher terrestrial-derived palynomorphs, and higher Fe contents related to increments in detrital ilmenite.

The Woodford shale Mo/U ratios and C_{40} organic biomarkers support the idea of stagnant or marine restricted conditions during the accumulation of the middle Woodford Shale deposits. In the Arbuckle Mountain region, the Woodford shale outcrops identified the F/F transitions based on conodont assemblages and magnetic susceptibility correlations. The middle Woodford in the Wyche-1 well recorded two positive carbon excursion events which correlated to the Upper and Lower Kellwasser anoxic-events. In addition, the transition between the upper Woodford and the pre-Walden shales recorded another positive isotopic excursion which was interpreted as the Devonian/Carboniferous (D/C) transition and correlative with the upper Woodford age based on conodont assemblages reported from the Lawrence uplift outcrops.

The top of the Upper Kellwasser event is associated globally with the F/F boundary. The F/F boundary was characterized by the end of the permanent euxinic conditions. This boundary

was also marked by a change from predominantly transgressive conditions, during the accumulation of the lower to middle Woodford, to marked regressive conditions identified in the upper Woodford. The regression can be associated with a global sea level drop, recorded by the end of the Famennian stage and according to some authors, caused by the first Late Devonian glacial events recorded in South America.

The distribution, contents and preservation of the organic matter (OM) in the Woodford Shale deposits was controlled by sedimentological and paleo-ecological conditions, which governed the marine productivity and redox conditions. These processes were largely influenced by relative sea level changes by controlling key primary productivity elements including: marine salinity, the influx of key nutrient (e.g. Fe-influx), water oxygenation, deep-water marine circulation and sedimentation/dilution rates. The widespread of anoxic benthic conditions during the F/F boundary still poorly understood. However, the preservation of the OM in the Woodford Shale was the result of deep-water stagnation, low dilution rates, high salinity/dense vertical oceanic stratification, deep-water oxygen depletion, with no clear evidences of a shallow marginal sill.

6. Acknowledgements

This research was funded by the Geological Society of America (GSA # 9248550) and the American Association of Petroleum Geologists (Jon R. Withrow Named-Grant) and Colfuturo grants gave to Carlos Molinares-Blanco. It was also funded by the generous and continuous support of companies affiliated to the Institute of Reservoir Characterization consortium - University of Oklahoma (IRC-OU). Devon energy and Schlumberger sponsored the drilling and logging of the research Wyche-1 core well. The work performed at the National High Magnetic Field Lab was supported by the National Science Foundation Cooperative Agreement No. DMR-1644779 and the State of Florida. CM deepest appreciation to Dr. Seth Young and Nevin Kozik for their incredible support and help during my time in the National Magnetic Lab in Tallahassee, Florida. Our gratitude with Emma Bachman and Dr. Andrew Elwood-Madden for their assistant during the XRD lab analysis and results interpretation. Sincere thanks go to Dr. Paul Philp, his students and staff at the Organic Geochemistry Laboratory, for helping me in rock preparation and letting use lab facilities for sampling preparations. Thanks to the colleagues from the Institute of Reservoir Characterization (IRC-OU) for discussions and support, especially to Emilio Torres and Andreina Liborius. Jing Zhang and Bryan Turner, who helped and taught the use and calibrations of HH-XRF analysis. Also, thanks to Dr. Douglas Elmore, Cory Terrel and Gerhard Heij for their kind assistance and support using the SEM-EDX OU lab. Extended gratitude to Ms. Brian Cardott (OGS) and Dr. Humberto Carvajal (Core-Lab) for sharing their insights into the Woodford and the Late Devonian black shales anoxia. Dr. Lynn Soreghan's talks about the Late Devonian South America glacial events were a good source of ideas. The paper benefited greatly from detailed thoughtful comments and the attentive oversight from two anonymous reviewers.

7. References

Abousleiman, Y., Tran, M., Hoang, S., Bobko, C., Ortega, A., and Ulm, F.J., 2007, Geomechanics Field and Laboratory Characterization of the Woodford Shale: The Next Gas Play: Proceedings of SPE Annual Technical Conference and Exhibition, doi:10.2523/110120-MS.

Adams, John A. S.; Weaver, C.E., 1958, Thorium-to-Uranium Ratios as Indicators of Sedimentary Processes: Example of Concept of Geochemical Facies: AAPG Bulletin, v. 42, p. 387–430, doi:10.1306/0BDA5A89-16BD-11D7-8645000102C1865D.

Algeo, T.J., and Ingall, E., 2007, Sedimentary Corg:P ratios, paleocean ventilation, and Phanerozoic atmospheric pO2: Palaeogeography, Palaeoclimatology, Palaeoecology, v. 256, p. 130–155, doi:10.1016/j.palaeo.2007.02.029.

Algeo, T.J., and Lyons, T.W., 2006, Mo-total organic carbon covariation in modern anoxic marine environments: Implications for analysis of paleoredox and paleohydrographic conditions: Paleoceanography, v. 21, p. 204–230, doi:10.1029/2004PA001112.

Algeo, T.J., and Maynard, J.B., 2004, Trace-element behavior and redox facies in core shales of Upper Pennsylvanian Kansas-type cyclothems: Chemical Geology, v. 206, p. 289–318, doi:10.1016/j.chemgeo.2003.12.009.

Algeo, T.J., and Rowe, H., 2012, Paleoceanographic applications of trace-metal concentration data: Chemical Geology, v. 324–325, p. 6–18, doi:10.1016/j.chemgeo.2011.09.002.

Algeo, T.J., and Tribovillard, N., 2009, Environmental analysis of paleoceanographic systems based on molybdenum-uranium covariation: Chemical Geology, v. 268, p. 211–225, doi:10.1016/j.chemgeo.2009.09.001.

Algeo, T.J., and Twitchett, R.J., 2010, Anomalous early Triassic sediment fluxes due to elevated weathering rates and their biological consequences: Geology, v. 38, p. 1023–1026, doi:10.1130/G31203.1.

Algeo, T.J., Berner, R.A., Maynard, J.B., and Scheckler, S.E., 1995, Late Devonian oceanic anoxic events and biotic crisis: “rooted’’ in the evolution of vascular land plants?” GSA Today, v. 5, doi:10.1130/GSAT01707GW.1.

Algeo, T.J., Lyons, T.W., Blakey, R.C., and Over, D.J., 2007, Hydrographic conditions of the Devono–Carboniferous North American Seaway inferred from sedimentary Mo–TOC relationships: Palaeogeography, Palaeoclimatology, Palaeoecology, v. 256, p. 204–230, doi:10.1016/J.PALAEO.2007.02.035.

Algeo, T.J., Scheckler, S.E., and Maynard, J.B., 2001, Effects of early vascular land plants on weathering processes and global chemical fluxes during the Middle and Late Devonian: Plants Invade the Land: Evolutionary and Environmental Perspectives, p. 213–236, doi:10.1056/NEJMra1201534.

Althoff, C.D., 2012, Characterization of depositional megacycles in the Woodford Trough of Central Oklahoma. [M.S. Thesis], University of Oklahoma. 99 p.

Ali, E.E., 2015, Integrated characterization of the Woodford Shale in southwest Cherokee Platform, Oklahoma: Norman, Oklahoma, University of Oklahoma. [M.S. Thesis], University of Oklahoma. 104 p.

Amorocho-Sanchez, J. D., 2012, Sequence stratigraphy and seismic interpretation of the Devonian-Lower Mississippian Woodford Shale in the Cherokee Platform: A characterization approach for unconventional reservoirs, numerous TOC calculated from

logs and seismic. [M.S. Thesis], University of Oklahoma. 109 p.
Amsden, T. W., 1980, Hunton Group (Late Ordovician, Silurian, and Early Devonian) in the Arkoma Basin of Oklahoma: Oklahoma Geological Survey Bulletin 129, 136 p.
Amsden, T. W., and Klapper, G., 1972. Misener sandstone (Middle-Upper Devonian), north-central Oklahoma: American Association of Petroleum Geologists Bulletin, v. 56, no. 12, pp. 2323–2334, doi: 10.1306/819a421e-16c5-11d7-8645000102c1865d
Becerra, D., Galvis, H., and Slatt, R., 2018, Lithofacies and stratigraphy of a complete Woodford Shale outcrop section in South Central Oklahoma: Geologic considerations for the evaluation of unconventional shale reservoirs: Interpretation, doi:10.1190/int-2017-0074.1.
Berner, R.A., and Kothavala, Z., 2001, Geocarb III: A revised model of atmospheric CO2over phanerozoic time: American Journal of Science, v. 301, p. 182–204, doi:10.2475/ajs.301.2.182.
Bohacs, K.M.K.K.M. et al., 2005, Production, Destruction, and Dilution-the Many Paths To Source-Rock Development: 61–101 p., doi:10.2110/pec.05.82.0061.
Bond, D.P.G., and Grasby, S.E., 2017, On the causes of mass extinctions: Palaeogeography, Palaeoclimatology, Palaeoecology, doi:10.1016/j.palaeo.2016.11.005.
Bond, D.P.G., and Wignall, P.B., 2008, The role of sea-level change and marine anoxia in the Frasnian-Famennian (Late Devonian) mass extinction: Palaeogeography, Palaeoclimatology, Palaeoecology, v.263, p. 107–118. doi:10.1016/j.palaeo.2008.02.015.
Bond, D., Wignall, P.B., and Racki, G., 2004, Extent and duration of marine anoxia during the Frasnian-Famennian (Late Devonian) mass extinction in Poland, Germany, Austria and France: Geological Magazine, v. 141, p. 173–193, doi:10.1017/S0016756804008866.
Bond, D.P.G., Zatoń, M., Wignall, P.B., and Marynowski, L., 2013, Evidence for shallow-water "Upper Kellwasser" anoxia in the Frasnian-Famennian reefs of Alberta, Canada: Lethaia, v. 46, p. 355–368, doi:10.1111/let.12014.
Bontempi, C, P., 2015, High resolution stratigraphy of thin bedded shales/radiolarians, Woodford Shale, Arbuckle Wilderness area, Murray County, Oklahoma: A new correlation tool. [M.S. Thesis], University of Oklahoma. 81 p.
Bruce, C.H., 1984, Smectite dehydration—its relation to structural development and hydrocarbon accumulation in northern Gulf of Mexico basin: American Association Petroleum Geologist Bulletin, v. 68, p. 673-683, doi: 10.1306/948855d9-1704-11d7-8645000102c1865d
Buggisch, W., 1991, The global Frasnian-Famennian »Kellwasser Event«: Geologische Rundschau, v. 80, p. 49–72, doi:10.1007/BF01828767.
Buggisch, W., and Joachimski, M.M., 2006, Carbon isotope stratigraphy of the Devonian of Central and Southern Europe: Palaeogeography, Palaeoclimatology, Palaeoecology, v. 240, p. 68–88, doi:10.1016/j.palaeo.2006.03.046.
Calvert, S.E., and Pedersen, T.F., 1993, Marine Sediments, Burial, Pore Water Chemistry, Microbiology and Diagenesis Geochemistry of Recent oxic and anoxic marine sediments: Implications for the geological record: Marine Geology, v. 113, p. 67–88, doi:10.1016/0025-3227(93)90150-T.
Canfield, D.E., 1994, Factors influencing organic carbon preservation in marine sediments: Chemical Geology, v. 114, p. 315–329, doi:10.1016/0009-2541(94)90061-2.

Cardona-Valencia, L. F., 2014, Integrated characterization of the Woodford Shale in the southern Cherokee Platform, Oklahoma. [M.S. Thesis], University of Oklahoma. 98 p.
Cardott, B.J., 2012, Thermal maturity of Woodford Shale gas and oil plays, Oklahoma, USA: International Journal of Coal Geology, v. 103, p. 109–119, doi:10.1016/j.coal.2012.06.004.
Cardott, B.J., and Chaplin, J.R., 1993, Guidebook for selected stops in the Western Arbuckle Mountains, southern Oklahoma: Oklahoma Geological Survey Special Edition, v. 93, p. 55.
Cardott, B.J., and Lambert, M.W., 1985, Thermal Maturation By Vitrinite Reflectance ofWoodford Shale, Anadarko Basin, Oklahoma.: American Association of Petroleum Geologists Bulletin, v. 69, p. 1982–1998, doi:10.1306/948878DE-1704-11D7-8645000102C1865D.
Chain, A. R., 2012, Stratigraphy and composition of the Woodford Shale in depositionally updip and downdip wells, Anadarko Basin, Oklahoma[M.S. Thesis], University of Oklahoma. 118 p
Claeys, P., Casier, J.G., and Margolis, S. V., 1992, Microtektites and mass extinctions: Evidence for a Late Devonian asteroid impact: Science, v. 257, p. 1102–1104, doi:10.1126/science.257.5073.1102.
Comer, J.B., and Hinch, H.H., 1987, Recognizing and quantifying expulsion of oil from the Woodford Formation and age-equivalent rocks in Oklahoma and Arkansas (USA).: American Association of Petroleum Geologists Bulletin, v. 71, p. 844–858, doi:10.1306/948878C5-1704-11D7-8645000102C1865D.
Connock, G.T., Nguyen, T.X., and Philp, R.P., 2018, The development and extent of photic-zone euxinia concomitant with Woodford Shale deposition: AAPG Bulletin, v. 102, p. 959–986, doi:10.1306/0726171602017224.
Copper, P., 1986, Frasnian-Famennian mass extinction and cold-water oceans: Geology, v. 14, p. 835-839, doi:10.1130/0091-7613(1986)14<835:FMEACO>2.0.CO;2
Copper, P., 2002, Reef development at the Frasnian/Famennian mass extinction boundary: Palaeogeography, Palaeoclimatology, Palaeoecology, v. 181, p. 27–65, doi:10.1016/S0031-0182(01)00472-2.
Crick, R.E., Ellwood, B.B., Feist, R., El Hassani, A., Schindler, E., Dreesen, R., Over, D.J., and Girard, C., 2002, Magnetostratigraphy susceptibility of the Frasnian/Famennian boundary: Palaeogeography, Palaeoclimatology, Palaeoecology, v. 181, p. 67–90, doi:10.1016/S0031-0182(01)00473-4.
Demaison, G.J., Moore, G.T., 1980, Anoxic environments and oil source bed genesis, Organic Geochemistry v. 2, p. 9–31, doi:10.1016/0146-6380(80)90017-0.
Ekwunife, I.C., 2017, Assessing Mudrock Characteristics, High-Resolution Chemostratigraphy, And Sequence Stratigraphy of The Woodford Shale in the McAlister Cemetery Quarry, Ardmore Basin, Oklahoma. [M.S. Thesis], University of Oklahoma. 125 p.
Elmore, R.D., Heij, G.W. and Wickard, A.K., 2016, Paragenesis of mineralized fractures and diagenesis of prominent North American shales: The Sedimentary Record: SEPM, v. 14, p. 4-10.
Ewing, T. E., compiler, 1991, Tectonic Map of Texas, and accompanying booklet, The Tectonic Framework of Texas (36 p.): The University of Texas at Austin, Bureau of Economic Geology, State Map SM 1, scale 1:750,000.
Filipiak, P., 2002, Palynofacies around the Frasnian/Famennian boundary in the Holy Cross Mountains, southern Poland: Palaeogeography, Palaeoclimatology, Palaeoecology, v. 181,

p. 313–324, doi:10.1016/S0031-0182(01)00483-7.
Froelich, P.N., Klinkhammer, G.P., Bender, M.L., Luedtke, N.A., Heath, G.R., Cullen, D., Dauphin, P., Hammond, D., Hartman, B., and Maynard, V., 1979. Early oxidation of organic matter in pemagic sediments of the eastern Equatorial Atlantic: suboxic diagenesis: Geochim. Cosmochim. Acta 43, p. 1075–1090. doi:10.1016/0016-7037(79)90095-4.
Galvis, H., Becerra, D., and R. Slatt, 2018, "Lithofacies and stratigraphy of a complete Woodford Shale outcrop section in South Central Oklahoma: Geologic considerations for the evaluation of unconventional shale reservoirs," Interpretation 6: SC15-SC27, doi:10.1190/INT-2017-0074.1
Ghosh, S., Galvis-Portilla, H.A., Klockow, C.M., and Slatt, R.M., 2018, An application of outcrop analogues to understanding the origin and abundance of natural fractures in the Woodford Shale: Journal of Petroleum Science and Engineering, doi:10.1016/j.petrol.2017.11.073.
Hillbun, K. et al., 2015, Upper Kellwasser carbon isotope excursion pre-dates the F-F boundary in the Upper Devonian Lennard Shelf carbonate system, Canning Basin, Western Australia: Palaeogeography, Palaeoclimatology, Palaeoecology, v. 438, p. 180–190, doi:10.1016/j.palaeo.2015.07.035.
Infante-Paez, L., 2015, Seismically-determined distribution of total organic carbon (TOC) in the Woodford Shale through integrated reservoir characterization, Payne County, Oklahoma. [M.S. Thesis], University of Oklahoma. 90 p.
Infante-Paez, L., L.-F. Cardona, B. McCullough, and R. Slatt, 2017, Seismic analysis of paleotopography and stratigraphic controls on total organic carbon: Rich sweet spot distribution in the Woodford Shale, Oklahoma, USA: Interpretation, v. 5, no. 1, p. T33-T47.
Isaacson, P.E., Díaz-Martínez, E., Grader, G.W., Kalvoda, J., Babek, O., and Devuyst, F.X., 2008, Late Devonian–earliest Mississippian glaciation in Gondwanaland and its biogeographic consequences: Palaeogeography, Palaeoclimatology, Palaeoecology, v. 268, p. 126–142, doi:10.1016/J.PALAEO.2008.03.047.
Jarvis, I., Burnett, W.C., Nathan, Y., Almbaydin, F.S.M., Attia, A.K. M., Castro, L.N., Flicoteaux, R., Hilmy, M.E., Husain, V., Qutawnnah, A.A., Serjani, A., Zanin, and Y.N., 1994, Phosphorite geochemistry: state ofthe art and environmental concerns: Eclogae Geol. Helv. 87, p. 643–700.
Joachimski, M.M., and Buggisch, W., 1993, Anoxic events in the late Frasnian - causes of the Frasnian- Famennian faunal crisis? Geology, doi:10.1130/0091-7613(1993)021<0675:AEITLF>2.3.CO;2.
Joachimski, M., Ostertag-Henning, C., Pancost, R., Strauss, H., Freeman, K.H., Littke, R., Sinninghe J.S., D., and Racki, G., 2001, Water column anoxia, enhanced productivity and concomitant changes in d13C and d34S across the Frasnian-Famennian boundary: (Kowala Holy Cross Mountains/Ploand), Chemical Geology, v. 175, p. 109–131, doi:10.1016/S0009-2451(00)00365-X.
Joachimski, M.M., Pancost, R.D., Freeman, K.H., Ostertag-Henning, C., and Buggisch, W., 2002, Carbon isotope geochemistry of the Frasnian-Famennian transition: Palaeogeography, Palaeoclimatology, Palaeoecology, v. 181, p. 91–109, doi:10.1016/S0031-0182(01)00474-6.
Johnson, J.G., Klapper, G., and Sandberg, C.A., 1985, Geological Society of America Bulletin Devonian eustatic fluctuations in Euramerica: Geological Society Of America Bulletin,

doi:10.1130/0016-7606(1985)96<567.
Johnson, K.S., and B.J. Cardott, 1992, Geologic framework and hydrocarbon source rocks of Oklahoma, *in* K.S. Johnson and B.J. Cardott, eds., Source rocks in the southern Midcontinent, 1990 symposium: OGS Circular 93, p. 21-37.
Jones, L. C., 2017, An integrated analaysis of Sequence Stratigraphy, petroleum geochemistry and Devonian mass extinction events in the Woodford Shale, southern Oklahoma. M.S. Thesis], University of Oklahoma. 198 p.
Kirkland, D. W., R. E. Denison, D. M., Summers, and J. R., Gormly, 1992, Geology and organic geochemistry of the Woodford Shale in the Criner Hills and western Arbuckle Mountains, Oklahoma, *in* Johnson K. S., Cardott, B. J., eds., Source rocks in the southern mid-continent: 1990 Symposium: OGS Circular v. 93, p. 38–69.
Klapper, G., Becker, R.T., and House, M.R. 1994, Definition of the Frasnian/Famennian Stage boundary: Episodes v. 16, p. 433–441
Klockow, C. M., 2017, Structural survey of the Woodford Shale at McAlister Cemetary Quarry, Carter County, Oklahoma. [M.S. Thesis], University of Oklahoma. 45p.
Kondas, M., Filipiak, P., Paszkowski M., Pisarzowska, A., Elmore, R., Jelonek, I., and Kasprzyk, M., 2018, The organic matter composition of the Devonian/Carboniferous deposits (South Flank of Arbuckle Anticline, Oklahoma, USA, International Journal of Coal Geology, v. 198, 1, p. 88-99, doi:10.1016/j.coal.2018.08.010
Kozik, N.P., Young, S.A., Bowman, C.N., Saltzman, M.R., and Them, T.R., 2019, Middle–Upper Ordovician (Darriwilian–Sandbian) paired carbon and sulfur isotope stratigraphy from the Appalachian Basin, USA: Implications for dynamic redox conditions spanning the peak of the Great Ordovician Biodiversification Event: Palaeogeography, Palaeoclimatology, Palaeoecology, doi:10.1016/j.palaeo.2019.01.032.
Lash, G.G., 2017, A multiproxy analysis of the Frasnian-Famennian transition in western New York State, U.S.A: Palaeogeography, Palaeoclimatology, Palaeoecology, v. 473, p. 108–122, doi:10.1016/j.palaeo.2017.02.032.
Lash, G.G., and Engelder, T., 2011, Thickness trends and sequence stratigraphy of the Middle Devonian Marcellus Formation, Appalachian Basin: Implications for Acadian foreland basin evolution: AAPG Bulletin, v. 95, p. 61–103, doi:10.1306/06301009150.
Lewan, M.D., 1984, Factors controlling the proportionality of vanadium to nickel in crude oils. Geochim. Cosmochim. Acta 48, p. 2231–2238, doi.org/10.1016/0016-7037(84)90219-9.
Lewan, M.D., and Maynard, J.B., 1982, Factors controlling enrichment of vanadium and nickel in the bitumen of organic sedimentary rocks: Geochimica et Cosmochimica Acta, v. 46, p. 2547–2560, doi:10.1016/0016-7037(82)90377-5.
Luning, S., and Kolonic, S., 2003, Uranium spectral gamma-ray response as a proxy for organic richness in black shales: Applicability and limitations, Journal of Petroleum Geology v. 26, p. 153–174, doi:10.1111/j.1747-5457.2003.tb00023.x
Lupker, M., France-Lanord, C., Galy, V., Lavé, J., and Kudrass, H., 2013, Increasing chemical weathering in the Himalayan system since the Last Glacial Maximum: Earth and Planetary Science Letters, v. 365, p. 243-252, doi:10.1016/j.epsl.2013.01.038
Maynard, S., 2016, Correlation of bioturbated facies, chemostratigraphym total organic carbon, and sequence stratigraphy in the Woodford Shale of south central Oklahoma. [M.S. Thesis], University of Oklahoma. 119 p.

McCullough, B. J., 2014, Sequence Stratigraphic framework and characterization of the Woodford Shale on the southern Cherokee Platform of Central Oklahoma. [M.S. Thesis], University of Oklahoma. 212 p.

McGhee, G.R., 1996, The Late Devonian mass extinctions: New York, Columbia University Press, 303 p.

Meyer, K.M., and Kump, L.R., 2008, Oceanic Euxinia in Earth History: Causes and Consequences: Annual Review of Earth and Planetary Sciences, doi:10.1146/annurev.earth.36.031207.124256.

Miceli-Romero, A., and Philp, R.P., 2012, Organic geochemistry of the Woodford Shale, southeastern Oklahoma: How variable can shales be? AAPG Bulletin, v. 96, p. 493–517, doi:10.1306/08101110194.

Molinares-Blanco, C.E., 2013, Stratigraphy and palynomorphs composition of the WoodfordShale in the Wyche Farm Shale Pit, Pontotoc County, Oklahoma: [M.S. Thesis], University of Oklahoma, 90 p.

Nesbitt, H.W., Young, G.M., 1982, Early Proterozoic climates and plate motions inferred from major element chemistry of lutite: Nature v. 299, p. 715–717, doi:10.1038/299715a0.

Northcutt, R. A., K. S. Johnson, and Hinshaw, G. C. 2001, Geology and petroleum reservoirs in Silurian, Devonian, and Mississippian rocks in Oklahoma, *in* Johnson, K. S. ed., Silurian, Devonian, and Mississippian geology and petroleum in the southern mid-continent: 1999 Symposium Oklahoma Geological Survey Circular: 105, p. 1–29.

O'Brien, N.R., and Slatt, R.M., 1990, Argillaceous Rock Atlas: New York, Springer-Verlag, 141 p.

Over, D.J., 1992a, Conodonts and the Devonian-Carboniferous boundary in the upper Woodford Shale, Arbuckle Mountains, south-central Oklahoma: Journal of Paleontology, v. 66, p. 293–311, doi:10.1017/S0022336000033801.

Over, D.J., 1992b, Paleontological Society Conodonts and the Devonian-Carboniferous Boundary in the Upper Woodford Shale , Arbuckle Mountains , South-Central Oklahoma Author (s): D . Jeffrey Over Published by : Paleontological Society Stable URL : http://www.jstor.org/sta: v. 66, p. 293–311.

Over, D.J., 2002, The Frasnian/Famennian Boundary in central and eastern United States: Palaeogeography, Palaeoclimatology, Palaeoecology, v. 181, p. 153–169, doi:10.1016/S0031-0182(01)00477-1.

Over, D.J., and J.E. Barrick, 1990, The Devonian/Carboniferous boundary in the Woodford Shale, Lawrence uplift, south-central Oklahoma, *in* Ritter, S.M. ed., Early to middle Paleozoic conodont biostratigraphy of the Arbuckle Mountains, southern Oklahoma: OGS Guidebook 27, p. 63-73.

Pedersen, T.F., and Calvert, S.E., 1990, Anoxia vs. productivity: What controls the formation of organic-rich sediments and sedimentary rocks?: American Association of Petroleum Geologists Bulletin, v. 74, p. 454–466.

Pollastro, R.M., 1993, Considerations and applications of the illite/smectite geothermometer in hydrocarbon-bearing rocks of Miocene to Mississippian age. Clays Clay Mineralogy, v. 41, p. 119-133, doi:10.1346/CCMN.1993.0410202.

Portas-Arroyal, R.M., 2009, Characterization and origin of fracture patterns in the Woodford Shale in southeastern Oklahoma for application to exploration and development. [M.S. Thesis], University of Oklahoma. 110 p.

Potter, P.E., Maynard, J.B., and Depetris, P.J., 2005, Mud and Mudstone; Introduction and Overview: Berlin, Springer-Verlag, 297 p.
Racki, G., 2005, Chapter 2 Toward understanding Late Devonian global events: few answers, many questions. Developments in Palaeontology and Stratigraphy, 20(C), 5–36, doi:10.1016/S0920-5446(05)80002-0.
Raiswell, R., and Berner, R.A., 1985, Pyrite formation in euxinic and semi-euxinic sediments.: American Journal of Science, v. 285, p. 710–724, doi:10.2475/ajs.285.8.710.
Raup, D.M., and Sepkoski, J.J., 1982, Mass extinctions in the marine fossil record: Science, v. 215, p. 1501–1503, doi:10.1126/science.215.4539.1501.
Roberts, C. T., and Mitterrer, R. M., 1992, Laminated Black Shale-Bedded chert cyclicity in the Woodford Formation, Southern Oklahoma, *in*: Johnson, K.S., and B. J. Cardott, eds., Source Rocks in the Southern Midcontinent, 1990 Symposium: OGS Circular v. 93, p. 330.
Rothman, D.H., 2002, Atmospheric carbon dioxide levels for the last 500 million years: Proceedings of the National Academy of Sciences, v. 99, p. 4167–4171, doi:10.1073/pnas.022055499.
Rowe, H., Hughes, N., and Robinson, K., 2012, The quantification and application of handheld energy-dispersive x-ray fluorescence (ED-XRF) in mudrock chemostratigraphy and geochemistry: Chemical Geology, v. 324–325, p. 122–131, doi:10.1016/j.chemgeo.2011.12.023.
Sandberg, C. A., Morrow, J. R., and W., Ziegler, 2002, Late Devonian sea-level changes, catastrophic events, and mass extinctions, *in* Catastrophic Events and Mass Extinctions: Impacts and Beyond, Koeberl C., MacLeod, K. G., eds., Geological Society of America, Special Paper no. 356, p. 473-487.
Saltzman, M.R., 2005, Phosphorus, nitrogen, and the redox evolution of the Paleozoic oceans: Geology, v. 33, p. 573–576, doi:10.1130/G21535.1.
Savoy, L.E., Mountjoy, E.W., 1995, Cratonic-margin and Antler-age foreland basin strata (Middle Devonian to Lower Carboniferous) of the southern Canadian Rocky Mountains and adjacent plains, *in* Dorobek, S.L., Ross, G.M. eds., Stratigraphic Evolution of Fore- land Basins: Soc. Sediment. Geol. Spec. Publ., v. 52, p. 213–231.
Serna-Bernal, A., 2013, Geological characterization of the Woodford Shale in the McAlister Cemetery Quarry, Criner Hills, Ardmore Basin, Oklahoma: [M.S. thesis], University of Oklahoma, 90 p.
Schindler, E., 1993, Event-stratigraphic markers within the Kellwasser crisis near the Frasnian/Famennian boundary (upper Devonian) in Germany: Palaeogeography, Palaeoclimatology, Palaeoecology, v. 104, p. 115–125, doi:10.1016/0031-0182(93)90124-2.
Sierra, R., Tran, M.H., Abousleiman, Y.N., and Slatt, R.M., 2010, Woodford Shale Mechanical Properties And the Impacts of Lithofacies: 44th US Rock Mechanics Symposium, doi:10.1093/bjc/azu106.
Slatt, R. M., and Y. Abousleiman, 2011, Merging sequence stratigraphy and geomechanics for unconventional gas shales: The Leading Edge, v. 30, p. 274–282, doi:10.1190/1.3567258.
Slatt, R.M., and O'Brien, N.R., 2011, Pore types in the Barnett and Woodford gas shales: Contribution to understanding gas storage and migration pathways in fine-grained rocks: AAPG Bulletin, v. 95, p. 2017–2030, doi:10.1306/03301110145.
Slatt, R.M., Portas, R., Buckner, N., Abousleiman, Y., O'Brien, N.R., Tran, M., Sierra, R., Miceli

Romero, A.A., Davis, R.C., and Wawrzyniec, T.F., 2011, Outcrop/behind outcrop (quarry), multiscale characterization of the Woodford gas shale, Oklahoma: Search and Discovery, v. 80138, p. 1–22, doi:10.1306/13321481M97441.

Slatt, R. M., Buckner, N., Abousleiman, Y., Sierra, R., Philp, P., Miceli-Romero, A., Portas, R., O'Brien, N., Tran, M., Davis, R., and T. Wawrzyniec, 2012, Outcrop/behind outcrop (quarry), multiscale characterization of the Woodford Gas Shale, Oklahoma, *in* Breyer, J., ed., Shale reservoirs—Giant resources for the 21st century: AAPG Memoir 97, p. 382-402.

Slatt, R.M., and Rodriguez, N.D., 2012, Comparative sequence stratigraphy and organic geochemistry of gas shales: Commonality or coincidence? Journal of Natural Gas Science and Engineering, v. 8, p. 68–84, doi:10.1016/j.jngse.2012.01.008.

Soreghan, G.S., Soreghan, M.J., and Hamilton, M.A., 2008, Origin and significance of loess in late Paleozoic western Pangaea: A record of tropical cold? Palaeogeography, Palaeoclimatology, Palaeoecology, v. 268, p. 234–259, doi:10.1016/j.palaeo.2008.03.050.

Streel, M., Caputo, M.V., Loboziak, S. and Melo, J.H.G., 2000, Late Frasnian–Famennian climates based on palynomorph analyses and the question of the Late Devonian glaciations: Earth-Science Reviews, 52(1-3), p. 121-173, doi: 10.1016/S0012-8252(00)00026-X.

Torres, E.J., R.M. Slatt, K.J. Marfurt, L.E. Infante, and L.A. Castillo, 2017, Identification of potential lacustrine stratigraphic intervals in the Woodford Shale, Oklahoma, using multi-attribute 3-D seismic displays and a supervised neural network: Unconventional Resources Technology Conference, URTeC 2692737, 13 p.

Tourtelot, H.A., 1979, Black Shale - Its deposition and diagenesis: Clay and Clay Minerals, v. 27, p. 313–321, doi:10.1346/CCMN.1979.0270501.

Treanton, J. A., 2014, Outcrop-derived chemostratigraphy of the Woodford Shale, Murray County, Oklahoma. [M.S. Thesis], University of Oklahoma. 83 p.

Tribovillard, N., Algeo, T.J., Lyons, T., and Riboulleau, A., 2006, Trace metals as paleoredox and paleoproductivity proxies: An update: Chemical Geology, v. 232, p. 12–32, doi:10.1016/j.chemgeo.2006.02.012.

Turner, B.W., Molinares-Blanco, C.E., and Slatt, R.M., 2015, Chemostratigraphic, palynostratigraphic, and sequence stratigraphic analysis of the Woodford Shale, Wyche Farm Quarry, Pontotoc County, Oklahoma: Interpretation, v. 3, p. SH1–SH9, doi:10.1190/INT-2014-0089.1.

Turner, B.W., and Slatt, R.M., 2016, Assessing bottom water anoxia within the Late Devonian Woodford Shale in the Arkoma Basin, southern Oklahoma: Marine and Petroleum Geology, v. 78, p. 536–546, doi:10.1016/j.marpetgeo.2016.10.009.

Turner, B.W., Tréanton, J.A., and Slatt, R.M., 2016, The use of chemostratigraphy to refine ambiguous sequence stratigraphic correlations in marine mudrocks. An example from the Woodford Shale, Oklahoma, USA: Journal of the Geological Society, v. 173, p. 854–868, doi:10.1144/jgs2015-125.

Tyson, R.V., Pearson, T.H., 1991, Modern and ancient continental shelf anoxia: an overview, *in*: Tyson, R.V., Pearson, T.H., eds., Modern and Ancient Continental Shelf Anoxia: Geol. Soc. Spec. Publ., v. 58, p. 1–26, doi.org/10.1144/GSL.SP.1991.058.01.01.

Urban, J.B., 1960, Microfossils of the Woodford Shale (Devonian) of Oklahoma, [M.S. Thesis]: University of Oklahoma, 77p.

Van Geldern, R., Joachimski, M.M., Day, J., Jansen, U., Alvarez, F., Yolkin, E.A., and Ma, X.P.,

2006, Carbon, oxygen and strontium isotope records of Devonian brachiopod shell calcite: Palaeogeography, Palaeoclimatology, Palaeoecology, v. 240, p. 47–67, doi:10.1016/j.palaeo.2006.03.045.

Walliser, O.H., 1995, Global events in the Devonian and Carboniferous, *in* Walliser, O.H., ed., Global Events and Event Stratigraphy in the Phanerozoic, Springer, Berlin, p. 225-250.

Wang, K., 1992, Glassy microspherules (microtektites) from an Upper Devonian limestone, Science v. 256, p. 1547–1550, doi: 10.1126/science.256.5063.1547

Wang, T., 2016, An organic geochemical study of Woodford Shale and Woodford-Mississippian Tight Oil from central Oklahoma [Ph.D dissertation], University of Oklahoma, 299 p.

Wignall, P.B., and Myers, K.J., 1988, Interpreting benthic oxygen levels in mudrocks: A new approach: Geology v. 16, p. 452–455. doi:10.1130/0091-613(1988)016<0452:IBOLIM>2.3.CO;2.

Wignall, P. B., and Newton, R., 1998, Pyrite framboid diameter as a measure of oxygen deficiency in ancient mudrocks: American Journal of Science v. 298, p. 537–552, doi: doi:10.2475/ajs.298.7.537.

Zhang, J., 2016, Comprehensive reservoir characterization of the Woodford Shale in parts of Garfield and Kingfisher Counties, Oklahoma; 24 cuttings samples from horizontal well in Garfield Cty. TOC/RockEval. [M.S. Thesis], University of Oklahoma. 142 p.